Structural Basis of Adenovirus Attachment to its Receptor CD46

Strukturelle Basis der Bindung des Adenovirus an seinen Rezeptor CD46

Dissertation

der Fakultät für Chemie und Pharmazie
der Eberhard-Karls-Universität Tübingen

zur Erlangung des Grades eines Doktors
der Naturwissenschaften

2008

vorgelegt von
David Persson

Tag der mündlichen Prüfung: 04. Juli 2008

Dekan: Professor Dr. L. Wesemann

1. Berichterstatter: Professor Dr. T. Stehle

2. Berichterstatter: Dr. N. Arnberg

The experimental part of this thesis was performed at the Interfaculty Institute for Biochemistry at the University of Tuebingen between June 2005 and April 2008, under the supervision Prof. Dr. Thilo Stehle.

"Millions saw the apple fall, but Newton was the one who asked why."
-Bernard Baruch

Abstract

Adenoviruses are common pathogens, causing a number of infectious diseases. They have been found in virtually all human organs, producing symptoms that range from the common cold to pneumonia (Hakim and Tleyjeh, 2008). Additionally, they also cause a variety of clinical symptoms, for example epidemic keratoconjunctivitis (EKC), pharyngoconjunctival fever (PCF), infantile gastroenteritis, cystitis and urinary tract infections. Individuals with poorly functioning immune systems are especially prone to severe and life-threatening infections. Among these are persons infected with HIV, or organ transplant patients (Hoffman, 2006). In 1977 Philip Sharp and Richard Roberts discovered the ability of Adenoviruses to split genes (e.g. splicing), and they were in 1993 awarded the Nobel Prize in Physiology and Medicine for their discovery. Today, Adenoviruses are mostly studied for the ability to be used as delivery vehicles in gene therapy. About 25% of all clinical gene therapy trials are performed with Adenovirus-based vectors, making Adenoviruses the largest group (Edelstein et al., 2007). In this thesis we exclusively studied Adenoviruses binding to the cellular receptor CD46, characterizing the interaction at an atomic level. We experimentally connected structure and function, defining the Adenovirus interaction with CD46. The structures presented in this thesis will have implications for future drug design, focusing on reducing complications due to Adenoviruses during organ transplantation. Furthermore, our findings will significantly improve general knowledge of Adenovirus:receptor interactions, which will facilitate the development of more efficient gene delivery vehicles.

Abbreviations

A	Ala	Alanine
C	Cys	Cysteine
D	Asp	Aspartic Acid
E	Glu	Glutamic Acid
F	Phe	Phenylalanine
G	Gly	Glycine
H	His	Histidine
I	Ile	Isoleucine
K	Lys	Lysine
L	Leu	Leucine
M	Met	Methionine
N	Asn	Asparagine
P	Pro	Proline
Q	Gln	Glutamine
R	Arg	Arginine
S	Ser	Serine
T	Thr	Threonine
V	Val	Valine
W	Trp	Tryptophan
Y	Tyr	Tyrosine

Ad	Adenovirus type
Ads	Adenoviruses
bp	Base pairs
CAR	Coxsackie adenovirus receptor
CDC	Centers for Disease control and prevention
Con A	Concanavalin A
DNA	Deoxyribonucleic acid
ds	Double stranded
E.coli	*Escherichia coli*

Eq	Equation
FFA	Fluorescence Focus Assay
ICTV	International Committee on Taxonomy of Viruses
IEC	Ion exchange chromatography
ITC	Isothermal titration calorimetry
JAM-A	Junctional adhesion molecule A
kDa	Kilo Dalton
LLG	Log likelihood gain
MCP	Membrane cofactor protein
MHC	Major histocompatibility complex
MQ	MilliQ water, deionized and filtered
MR	Molecular replacement
NiNTA	Nickel (II) nitrilotriacetic acid
NPC	Nuclear pore complex
PBS	Phosphate buffered saline
PDB	Protein data bank
rms	Root mean square
RNA	Ribonucleic acid
SAP	Shrimp alkaline phosphatase
SCR	Short consensus repeat
SDS-PAGE	sodium dodecylsulfate polyacrylamide gel electrophoresis
SPR	Surface plasmon resonance
U.S.	United States
UV	Ultra violet
Wt	Wild type
Å	Ångström

1 Introduction

1.1 History

It was only about 100 years ago, at the end of the nineteenth century that the first viral pathogen was discovered. A pathogen was then defined as an organism that could be observed with a microscope, cultivated in nutrient medium, and be retained by filters. At this point, apart from a few toxins, very few infectious agents did not fulfill these criteria. In 1898, Dmitri Iwanowski was able to show that the causative agent of a mosaic disease of tobacco plants did not fulfill any of the criteria. Iwanowski was unimpressed by his findings, but in 1898 Martinus Willem Beijerinck repeated Iwanowski's experiments and discovered a new infectious agent that he called *contagium vivum fluidum*, what we today know as a virus. In the same year, Loeffler and Frosch came to the same conclusion regarding the cause of foot and mouth disease. This disease could be transferred from animal to animal with large dilutions in each passage, suggesting a replicating pathogen and not a toxin (Dimmock, 2007). Today, some properties are known to all viruses and thus define a virus.
Viruses have:

- a nucleic acid genome of either DNA or RNA
- genomes associated with protein that at its simplest forms the virus particle, but in some viruses this nucleoprotein is surrounded by additional protein or a lipid bilayer
- the ability to reproduce only in living cells
- the ability to recognize the correct host cell and gain entry to its cytoplasm by use of the outer most proteins

Adenoviruses (Ads) were isolated and cultured for the first time in 1953 by Wallace P. Rowe and colleagues (Rowe et al., 1953). The virus was isolated from adenoids and tonsils in children, where it caused a degeneration of epithelial-like cells. The symptoms caused by this viral agent were called *adenoid*

degenerating (A.D), *adenoid-pharyngeal conjunctival* (APC) and *acute respiratory disease* (ARD). The name Adenovirus was used for the first time in 1956, although possible adenovirus symptoms are documented 100 years earlier (Dingle and Langmuir, 1968). In 1962, it was shown that Adenoviruses also have a tumor activity in mice and hamsters (Fields, 1996), providing the first evidence of a human pathogen causing malignant tumors in an animal model. To date, no convincing results have been obtained of a malignant tumor activity in humans. In total, five polygenetic genera of Adenoviruses have been defined, which infect a broad range of host organisms.

1.2 Taxonomy

Adenoviruses have so far only been isolated from vertebrates. The *Adenoviridae (Benkö, 2006)* family of viruses is divided into four defined genera and one suggested genus according to the International Committee on Taxonomy of Viruses (ICTV) (Büchen-Osmond, 2003). The first genus is *Atadenoviridae (Benkö, 2006)* with a name reflecting the high AT base pair content in the viral genome. The genus infects ruminants (Bartha, 1969; Boros et al., 1985; Lehmkuhl and Cutlip, 1999), birds (Harrach et al., 1997), snakes (Benkö et al., 2002; Farkas et al., 2002) and marsupial hosts (Thomson et al., 2002). The second genus, *Aviadenoviridae (Benkö, 2006)*, infects exclusively birds (Schrenzel et al., 2005) and a third genus *Siadenoviridae (Benkö, 2006)* infecting birds and frogs (Davison et al., 2000; Pitcovski et al., 1998). The fourth genus is *Mastadenoviridae (Benkö, 2006)* and infects exclusively mammals. One adenoviruses genus, *Ichtadenoviridae*, infects fish but is not yet accepted by the ICTV (Benkö et al., 2002; Kovacs et al., 2003). Each genus is further divided into species with names from the host and letters from the alphabet. Species designation of Adenoviruses depends on a number of characteristics like oncogenicity, cross reacting antibodies, and agglutination properties, among others.

In this study we exclusively worked with human Adenoviruses. When we refer to Adenoviruses (or Ads) we always imply human Adenoviruses. The human adenoviruses consist of a total of 51 serotypes classified into six subgenera, designated A-F, that cause a wide range of symptoms (Benkö, 2006) (Table 1).

Table 1. Properties of human adenoviruses species A-F

Species	Serotype	Infects
A	12, 18, 31	Intestine
B:1	3, 7, 16, 21, 50	Respiratory tract, eye
B:2	11, 14, 34, 35	Respiratory and/or urinary tract, eye
C	1, 2, 5, 6	Respiratory tract
D	8-10, 13, 15, 17, 19, 20, 22-30, 32, 33, 36, 37-39, 42-49, 51	Eye, intestine
E	4	Respiratory tract, eye
F	40, 41	Intestine

An additional term used for classification is the "prototype". The first strain isolated is normally the prototype strain, indicated by a "p" for prototype (for example Ad11p). Strains differing from the prototype are designated type "a, b, c" (for example Ad11a). The isolates are also given a specific strain name (for example Ad11p: Slobitski).

1.3 The Adenovirus structure

Adenoviruses are non-enveloped dsDNA viruses, between 70-90 nm in size, with icosahedral symmetry (Brenner and Horne, 1959). The spherical capsid has a diameter of about 900 Å (Stewart et al., 1991), with an estimated molecular weight of $150x10^6$ Da including DNA (Burnett, 1985; Burnett et al., 1985). Adenoviruses, regardless of which host they infect, all share this morphology. The 252 "capsid building blocks" forming the external surface consist of 240 copies of the hexon, arranged such that they have six fold symmetry, and 12 pentons at the vertices of the icosahedron with five fold symmetry. From each center of the penton an elongated fiber protrudes that terminates in a globular knob. The knobs primarily mediate cellular attachment, whereas the penton bases trigger the viral uptake (Figure 1).

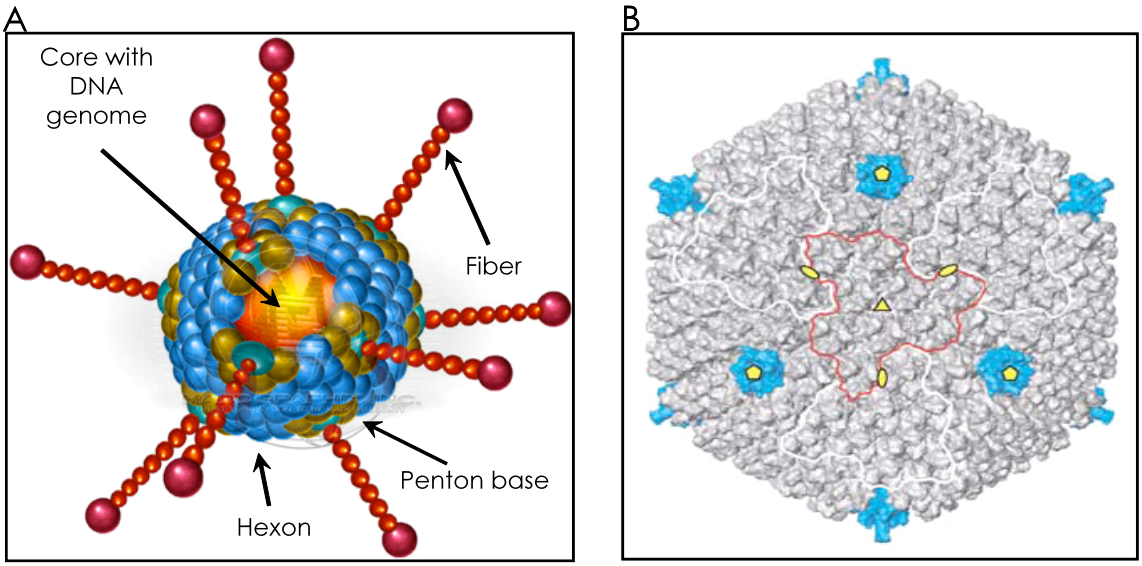

Figure 1. The adenovirus particle. (A) Drawing of the adenovirus particle, with different structural proteins marked in: olive (penton), green (penton Base), blue (hexon) and red (fiber). Picture modified from Madd Graphix Inc (www.maddgraphix.com). (B) Quasi-atomic model of the Ad5 particle at a resolution of 10 Å. The yellow pentagons indicate the five fold rotation axes, the triangles the three fold rotation axes, and the ellipses the two fold rotation axes. The outer edge of one hexon trimer is outlined in red. Each facet is built up by four trimers of the hexon, here outlined in red and white. Figure B obtained from Fabry (Fabry et al., 2005).

There are in total 11 structural proteins, but only the major capsid proteins will be described here in greater detail (hexon, penton and fiber). The virus also encodes about 30 non-structural proteins. These will not be discussed as they are of no importance for receptor interactions, which is the focus in this thesis, but possess regulatory and catalytic functions (San Martín, 2003).

1.4 Adenovirus structural proteins

1.4.1 Hexon (polypeptide II)

The hexon protein is the most abundant protein of the adenovirus particle. It is responsible for 63% of its total protein mass (Burnett et al., 1985), and contains about 950 amino acids. The first X-ray structure of the Ad2 hexon was published in 1985, but was followed by several additional hexon structures (Athappilly et al., 1994; Burnett et al., 1985; Roberts et al., 1986; Rux and Burnett, 2000; Rux et al., 2003) (Figure 2A-B). The hexon folds into two 8 stranded jellyroll like β-sheets (Voet Donald, 2004). The top of the molecule contains three loops and makes up most

of the outer surface of the capsid. With the crystal structure, a quasi atomic model was built by docking the Ad2 hexon into a 35 Å resolution cryo-EM reconstruction from 1991 (Athappilly et al., 1994; Stewart et al., 1991; Stewart et al., 1993). The reconstruction has been drastically improved since then, and the best available structure is now at a resolution of 10 Å, built with the Ad5 hexon (Fabry et al., 2005) (Figure 1B).

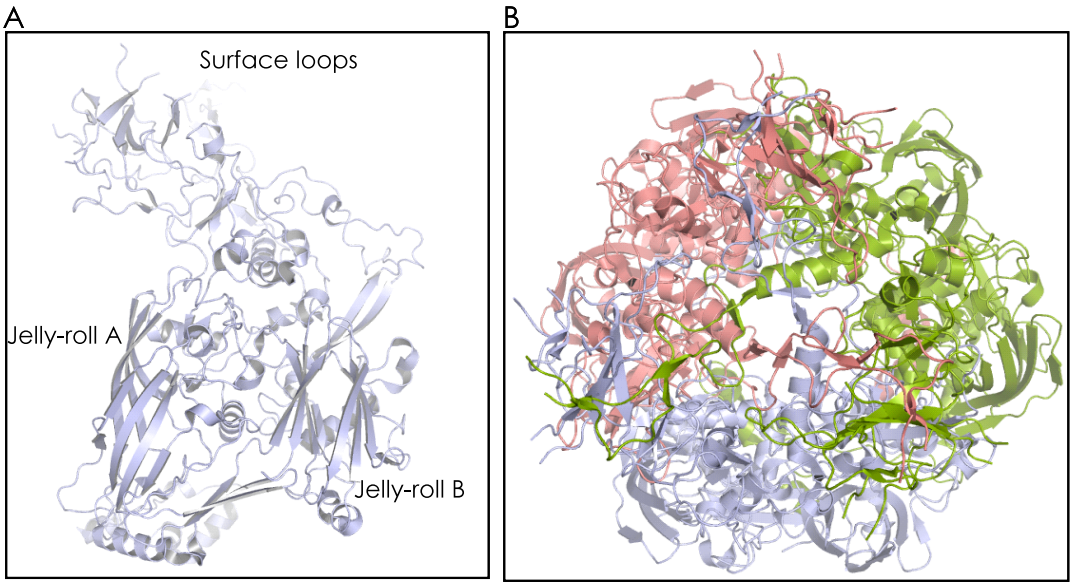

Figure 2. Cartoon representation of the major capsid component, the hexon of Ad5 (PDB accession number 1P30). (A)Side view of one protomer in the trimer, showing the two jelly roll β-sheets and the surface-exposed loops. (B) The hexon polypeptide forms trimers shown in blue, green and red. The view is along the three fold rotation axis, looking down onto the capsid. Figures made in PyMOL (DeLano, 2002).

The hexon trimers have a remarkable stability due to their unusual topology (Rux et al., 2003). The N-terminus of each hexon chain spans the base of the molecule, making contacts with each of the three subunits. The hexon retains its physical and immunological characteristics even after exposure to 8 M urea (Shortridge and Biddle, 1970). The observed high conservation of amino acids at the base of the hexon molecule is probably due to packing restraints within the capsid (Rux et al., 2003). The hexon can be exchanged among different serotypes (Gall et al., 1998; Youil et al., 2002), indicating that the substitutions in the sequence are mainly in surface exposed loops. The hypervariable regions are the major targets for antigenic determinants, as expected for a specific immune response (Crawford-Miksza and Schnurr, 1996).

1.4.2 Penton base (polypeptide III)

The penton base "glues" each of the hexon trimers together through its position at the 12 five fold rotation axes in the virus capsid. The second function for the penton base is during internalization of the virus particle, when its Arg-Gly-Asp (RGD) motif interacts with integrins of the α_v type (Nemerow and Stewart, 1999). Early EM studies showed that the pentamer has a hole with a diameter of 30 Å centered at the five fold axis (Stewart et al., 1991; Stewart et al., 1993) that fits the anchoring peptide of the fiber knob. Two crystal structures of the Ad2 penton base were solved in 2005 (Zubieta et al., 2005) (Figure 3), one of just the penton base, and a second of the penton base in complex with the conserved anchoring peptide of a fiber knob (Zubieta et al., 2005). The penton base has a fold similar to the hexon, with the stable jelly-roll □-barrel domain forming the base and loop extensions. Sequence comparisons among the pentons have shown large diversity in the surface-exposed loops containing the RGD motif, possibly determining the tropism of the different types (Madisch et al., 2007). The penton base is also involved in the agglutination of erythrocytes, one of the criteria for grouping the Ads (A-F) (Wadell and Norrby, 1969).

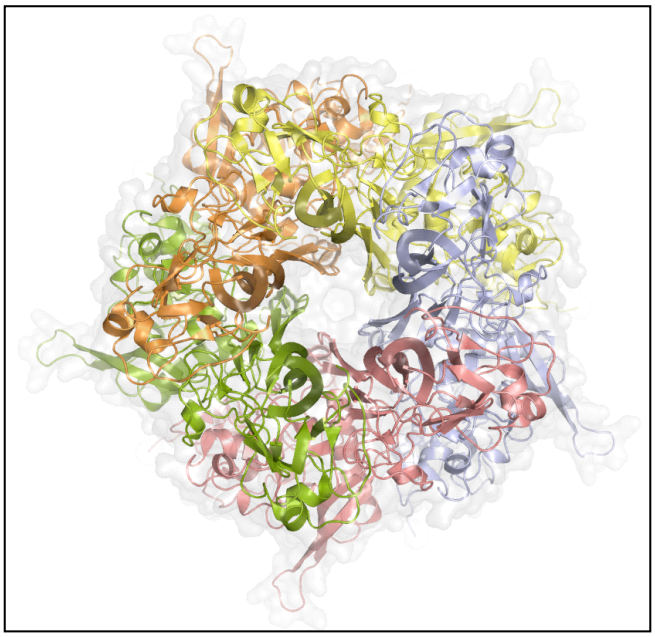

Figure 3. Cartoon representation of the Ad2 penton base (PDB accession number 1X9P). Each chain is colored differently. The view is along the five fold axis, looking down onto the particle. The hydrophobic N-terminal tail of the fiber protein is inserted into the large hole at the center. Figure made in PyMOL (DeLano, 2002).

1.4.3 Fiber (polypeptide IV)

The trimeric fiber protein is inserted into the penton base and protrudes from each of the 12 vertices of the adenovirus capsid. Its structure can be divided into three domains: the N-terminal tail, anchoring the protein to the penton base, the shaft, and the C-terminal knob. A wide variation of the number of repeats (repetitive amino acids in the sequence) in the shaft is observed, ranging from 6 in Ad3 to 22 in Ad5, probably influencing the viral tropism (Green et al., 1983). The first knob structure to be solved was that of Ad5 in 1994 (Xia et al., 1994). The crystal structure confirmed stoichiometric analyses indicating that the fiber is a homotrimeric protein (van Oostrum and Burnett, 1985). The result was controversial due to the symmetry mismatch as the trimeric fiber is positioned on a five fold rotation axis. With the crystal structure of the fiber knob (Xia et al., 1994) it became clear why the knob was never seen in early EM constructions. One reason for this is that five fold symmetry averaging was employed to produce the density maps for the virions. Since the trimers do not have five fold symmetry, they were averaged out of the images (Stewart et al., 1991). Although the penton and the hexon also contain an eight-stranded □ barrel fold forming the core of the protein, the topologies of the □ barrels differ from that of the fiber (Figure 4). In additional the knob barrels have much shorter and less flexible loops. Several knob structures have been solved from almost all species (species A: Ad12, Species B: Ad3, Ad11 and Ad35, species C: Ad2 and Ad5, Species D: Ad19 and Ad37, Species F: Ad41) (Bewley et al., 1999; Burmeister et al., 2004; Durmort et al., 2001; Persson et al., 2007; Seiradake and Cusack, 2005; van Raaij et al., 1999a; Wang et al., 2007). Moreover, the structure of the canine Ad2 knob (Seiradake et al., 2006) is also known.

The overall structures of all crystallized knobs are similar, but they differ in the loop areas determining receptor specificity (Bewley et al., 1999; Cusack, 2005; Persson et al., 2007). Moreover, the overall fold is also similar to the reovirus attachment protein □1 (Chappell et al., 2002), which allows swapping of fibers between reovirus and adenovirus (Mercier et al., 2004). A single crystal structure of a fiber shaft of Ad2 has been successfully solved. The Ad2 structure contains four repeats of the shaft and is the only structural information available on that

region of the fiber (van Raaij et al., 1999b). The repeats have a novel triple beta spiral fold with a unique helical packing, explaining the repetitive pattern of glycine, proline and hydrophobic residues in the sequence. Interestingly, this fold is also shared with the reovirus attachment protein □1. Knob-less viruses can be constructed but leak DNA and are less stable, indicating that the fiber protein has an important role in stability (Schoehn et al., 1996; Von Seggern et al., 1999).

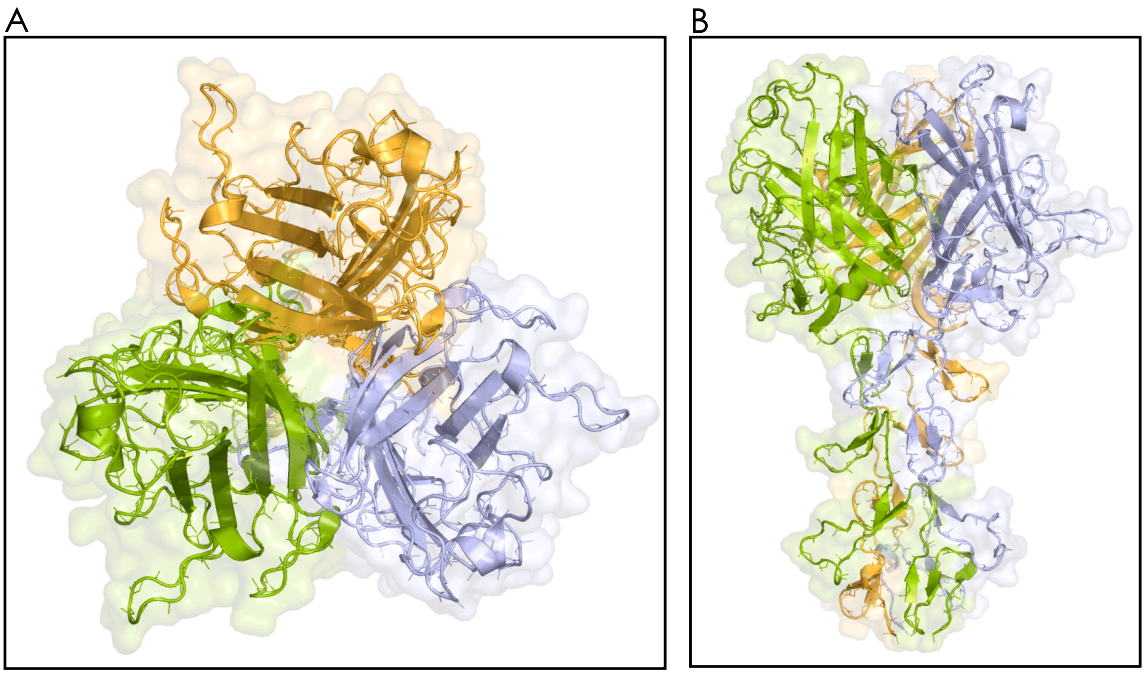

Figure 4. Cartoon/surface representation of the Ad2 trimer (PDB accession number 1QIU). The protomers are shown in green, blue and orange. (A) Top view along the three fold axis. (B) Side view of the same trimer, showing four repeats of the adenovirus shaft. Figures made in PyMOL (DeLano, 2002).

1.5 Adenoviruses and the host

Ads normally enter the host through the mouth or the ocular conjunctiva. Some types, especially species C Ads, can be latent in young children and be shed (sporadic release of viral particles) for months, spreading through the fecal-oral route. The virus normally manifests locally in the eyes and pharynx before migration to the primary tissue, which is the optimal tissue for replication. This suggests that viral particles are present in the blood stream at some stage, i.e. the virus is viremic.

1.6 The Adenovirus life cycle

The process of passing the membrane is called internalization, or penetration, of the virus particle. For this process much more is known for enveloped viruses than non-enveloped viruses. Enveloped viruses enter cells by membrane fusion, whereas non-enveloped viruses use membrane lysis or pore formation (Marsh and Helenius, 2006). For Ads the uptake of the viral particle is a stepwise process that differs depending on Ad type and receptor usage (Figure 5). In short, the first step is the primary interaction between the cellular receptor and the fiber protein of the virus capsid, associating the capsid with the cell surface. The primary attachment receptor is mostly an "anchoring event". Next, the penton base interacts with integrins. This triggers uptake by clathrin mediated endocytosis and the transport of incoming viruses together with their receptors into early and late endosomes (Marsh and Helenius, 2006). The uptake is followed by dismantling of the capsid and endosomal escape (early endosome for species C Ads and late endosome for non-species C Ads) (Miyazawa et al., 2001). Several proteins have been suggested for triggering the escape (penton base, fiber knob, protease and polypeptide VI) (Medina-Kauwe, 2003; Vellinga et al., 2005). As the endosome maturates and pH drops, the capsid proteins change conformation and the partially degraded particle penetrates the membrane (Seth 1985, Greber 1993). Before docking to the nuclear membrane and injection of viral DNA, the virus relocates from the endosome to the nucleus by bidirectional movement along microtubule. The mechanism of importing the adenovirus DNA is a Ca^{2+} dependent process (Greber et al., 1997). Additionally, the role of the non-structural adenovirus protease in degrading the capsid at NPC is of importance. After replication in the nucleus, the virus is released by inducing cell lysis.

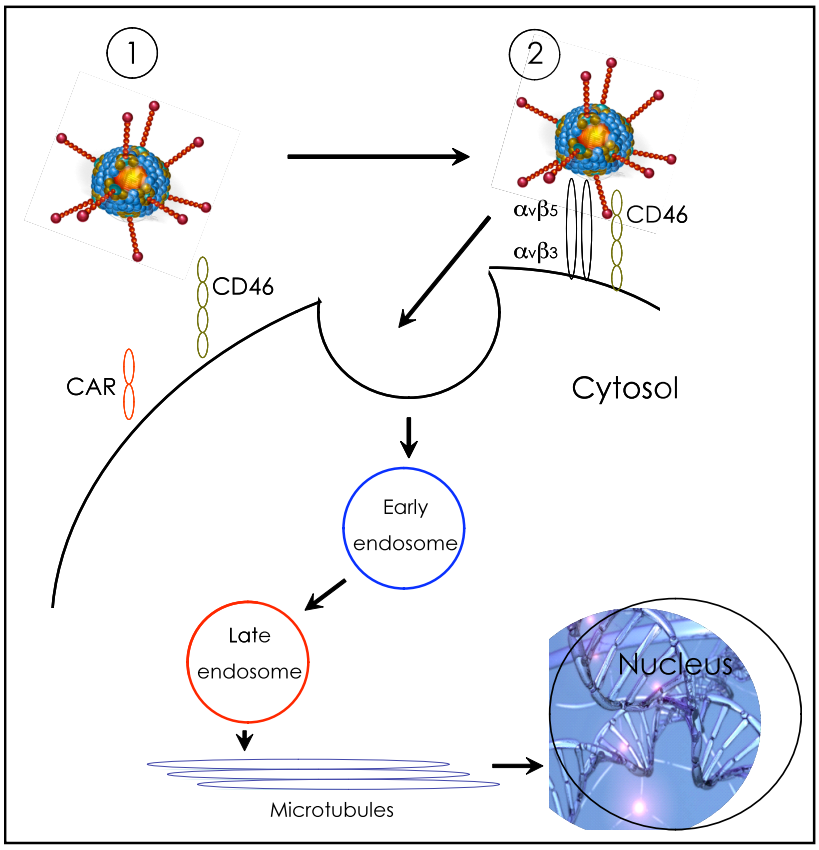

Figure 5. Schematic drawing of the internalization of an Adenovirus particle. Primary high affinity interaction with CD46 or CAR docks the virus to the cell surface. The binding event allows secondary interactions with integrins that trigger uptake by clathrin coated endocytosis. In the early endosome (species C, e.g. Ad5, blue circle), or late endosome (species B, e.g. Ad7, red circle), the particles escape due to altered conformation of structural proteins triggered by the drop in pH. The particles are engaged in bi-directional movement along microtubules and dock at the NPC, where the DNA is injected.

1.7 The Adenovirus receptors

The first step in a virus life cycle is the attachment to a cellular receptor prior to internalization of the capsid (Marsh and Helenius, 2006). The primary interaction can range from high- (Kirby et al., 1999; Persson et al., 2007) to low interaction (Burmeister et al., 2004; Neu et al., 2008) affinity. Viruses normally attach to a protein on the cell surface but also carbohydrates, and very occasionally lipids, are used (Dimmock, 2007). The receptor usage often, but not always, determines the host range, as well as the tropism of the virus. This explains why virus replication is limited to a certain type of tissue, even though the primary attachment receptor may be present on many cells (Flint, 2004). For Ads three

receptors have been confirmed; CAR, α2,3 linked sialic acid, and CD46. However, two more receptors are currently being investigated, CD80/CD86 (Short et al., 2004; Short et al., 2006) and the unknown "receptor X" (Tuve et al., 2006). The consequences for the adenovirus biology by using CD80/CD86 and "receptor X" are not clear, and more data is required for an understanding of the attachment processes with these proteins.

1.7.1 The Coxsackie Adenovirus Receptor (CAR)

Many Ads from different groups attach to cells by engaging the coxsackie- and adenovirus receptor (CAR), a member of the immunoglobulin superfamily and a component of tight junctions (Cohen et al., 2001). CAR is a 46 kDa homodimeric protein that functions primarily as the receptor for species A, C, D, E and F (Carson, 2001). Sequence analysis indicates a single membrane spanning domain dividing the 107 amino acid long cytoplasmic tail from the 216 amino acids in the extracellular domain. CAR is located on the basolateral surface of cells in the respiratory tract, where, surprisingly, it is inaccessible to viruses. Ad infections can only occur after a transient break of the epithelia, exposing the CAR dimer (Flint, 2004). A structural basis for the interaction between Ad12 (species A adenoviruses) and CAR (truncated version with one of the two domains, D1) was published in 1999 (Bewley et al., 1999) (Figure 6). In the structure, the main binding site on the adenovirus knob was located in the AB-loop, with several water-filled cavities and multiple water molecules bridging interactions. Three structures of the interaction between Ads and CAR are known (Bewley et al., 1999; Seiradake et al., 2006), one of them with canine Ad type 2 (Seiradake et al., 2006). In all structures, the knob engages the CAR-D1 protein in a similar fashion and binds with a very similar affinity, which is in the range of 15 nM (Kirby et al., 2000; Wickham et al., 1993).

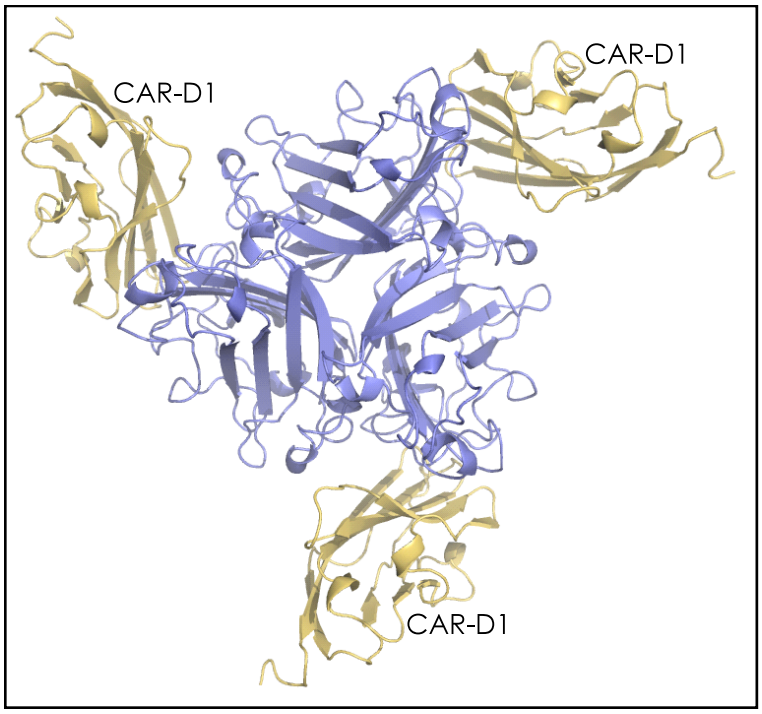

Figure 6. Cartoon representation of the Ad12 knob in complex with the N-terminal domain of CAR (CAR-D1) (PDB accession number 1KAC). The Ad12 knob shown in blue and CAR-D1 is in yellow. The view is along the three fold rotation axis, looking down the fiber. Figure made in PyMOL (DeLano, 2002).

1.7.2 Sialic acid

Sialic acid, (N-acetyl-neuraminic-acid) is widely expressed on animal tissues, and is normally found in glycoproteins and gangliosides (Angata and Varki, 2002; Varki, 2007). A small group of species D adenoviruses (Ad9, Ad19 and Ad37), causing primarily EKC, have been shown to use α2-3 linked sialic acid for cellular attachment, as opposed to CAR (Arnberg et al., 2000a; Arnberg et al., 2002a; Arnberg et al., 2000b; Arnberg et al., 2002b). They all bind CAR (Kirby et al., 2001; Seiradake et al., 2006), but sialic acid offers a more effective infectious route. These three knobs have a particularly positive surface at physiological pH, in comparison to Ads causing mild ocular infections or respiratory infections, allowing interactions with sialic acid in a charge dependent matter (Arnberg et al., 2002a).

The crystal structures of Ad37 and Ad19 (species D Ads) in complex with α2-3 sialyl lactose have been solved, providing a structural basis for the adenovirus-sialic acid interaction (Burmeister et al., 2004) (Figure 7). The binding

epitope is located at the positively charged top of the trimer, binding three copies of α2-3 sialyl lactose molecules used as receptor analogs. A correlation between shaft length and sialic acid binding has been proposed (Wu et al., 2003).

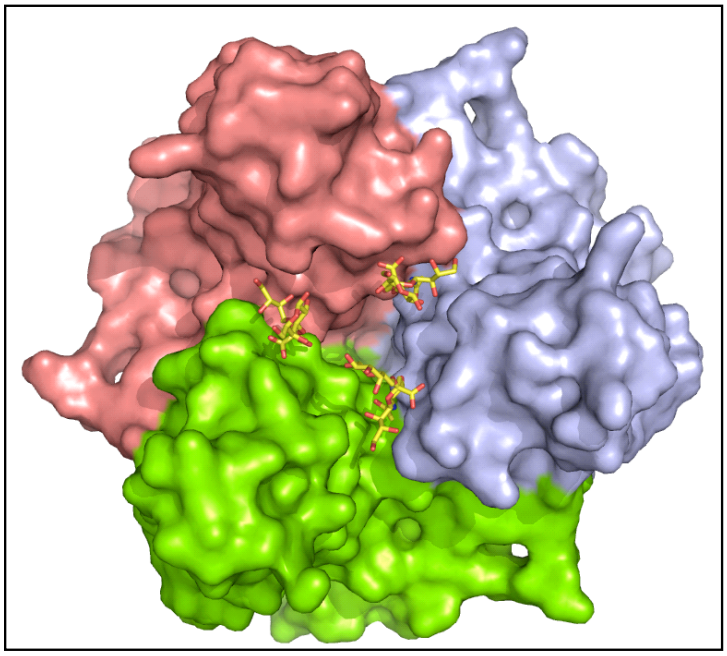

Figure 7. Surface representation (contact surface calculated with a 1.4 Å probe) of the Ad37 knob in complex with α2-3 sialyl lactose (PDB accession number 1UXA). The three chains of the Ad knob are shown in green, blue and red. The α2-3 sialyl lactose is represented with a stick model. The view is along the three fold rotation axis looking down the fiber. Figure made in PyMOL (DeLano, 2002).

1.7.3 Membrane cofactor protein (MCP or CD46)

CD46 (MCP) is a key component in the alternate pathway of the innate immune system where it protects self tissue against complement activation. CD46 was discovered when searching for C3b and C4b proteins of peripheral blood cells and was co-purified using affinity chromatography with CD35 (complement receptor 1) and CD21 (complement receptor 2) (Liszewski et al., 2005). CD46 was later found to inhibit complement activation by binding separately to C3b or C4b and stabilizing them for proteolytic cleavage by factor I, a plasma protein in the trypsin protease family (Liszewski et al., 1991). Inactivation of C3b and C4b inhibits continued complement activation and thus the formation of the membrane attack complex (Liszewski et al., 1996). CD46 provides an intrinsic defense in that it protects cells on whose surface it is expressed. Its broad tissue

distribution is accounted for by the necessity of guarding any cells that may be exposed to complement from its inappropriate activation. CD46 is expressed in four different isoforms generated by alternative splicing (BC1, BC2, C1 or C2) (Post et al., 1991; Riley-Vargas et al., 2004; Russell, 2004). All share the same extracellular portion. CD46 contains four short consensus repeat (SCR or CCP) modules, containing one N-linked glycosylation site each in SCR1 and SCR2, and one predicted in SCR4. In 1999, the crystal structure of the N-terminal two repeats of CD46 was published (Casasnovas et al., 1999) (Figure 8). The SCR1-SCR2 chain folds into two compact β-barrels, each containing a four stranded antiparallel β-sheet. N-linked glycans are attached to Asn49 and Asn80. The glycans cover the majority of one side of the molecule, facing each other and stabilizing a distinct 60° bend between SCR1 and SCR2. Following the four SCRs, a 25 amino acid sequence rich in serine, threonine and proline residues (the STP region) is present. This region is targeted for alternative splicing. Even though three exons (A, B and C) code for the STP region, expression occurs exclusively from exons B + C or C alone (Liszewski et al., 2005). The STP region contains several possible sites for O-linked glycosylation. Following the transmembrane region is a short C-terminal cytoplasmic tail containing one of two possible sequences, CYT-1 or CYT-2, that are linked to cell signalling (Liszewski et al., 2005). The role of CD46 in cell signalling is not well characterized, however crosslinking of CD46 using DLG4, a scaffold protein important for neural signalling, altered the polarization of human epithelial cells (Ludford-Menting et al., 2002). Increasing amounts of data regarding CD46 and immune signalling have suggested that CD46 provides a link between innate and acquired immune function, possibly by influencing immune cell signalling and antigen processing (Elward et al., 2005; Russell, 2004).

In addition to species B Ads, measles virus, human herpes virus 6, group A *Streptococcus pyogenes*, *Neisseria gonorrhoeae, and Neisseria meningitidis* have all been found to utilize CD46 as a specific cellular receptor (Cattaneo, 2004; Gaggar et al., 2003; Giannakis et al., 2002; Gill and Atkinson, 2004; Greenstone et al., 2002; Kirchner et al., 2005; Marttila et al., 2005; Santoro et al., 1999; Segerman et al., 2003a; Segerman et al., 2003b; Segerman et al., 2006). Some of these pathogens only use CD46 for cellular entry, but others also alter

expression and signalling, thus affecting immune response against the pathogen (Cardoso et al., 1995; Gerlier et al., 1994). Taken together, these pathogens contribute significantly to morbidity and mortality all over the world, and CD46 is therefore sometimes referred to as a "pathogen magnet" (Liszewski et al., 2005).

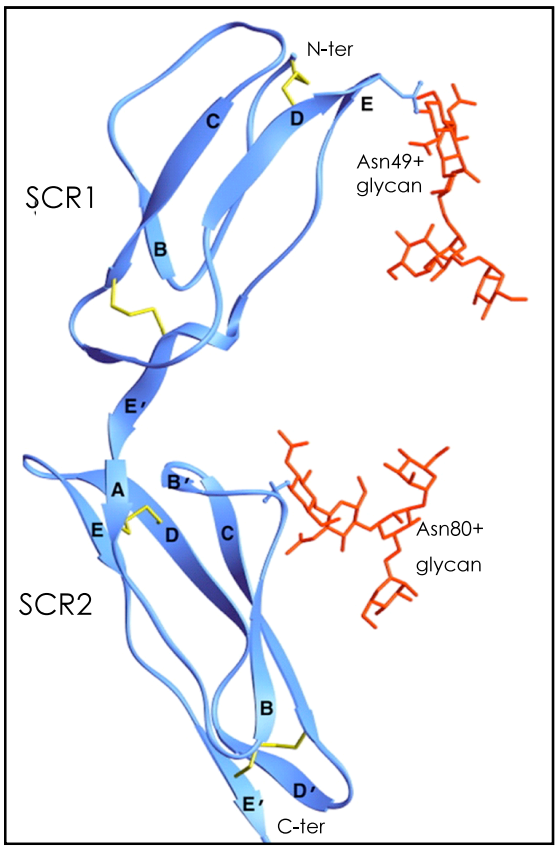

Figure 8. Cartoon representation of CD46 SCR1-SCR2, with the glycans displayed as red stick models and disulfide bonds as yellow sticks (PDB accession number 1CKL). Figure modified from Casasnovas et al., 1999.

1.7.4 The role of integrins as entry receptors

Integrins are an important family of cell adhesion proteins involved in cell migration and signalling (Hynes, 2002). These proteins are large heterodimers composed of α and β subunits, making transmembrane connections to the cytoskeleton and activating several signalling pathways (Nemerow and Stewart, 1999; Ruoslahti, 1997; Xiong et al., 2001). There at least 24 members of the integrin family, divided into four groups, and they bind different receptors as diverse as the Leukocyte specific receptor, Laminin receptor, Collagen receptors and receptors containing RGD motifs (Hynes, 2002). Integrins are co-receptors for Ads, and interactions between the penton base and integrins activates, among

others, phosphatidylinositol 3-kinase, Rac and Cdc42, resulting in the polymerization of actin- and clathrin-mediated endocytosis (Li et al., 1998a; Li et al., 1998b; Marsh and Helenius, 2006; Nemerow and Stewart, 1999). Several Ads have been shown to use integrins $\alpha_v\beta_5$ or $\alpha_v\beta_3$ for internalization (Greber, 2002; Li et al., 1998b; Nemerow and Stewart, 1999). However, some reports indicate that $\alpha_v\beta_1$ might also promote internalization due to its high expression levels on certain tumor cells (Li et al., 2001). In addition integrins $\alpha_3\beta_1$, $\alpha_5\beta_1$, $\alpha_M\beta_2$, and $\alpha_L\beta_1$ have also been implicated in Ad entry (Davison et al., 1997; Salone et al., 2003); Huang 1996).

The penton base RGD-motif (Zubieta et al., 2005) interacts with integrins $\alpha_v\beta_5$ and/or $\alpha_v\beta_3$, probably at the interface between the α and β subunits, as indicated by the $\alpha_v\beta_3$ structure in complex with a cyclic RGD-peptide (Xiong et al., 2001). This interaction is thought to trigger clathrin coated endocytosis. Cryo-EM images of the penton base show a protruding loop with a high flexibility that turned out to contain the RGD motif (Stewart et al., 1991). Unfortunately, in the X-ray structure of the Ad2 penton base, the RGD motif can not be seen due to high flexibility (Zubieta et al., 2005). Mutation or deletion of the RGD motif delays the uptake of the viral particle (Bai et al., 1993), as well as producing an impaired endosomal escape for members of several species (Shayakhmetov et al., 2004).

1.8 Species B Adenoviruses

The species B Adenoviruses are further divided into species B:1 (Ad3, Ad7, Ad16, Ad21, Ad50) and B:2 (Ad11, Ad14, Ad34, Ad35) according to their tropism. Species B:1 Ads mainly cause eye infections and respiratory tract infections, but also systemic infections and diarrhea. Species B:2 Ads primarily cause persistent infections of the urinary tract and kidneys, rarely causing eye and respiratory infections, and they are potentially lethal in immunocompromised hosts (Leen and Rooney, 2005; Levy et al., 1990). Ad3 and Ad7 cause infections in humans more frequently than the other species B adenoviruses, and neutralizing antibodies against these two are thus found in an overall higher percentage in humans (Metzgar et al., 2005; Vogels et al., 2003). Some species B adenoviruses

(Ad3, Ad7, Ad14, Ad16 and Ad21) are weakly oncogenic, causing tumors in a small proportion of hamsters after 4-18 months (Fujinaga and Green, 1967).

The receptor usage of species B adenoviruses is not completely clear but CD46 has been shown to be a major receptor for most adenoviruses in this group (Gaggar et al., 2003; Segerman et al., 2003a; Segerman et al., 2003b; Sirena et al., 2004). Ad7 and Ad3 can infect BHK cells when they are transfected with human CD46, as well as CD46-expressing A549 cells (Fleischli et al., 2007; Fleischli et al., 2005). Other studies have found that Ad3 and Ad7 do not use CD46 as a receptor (Marttila et al., 2005). In addition, a second group B receptor has recently been identified on human stem and tumor cells. This receptor is thought to be used by Ad7 and Ad14, but not by the closely related Ad11 (Tuve et al., 2006). The picture is further complicated by data showing that the group D Ad37 appears to bind CD46 in a calcium-dependent manner (Wu et al., 2004). In this case, binding of Ad37 to CD46 could be blocked with an antibody raised against the N-terminal 19 residues of CD46 (Wu et al., 2004).

1.9 Clinical relevance

1.9.1 Gene therapy

Gene therapy is used to introduce new genes into cells, often for the purpose of treating disease or in order to restore or add gene expression. However, the delivery of a gene does not necessarily have to complement a deficiency, but can also specifically introduce a toxic compound, trigger an immune response, or lead to apoptosis of specific cell types (i.e. cancer cells) (Gardlik et al., 2005). There are two forms of viruses commonly used in gene therapy trials; (i) Non-lytic viruses, including retroviruses and lentiviruses, which leave the host cell intact by budding off the cellular membrane and (ii) lytic viruses, including adenoviruses and human herpes simplex virus, which leave the cell by lysis (Bangari and Mittal, 2006b; Gardlik et al., 2005). As the adenovirus particle is particularly well studied and its transgene will remain episomal, this virus has become especially useful as a tool in gene therapy. Ad vectors are easily propagated to high titers, can be modified without difficulty, and have high transduction efficiency (Ritter et al., 2002). The use of a primary and secondary receptor offers several modes of

altering cellular tropism (Wickham, 2003), by modifying the penton (Einfeld et al., 1999), hexon (Vigne et al., 1999) or fiber (Michael et al., 1995; Wickham et al., 1997). The first generation of Ad vectors was replication deficient, due to the insertion in the E1 region, and caused a notable immune response in two steps. The response was first against the injected virions, the second one against the newly synthesized proteins in the host cell. The second generation of vectors contained additional deletions in the E2 and E4 genes. However, a longterm expression that does not lead to CPE has not yet been achieved. The newest generations of Ad vectors, called "gutless vectors", contain only cis-acting terminal repeats and lead to a very limited immune response. Unfortunately, these vectors can only replicate when complemented (Gardlik et al., 2005).

Most gene delivery studies involving Ad vectors have been performed using the CAR binding Ad5. The current challenge is to obtain high gene delivery in cell types expressing low levels, or no, CAR at all. Among these cell types are many advanced tumor cells, skeletal muscle cells, smooth muscle cells, peripheral blood cells, hematopoietic stem cells and dendritic cells (Mizuguchi and Hayakawa, 2004). However, new strategies for improving the low transduction rate in some cell lines include the insertion of an RGD-motif in the HI- or IJ-loop of the fiber protein (Borovjagin et al., 2005). Retargeting experiments of Ad5 vectors inserting a RGD motif in the HI-loop increased the transduction of esophageal cancer cell lines up to 800 fold (Buskens et al., 2003). Since the discovery of CD46 as a cellular receptor for species B adenoviruses, two vectors based on CD46 binding serotypes (Ad11 and Ad35) have been tested (Brouwer et al., 2007; Stone et al., 2005). These vectors have the benefit of lower pre-existing immunity (Bangari and Mittal, 2006a) in comparison to Ad5. Furthermore, CD46 is ubiquitously expressed, which allows transduction of cells expressing low levels of CAR. So far, no studies have reported a cross reactivity of neutralizing antibodies against Ad11, and Ad35, which allows for immunization without an increased immune response (Holterman et al., 2004). Observed down-regulation of CD46 has implications for gene delivery using the species B adenoviruses (Larochelle et al., 2008).

1.9.2 Vaccination and treatment

Over the last decades, up to 80% of new military recruits in the U.S have acquired lower respiratory tract infections during the first three weeks of training, and 20% of these needed to be hospitalized. The most common diagnosis, in 60% of the cases, is an Ad4 infection followed by Ad7 infection (Xu and Erdman, 2001). However, this also led in 1971 to a vaccination program of new recruits using a live encapsulated enteric vaccine, first for Ad4 but later also for Ad7. The program was abandoned in 1999 due to economical reasons (Metzgar et al., 2007). Very recent outbreaks of severe upper respiratory tract infections caused by Ad14 and Ad21, with fatal outcome in healthy individuals, have renewed interest in vaccination, interestingly against Ad4 and Ad7 (Metzgar et al., 2007). Earlier vaccinations probably also allowed protection against Ad14, by cross reactivity between Ad7 and Ad14, due to the very high homology (CDC, 2007; Metzgar et al., 2007), thus protecting against both Ad7 and Ad14. A new effective vaccination program for the U.S army is therefore anticipated by 2008 (Russell et al., 2006).

CD46 binding Ads have long been implicated in the pathogenesis of disease that occurs in the peri-transplant period, including severe nephritis with graft loss, hemorrhagic cystitis, hemophagocytic syndrome, and fatal multi-organ system infections (Akiyama et al., 2001; Levy et al., 1990; Liles et al., 1993). However, recent Ad infections with a lethal outcome of normal healthy individuals are very alarming and indicate that Ads could become a larger problem in the future, underscoring the need for an effective treatment, and possibly vaccination.

1.10 Aim

The overall aim of this work was to provide a structural basis for the attachment of Ads to the human CD46 protein, which functions as the cellular receptor for several pathogenic Ads. We designed a combination of structural and functional analyses in order to determine the requirements for a functional interaction of Ad knobs with CD46. Key questions to be answered by our research were: What defines the Ad epitope necessary for a productive interaction with CD46? Which region of CD46 is recognized by Ad knobs? Are there structural rearrangements in either protein upon complex formation? Do different CD46-binding Ad knobs differ in their interaction with the receptor, either at the structural level, or in their relative affinities? Can one engineer Ad knob mutations with altered CD46-binding properties? Does the Ad knob binding site for CD46 overlap with previously known ligands for Ad knobs? Does CD46 engage Ads with a region also involved in physiologic interactions?

Answering these questions will help to provide a foundation for the rational design of drugs that might prevent infections of Ads that interact with CD46. Moreover, these studies were also thought to have implications for gene therapy, since it is desirable to limit the distribution of some Ad type vectors by focusing transduction to cell-, organ- or tissue specific molecules. Such strategies could potentially be explored by subtly modifying the interaction with CD46 in order to retarget Ad vectors for treatment of cancer, hereditary disorders and infectious diseases. Knowledge about the precise mechanism of interaction between the virus and its receptor is essential to perform such studies.

2 Materials

2.1 Equipment

2.1.1 General purpose equipment

Autoclave V95	Systec, Wettenberg, Germany
Shaker Intelli-Mixer	NeoLab®, Heidelberg, Germany
Icemaker	Scotsman, Milan, Italy
Gel dryer Slab 2300	LKB, Bromma, Sweden
Microwave NN-E203 WB	Panasonic, Hamburg, Germany
Mini Protean 3 Cell	Bio-Rad, Munich, Germany
Mini Sub-Cell GT	Bio-Rad, Munich, Germany
Shaker Dos-10L	NeoLab®, Heidelberg, Germany
PCR-Cycler iCycler	Bio-Rad, Munich, Germany
pH-Meter PB-11	Sartorius, Göttingen, Germany
Photometer SmartSpec™ Plus	Bio-Rad, Munich, Germany
Pipette Mettler (2.5 µl)	Mettler Toledo, Columbus, USA
Pipettes Pipetman	Gilson, Middleton, USA
PowerPac Basic	Bio-Rad, Munich, Germany
Quartz Cuvette (75 µl)	Helma, Jena, Germany
SpeedVac Heto Vacuum Centrifuge	Heto, Allerod, Denmark
Thermoshaker Unitron	InforsHT, Bottmingen, Switzerland
Transilluminator Universal Hood II	Bio-Rad, Munich, Germany
Scale 323S-OCE	Sartorius, Göttingen, Germany
Scale 4202S-OCE	Sartorius, Göttingen, Germany
Scale Genius	Sartorius, Göttingen, Germany
Centrifuge 5414D	Eppendorf, Wesseling-Bertzdorf, Germany
Centrifuge J2-21	Beckman, Langenselbold, Germany
Centrifuge Multifuge 1L-R	Kendro, Langenselbold, Germany
Centrifuge Sorvall RC-6	Kendro, Langenselbold, Germany
Sorvall Rotor SS34	Kendro, Langenselbold, Germany
Sorvall Rotor SLC4000	Kendro, Langenselbold, Germany
Sorvall Rotor 75002000	Kendro, Langenselbold, Germany
Hera Cell 240 incubator	Thermo Scientific, South Logan, USA

2.1.2 Chromatography

Analytical FPLC Smart	GE Healthcare, Uppsala, Sweden
FPLC BioLogic Duo Flow	Bio-Rad, Munich, Germany
FPLC GE Healthcare	GE Healthcare, Uppsala, Sweden
HisTrap column HP 1 ml	GE Healthcare, Uppsala, Sweden
Concanavalin A Sepharose	GE Healthcare, Uppsala, Sweden
Gelfiltration column Superdex® 200 HiLoad (16/60)	GE Healthcare, Uppsala, Sweden
Gel filtration column Superdex® 200 HR 2ml	GE Healthcare, Uppsala, Sweden
Gel filtration column Superdex® 200 HR (10/30)	GE Healthcare, Uppsala, Sweden
Ion Exchange column MonoQ 5/50	GE Healthcare, Uppsala, Sweden
Homogenizer EmulsiFlex®-C3	Avestin, Ottawa, Canada
Sonicator Digital Sonifier 250	Branson, Danbury, USA
Peristaltic pump Econo Pump	Bio-Rad, Munich, Germany
UV Detector Uvicord SII	GE Healthcare, Uppsala, Sweden

2.1.3 X-ray crystallography equipment

Cryosystem X-Stream	Rigaku/MSC, The Woodlands, USA
Detector MAR 345 dtb	Mar research, Hamburg, Germany
Rotating Anode Micromax 007 HF	Rigaku/MSC, The Woodlands, USA
Digital Microscope with polarization filter MZ16	Leica, Wetzlar, Germany
Microscope S6E	Leica, Wetzlar, Germany
Optics Varimax HF	Rigaku/MSC, The Woodlands, USA
Detector MAR ccd 225	Mar research, Hamburg, Germany
Detector ADSC Q315	Area detector systems corporation, Poway, USA
Pilatus pixel detector	Swiss Light Source, Villigen, Switzerland
Depression wells	Hampton research, Aliso Viejo, USA
Fiber loops/ magnetic bases	Hampton research, Aliso Viejo, USA
96 well crystallization plates	Art Robbins, Sunnyvale, USA
24 well crystallization plates	Hampton research, Aliso Viejo, USA
22mm siliconized cover slides	Hampton research, Aliso Viejo, USA

2.1.4 Software

CCP4	CCP4, 1994
CNSsolve	Brunger et al., 1998
Coot	Emsley et al., 2004
HKL package	HKL research Inc., Charlottesville, USA
Mar345dtb	Mar research, Hamburg, Germany
PyMOL	DeLano, 2002
Ribbons	Carson, 1997
GRASP	Nicholls et al., 1991
RAVE package	Kleywegt et al., 2001
XDS package	Kabsch, 1993
Origin 7.0 plus ITC	MicroCal, Milton Keynes, United Kingdom
Excel	Microsoft, Washington, USA

2.1.5 Filters and kits

0.45 µm Nitrocellulose membrane	Millipore, Schwabach, Germany
Amicon Ulra 4 Concentrator	Millipore, Schwabach, Germany
Amicon Ultra 15 Concentrator	Millipore, Schwabach, Germany
Centricon Plus-70 Concentrator	Millipore, Schwabach, Germany
PCR purification kit	Qiagen, Hilden, Germany
Promega Miniprep kit	Promega, Mannheim, Germany

2.2 Cloning and expression

2.2.1 Bacterial strains

Strain	Genotype	Company
DH5α	*fhuA2* □*(argF-lacZ)U169 phoA glnV44* □*80* □*(lacZ)M15 gyrA96 recA1 relA1 endA1 thi-1 hsdR17*	Personal stock from Prof. Dr. Stehle
Nova Blue	*endA1 hsdR17* (r_{K12}^{-} m_{K12}^{+}) *supE44 thi-1 recA1 gyrA96 relA1 lac* F□[*proA*$^{+}$*B*$^{+}$ *lacI*^{q}*ZΔM15*::Tn*10*] (Tet^{R})	Merck (Novagen), Darmstadt, Germany
Rosetta 2 (DE3)	F^{-} *ompT hsdS*$_{B}$(r_{B}^{-} m_{B}^{-}) *gal dcm* (DE3) pRARE2 (Cam^{R})	Merck (Novagen), Darmstadt, Germany

2.2.2 Eukaryotic cell lines

CHO Lec 3.2.8.1 (Stanley, 1989)
A549 (University of Umeå)

2.2.3 Bacterial expression plasmid

For all bacterial expression the pET-15b plasmid (gene map at: www.merckbiosciences.co.uk) (Merck (Novagen), Darmstadt, Germany) was used.

2.2.4 CHO cell expression plasmid

The CHO-cells were transfected using the pBJ5-GS plasmid (Lonza, Basel Switzerland)

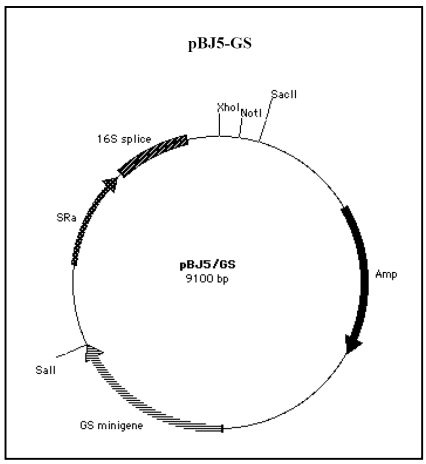

Figure 9. Gene map of the pBJ5-GS plasmid (Figure obtained from www.its.caltech.edu).

2.2.5 PCR-reactions

Pfu-ultra (Stratagene, La Jolla, Canada)
10x Pfu-ultra buffer (Stratagene, La Jolla, Canada)
TaqLC-polymerase (Fermentas, St. Leon-Rot, Germany)
10X buffer $-MgCl_2$ $+(NH_4)_2SO_4$ (Fermentas, St. Leon-Rot, Germany)

2.2.6 Primers

For all Ad knob constructs the following primers were used. The amino acid numbers cloned into the construct are given in parenthesis. The restriction recognition sequence is underlined. The oligo nucleotides were ordered from Biomers (Ulm, Germany).

Primers for wt proteins

Construct (amino acid number)	Primer sequence 5'-3'
Ad11 (118-325) Fw-Nde1	GGGAATTCCATATGGGACTTACATTCAATTCAAACAACAT
Ad11 (118-325) Rev-BamH1	TGGTATGGATCCTCAGTCGTCTTCTCTGATGTAGTAAAA
Ad7 (118-325) Fw-Nde1	GGAATTCCATATGTTGGGAGAAGGACTTACATTC
Ad7 (118-325) Rev-BamH1	TGGTATGGATCCTCAGTCGTCTTCTCTAATG
Ad14 (123-325) Fw-Nde1	GGGAATTCCATATGAACAACATTTGCATTGATGECAAT
Ad14 (123-325) Rev-BamH1	TGGTATGGATCCTCAGTCGTCTTCTCTGATGTAGTAAAA
Ad35 (118-325) Fw-Nde1	GGGAATTCCATATGTTAAAATTTAACAACGGTGACATT
Ad35 (118-325) Rev-BamH1	GTATGGATCCTTAGTTGTCGTCTTCTGTAATGTAAGA
Ad35short (123-325) Fw-Nde1	GGGAATTCCATATGGGTGACATTTGTATAAAGGAT
Ad35short (123-325) Rev-BamH1	GTATGGATCCTTAGTTGTCGTCTTCTGTAATGTAAGA
Ad21 (118-325) Fw-Nde1	GGGAATTCCATATGTTAAAATTTAACAACGGTGACATT
Ad21 (118-325) Rev-BamH1	TGGTATGGATCCTTAGTTGTCGTCTTCTCTAATATAAGA

Primers for mutant proteins (Mutation shaded in grey)

Construct (amino acid number)	Primer sequence 5'-3'
Ad11-N245S (118-325) Fw	GCCTATCCTTTCTCCGATAATTCTAGAG
Ad11-N245S (118-325) Rev	CTCTAGAATTATCGGAGAAAGGATAGGC
Ad11-R279Q (118-325) Fw	ATGCTTAACCAGAGAGCAATAAAT
Ad11-R279Q (118-325) Rev	ATTTATTGCTCTCTGGTTAAGCGT
Ad11-R279S (118-325) Fw	ATGCTTAACTCTAGAGCAATAAAT
Ad11-R279S (118-325) Rev	ATTTATTGCTCTAGAGTTAAGCAT
Ad11-R280G (118-325) Fw	ATGCTTAACCGATCCGCAATAAAT
Ad11-R280G (118-325) Rev	ATTTATTGCGGATCGGTTAAGCAT
Ad11-I282L (118-325) Fw	AACCGAAGAGCACTTAATGACGAGACA
Ad11-I282L (118-325) Rev	TGTCTCGTCATTAAGTGCTCTTCGGTT
Ad11-N283S (118-325) Fw	CCGAAGAGCAATATCCGACGAGACATCATATT
Ad11-N283S (118-325) Rev	AATATGATGTCTCGTCGGATATTGCTCTTCGG
Ad11-D284S (118-325) Fw	CCGAAGAGCAATAAATTCCGAGACATCATATT
Ad11-D284S (118-325) Rev	AATATGATGTCTCGGAATTTATTGCTCTTCGG
Ad7-Q279R (118-325) Fw	CTGTCATGCTTAACCGAAGAGCATTAAATA
Ad7-Q279R (118-325) Rev	TATTTAATGCTCTTCGGTTAAGCATGACAG

Sequencing primers

Primer name	Primer Sequence 5'-3'
T7 Promoter	TAATACGACTCACTATAGGG
T7 Terminator	GCTAGTTATTGCTCAGCGG

2.2.7 Restriction enzymes

All restriction enzymes were obtained from Promega (Mannheim, Germany) and used in the supplied buffers.

Restriction Enzyme	Recognition sequence	Digestion type	Buffer
BamH1	G□GATC C C CTAG□G	Sticky end	D
Nde1	CA□TA TG GT AT□AC	Sticky end	D
Xho1	C□TCGA G G AGCT□C	Sticky end	D

2.2.8 Ligation of plasmids

Shrimp Alkaline Phosphatase (SAP) (Fermentas, St. Leon-Rot, Germany)
T4-DNA ligase (Fermentas, St. Leon-Rot, Germany)
5x rapid ligation buffer (Fermentas, St. Leon-Rot, Germany)

2.3 Cell culture

2.3.1 Bacterial expression

LB medium for bacterial growth
LB-Broth (Sigma, Munich, Germany) supplemented with 50 mM Ampicillin (Sigma, Munich, Germany)

LB agar
LB-Broth (Sigma, Munich, Germany) supplemented with 50 mM Ampicillin (Sigma, Munich, Germany)
14 g Bacto-agar (Roth, Karlsruhe, Germany)/l LB-Broth

Induction
IPTG (Isopropyl □-D-thiogalactopyranoside) (Peqlab, Erlangen, Germany)

2.3.2 CHO cell expression

CHO cell culture medium
5% Fetal Calf Serum (PAA, Cölbe, Germany)
20 mM GS-supplement (PAA, Cölbe, Germany)
5 mM Antibiotics (PEST) (PAA, Cölbe, Germany)
750 µM HEPES (Roth, Karlsruhe, Germany)
10 µM MSX (Sigma, Munich, Germany)

Passage of cells
Trypsin/EDTA (PAA, Cölbe, Germany)

2.4 Protein chemistry

2.4.1 DNA electrophoresis

100 bp DNA Marker (Fermentas, St. Leon-Rot, Germany)
Bacto Agar (Roth, Karlsruhe, Germany)

2.4.2 SDS-PAGE

10 x SDS Running buffer (Roth, Karlsruhe, Germany)
1 M Glycine buffer pH 6.8 (Roth, Karlsruhe, Germany)
1 M Glycine buffer pH 8.8 (Roth, Karlsruhe, Germany)
APS (Roth, Karlsruhe, Germany)
TEMED (Roth, Karlsruhe, Germany)
Unstained protein marker (Fermentas, St. Leon-Rot, Germany)
Comassie stain (Fluka, Steinheim, Germany)
β-Mercapto-ethanol (Roth, Karlsruhe, Germany)

2.4.3 Concentration determination of protein

Biorad Protein Assay (Bio-Rad, Munich, Germany)

2.4.4 Deglycosylation

EndoH (New England Biolabs, Ipswich, USA)

2.5 SPR

2.5.1 SPR buffers

HBS-EP running buffer (CM5-Chip)
10 mM HEPES pH 7.4 at 25 °C (Roth, Karlsruhe, Germany)
150 mM NaCl (Roth, Karlsruhe, Germany)
0.005 % v/v surfactant P20 (GE Healthcare, Uppsala, Sweden)
3 mM EDTA (Sigma, Munich, Germany)

HBS-P running buffer (Ni-Chip)
10 mM HEPES pH 7.4 at 25 °C (Roth, Karlsruhe, Germany)
150 mM NaCl (Roth, Karlsruhe, Germany)
0.005 % v/v surfactant P20 (GE Healthcare, Uppsala, Sweden)
50 mM EDTA (Sigma, Munich, Germany)

HBS-P stripping buffer (Ni-Chip)
10 mM HEPES pH 7.4 at 25 °C (Roth, Karlsruhe, Germany)
150 mM NaCl (Roth, Karlsruhe, Germany)
0.005 % v/v surfactant P20 (GE Healthcare, Uppsala, Sweden)
350 mM EDTA (Sigma, Munich, Germany)

Chip generation buffer
HBS-P buffer
5 mM $NiCl_2$ (Sigma, Munich, Germany)

2.5.2 BiaCore chips

CM5 (GE Healthcare, Uppsala, Sweden)
NiNTA (GE Healthcare, Uppsala, Sweden)

2.6 Crystallization

2.6.1 Crystallization screens

Screen	Conditions	Manufacturer	Reference
Wizard screens 1 and 2	192	Emerald BioScience, Bainbridge Island, USA	---- ----
Hampton screens 1 and 2	192	Hampton Research, Aliso Viejo, USA	(Cudney et al., 1994; Jancarik and Kim, 1991)
PEG/Ion screen	48	Hampton Research, Aliso Viejo, USA	---- ----
Hampton Lite	48	Hampton Research, Aliso Viejo, USA	(Jancarik and Kim, 1991; McPherson, 1990)
Additive screen 1	24	Hampton Research, Aliso Viejo, USA	(Cudney et al., 1994; Sousa, 1995)

2.6.2 Crystallization reagents

Chemical	Manufacturer
PEG200	Sigma, Munich, Germany /Fluka, Steinheim, Germany
PEG400	Sigma, Munich, Germany /Fluka, Steinheim, Germany
PEG600	Sigma, Munich, Germany /Fluka, Steinheim, Germany
PEG1000	Sigma, Munich, Germany /Fluka, Steinheim, Germany
PEG3350	Sigma, Munich, Germany /Fluka, Steinheim, Germany
PEG6000	Sigma, Munich, Germany /Fluka, Steinheim, Germany
PEG8000	Sigma, Munich, Germany /Fluka, Steinheim, Germany
Sodium acetate	Sigma, Munich, Germany
Sodium phosphate	Sigma, Munich, Germany
MES	Sigma, Munich, Germany
HEPES	Roth, Karlsruhe, Germany
TRIS	Sigma, Munich, Germany

Chemical	Manufacturer
CHES	Sigma, Munich, Germany
Glycine	Roth, Karlsruhe, Germany
Bicine	Sigma, Munich, Germany
$MgCl_2$	Merck, Darmstadt, Germany
Glycerol	Sigma, Munich, Germany
MPD	Sigma, Munich, Germany
Glucose	Roth, Karlsruhe, Germany
NaCl	Roth, Karlsruhe, Germany
$CaCl_2$	Merck, Darmstadt, Germany
$ZnCl_2$	Fluka, Steinheim, Germany
$ZnSO_4$	Fluka, Steinheim, Germany

2.7 Buffers

2.7.1 Generation of competent cells

Tfb I
100 mM RbCl (Sigma, Munich, Germany)
10 mM $CaCl_2$ (Merck, Darmstadt, Germany)
50 mM $MnCl_2$ (Sigma, Munich, Germany)
30 mM K Acetate (Sigma, Munich, Germany)
15% Glycerol (Sigma, Munich, Germany)

Tfb II
10 mM MOPS (Sigma, Munich, Germany)
75 mM $CaCl_2$ (Sigma, Munich, Germany)
10 mM RbCl (Sigma, Munich, Germany)
15% Glycerol (Sigma, Munich, Germany)

2.7.2 Buffers protein purification

Lysis buffer
50 mM NaH_2PO_4 pH 8.0 (Sigma, Munich, Germany)
20 mM Imidazole (Sigma, Munich, Germany)
300 mM NaCl (Roth, Karlsruhe, Germany)

His-Trap wash buffer
50 mM NaH_2PO_4 pH 8.0 (Sigma, Munich, Germany)
50 mM Imidazole (Sigma, Munich, Germany)
500 mM NaCl (Roth, Karlsruhe, Germany)

His-Trap elution buffer
50 mM NaH_2PO_4 pH 8.0 (Sigma, Munich, Germany)
300 mM Imidazole (Sigma, Munich, Germany)
500 mM NaCl (Roth, Karlsruhe, Germany)

Gel filtration buffer
20 mM HEPES pH 7.4 (Roth, Karlsruhe, Germany)
150 mM NaCl (Roth, Karlsruhe, Germany)

Ion exchange buffer A
20 mM HEPES pH 7.4 (Roth, Karlsruhe, Germany)

Ion exchange buffer B
20 mM HEPES pH 7.4 (Roth, Karlsruhe, Germany)
1.0 M NaCl (Roth, Karlsruhe, Germany)

Con A Sepharose equilibration buffer
20 mM HEPES pH 7.4 (Roth, Karlsruhe, Germany)
500 mM NaCl (Roth, Karlsruhe, Germany)
1 mM $MgCl_2$ (Merck, Darmstadt, Germany)
1 mM $CaCl_2$ (Merck, Darmstadt, Germany)
1 mM $MnCl_2$ (Sigma, Munich, Germany)

Con A Sepharose wash buffer
20 mM HEPES pH 7.4 (Roth, Karlsruhe, Germany)
1.0 M NaCl (Roth, Karlsruhe, Germany)
1 mM $CaCl_2$ (Sigma, Munich, Germany)
1 mM $MnCl_2$ (Sigma, Munich, Germany)

Con A Sepharose elution buffer
20 mM HEPES pH 7.4 (Roth, Karlsruhe, Germany)
500 mM NaCl (Roth, Karlsruhe, Germany)
12.5% w/v methyl-□-D-mannopyranoside (Sigma, Munich, Germany)
1 mM $MgCl_2$ (Merck, Darmstadt, Germany)
1 mM $CaCl_2$ (Merck, Darmstadt, Germany)
1 mM $MnCl_2$ (Sigma, Munich, Germany)

Con A Sepharose regeneration high pH buffer
100 mM TRIS pH 8.5 (Sigma, Munich, Germany)
500 mM NaCl (Roth, Karlsruhe, Germany)

Con A Sepharose regeneration low pH buffer
100 mM Citric acid pH 4.5 (Fluka, Steinheim, Germany)
500 mM NaCl (Roth, Karlsruhe, Germany)

Con A Sepharose regeneration storage buffer
Acetate pH 6.0 (Sigma, Munich, Germany)
1 M NaCl (Roth, Karlsruhe, Germany)
1 mM $MgCl_2$ (Merck, Darmstadt, Germany)
1 mM $CaCl_2$ (Merck, Darmstadt, Germany)
1 mM $MnCl_2$ (Sigma, Munich, Germany)

3 Methods

3.1 Molecular biology

3.1.1 Polymerase Chain Reaction (PCR)

The PCR reaction (Mullis et al., 1986) was used for amplification of the fiber gene of several species B adenoviruses (Ad7, Ad11, Ad14, Ad21 and Ad35) (see Appendix). Primers for each PCR reaction were manually constructed fitting the type sequence obtained from Genebank (GenBank, 2008) (see Materials section 2.2.6, Appendix 7.1). In this thesis, more detailed information about the recombinantly expressed proteins can be found in the Appendix. Several mutations were constructed by Overlap Extension PCR with the mutation introduced using a second set of primers. Briefly, the second sets of primers are constructed to contain a mismatch with the mutation at the center. The mutation is then introduced in two steps (Figure 10) by generating half of each gene in separate test tubes (reaction A). The two halves are then fused in a second reaction B using the wt flanking primers (see Materials section 2.2.6). Both reactions were performed at optimal annealing temperature (5 °C below the primer melting temperature), using 10 pMol of primer and 100 ng of insert. For reaction B, 100 ng of each fragment was used.

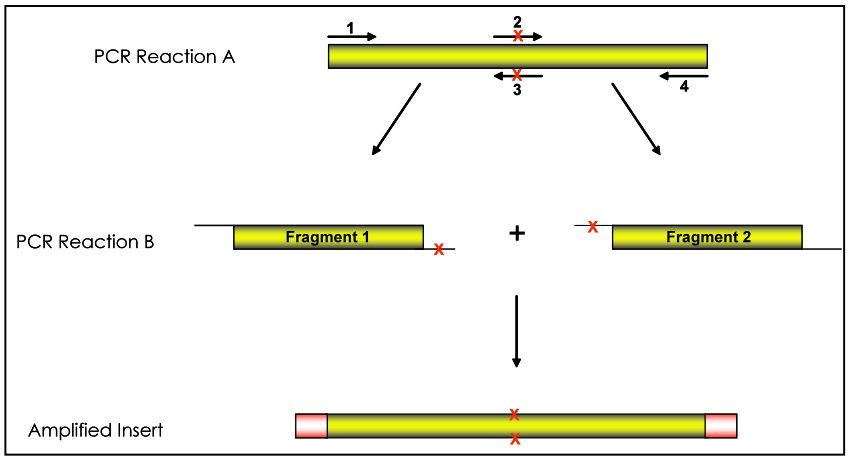

Figure 10. Overlap extension PCR. The mutation is introduced on a second set of primers in two PCR reactions. In reaction one primer pair 1+3 and 2+4 are used, in reaction two primer pair 1+4 generating an insert with mutation and flanking restriction enzyme cutting sequences.

3.1.2 Purification of plasmid DNA

In this work, purification of amplified insert was performed using a PCR purification kit from Qiagen according to the manufacturer's instructions. The amplified plasmids were purified by pelleting the plasmids ethanol at -80 °C over night. All DNA concentrations were measured using absorbance at a UV wavelength of 260 nm (A260) or 280 nm (A280) with a spectrophotometric analysis. DNA bases absorb UV light at 260 nm. The concentration of pure double-stranded DNA at an A260 of 1.0 is 50 mg/ml. Since there is a linear relationship between absorbance and DNA concentration, the following formula can be used (Eq. 1):

$$C_{unknown}(\mu g/ml) = 50\mu g/ml \times A260_{measured} \times Dilution \qquad \text{Equation 1}$$

Aromatic amino acids in proteins absorb UV light at 280 nm. Thus, by dividing A260/A280 one gets a constant direct proportional to the protein contamination in the sample, i.e. an indication of DNA purity

3.2 Restriction enzyme digestion and plasmid ligation

3.2.1 Adenovirus knob

The amplified insert was digested by double digestion using Promega enzymes in the appropriate supplied buffers, according to the manufacturer's instructions (in all cases buffer D). After dephosphorylation using SAP, in buffer D, the linearized plasmid was mixed with a three fold excess of insert. Ligation was then performed using T4 DNA ligase (Fermentas), in rapid ligation buffer at 20 °C, according to the manufacturer's protocol. The pET15-b vector was used, which contains a thrombin cleavable N-terminal hexahistidine tag. The plasmid was transformed into *E. coli* Nova Blue or *E. coli* DH5α cells using a heat shock protocol (incubation of 5 min on ice, 42 °C for 1 min, 5 min on ice), followed by incubation at 37 °C in LB medium without ampicillin (see Materials section 2.3.1). Amplified and purified plasmids were sequenced using the Value Read Package

service at MWG (Eurofins group, Germany) using the T7 Promoter and T7 Terminator primers (see Materials section 2.2.6).

3.2.2 Human CD46

The stable cell lines used for expression of the two CD46 constructs were produced by Jose M. Casasnovas. cDNA coding for amino acids 35-160 (CD46 SCR1-SCR2) or 35-288 (CD46 SCR1-SCR4) of human CD46 was cloned into the pBJ5-GS expression vector, which contains a glutamine synthetase enzyme for selection as described elsewhere (Bebbington et al., 1992; Casasnovas et al., 1999). Stable transfectants were selected by increasing amounts of methionine sulfoxime. The cells have four independent mutations in the N- and O-glycosylation pathways (Stanley, 1989), resulting in N-linked carbohydrates of the high mannose type ranging from Man_5 to Man_9. O-glycosylation is homogenous, with only a single GalNAc residue attached per site.

3.3 Protein chemistry

3.3.1 Protein expression

The expression of recombinant protein was driven by the LacZ promoter through addition of IPTG. IPTG is not hydrolyzable by the cell and is therefore kept at a constant concentration during the entire expression.

3.3.1.1 Adenovirus knob

E. coli Rosetta 2 (DE3) cells were transformed as described in the Methods section 3.2.1, and used for expression of all recombinant knobs. A glycerol stock was prepared for all constructs using 3 ml of an 8 hrs old culture, supplemented with 20% glycerol. During expression, the cells were grown at 37 °C to an OD_{600} of 0.6 and induced for 16 hrs at 20 °C, using 1 mM of IPTG. The cells were then pelleted, using a Sorvall RC6 centrifuge and a SLC 4000 (Sorvall) rotor at 4000 g for 20 min, and resuspended in 10 ml lysis buffer, per liter of culture (see Materials section 2.7). The resuspended pellet was supplemented with 1 mM phenylmethylsulphonylfluoride (PMSF) for protease inhibition. The cells were lysed using a high pressure homogenizer (EmulsiFlex-C3). The lysate was cleared by centrifugation at 20.000 g using a SS34 rotor (Sorvall) for 90 min followed by

filtration of the supernatant through a 0.45 µm nitrocellulose filter membrane (Millipore).

3.3.1.2 Human CD46

The CHO-cells were grown in Ex-cell™302 CHO serumfree medium (SAFC Biosciences) supplemented with 1x glutamine (50x stock, SAFC Biosciences), 5% Fetal Calf Serum (Gibco) and 1x Penicillin/Streptavidin (100X stock, PAA) (see Materials section 2.3.2). Cells from four 95% confluent 175 ml cell culture flasks were harvested using Trypsin/EDTA (1x stock PAA), pelleted at 2000 g, resuspended in 10 ml of fresh medium and then transferred to a roller bottle flask (Greiner) in 300 ml of medium. After three days, rotating at 37 °C with 5% CO_2 (Hera Cell 240 incubator), the medium was replaced. Dead detached cells were removed by centrifugation at 4000 g for 10 min, and the collected cell supernatant frozen at -20 °C for storage. The cells in the roller bottles were discarded after 4 weeks of protein production.

3.4 Protein purification

All proteins were purified and stored at either 4 °C, or if possible -80 °C. Some mutants tended to precipitate upon freezing.

3.4.1 Adenovirus knob purification

The following purification procedure explains how the Ad11 knob was purified, but the very same protocol was used for all other knobs described in this thesis. Detailed information about buffers used here can be found in the Materials section 2.7 of this thesis.

3.4.1.1 General – His-Trap chromatography

Histidine-tagged (His-tagged) proteins have a high selective affinity for Ni^{2+} several divalent metal ions. Consequently, a protein containing a histidine tag binds strongly to a metal-ion charged medium while other cellular proteins bind only weakly. Histidine-tags are small and can therefore be less disruptive to the properties of the proteins to which they are attached. Elution is performed by competing out the interaction between the His-tag and the Ni^{2+} by increasing concentrations of imidazole.

3.4.1.2 Adenovirus knob purification – His-Trap chromatography

The cleared supernatant was filtered through a 0.45 µm nitrocellulose membrane (Millipore) and applied to a Ni-charged 1 ml His-Trap HP column (Amersham Biosciences) for affinity purification at a flow rate of 1 ml/min using an ÄKTA™ system (GE Healthcare) at 4 °C. After washing with 20 column volumes of His-Trap wash buffer the protein was eluted using a 60 ml three step gradient at 20%, 50% and 100% HisTrap elution buffer (e.g 100 mM imidazole, 250 mM imidazole and 500 mM imidazole) collecting 2 ml fractions.

3.4.1.3 General - size exclusion chromatography

Gel filtration is a useful technique for handling biomolecules that are sensitive to changes in pH, concentration of metal ions or co-factors and harsh environmental conditions. Separations can be performed in the presence of essential ions or cofactors, detergents, urea, guanidinium hydrochloride, at high or low ionic strength, at 37 °C or in the cold room according to the requirements of the experiment. Gel filtration separates molecules according to differences in Stokes radius as they pass through the gel filtration medium. Large molecules elute from the column first, followed by smaller molecules.

3.4.1.4 Adenovirus knob purification – size exclusion chromatography

The cleaved protein was spun down, filtered through a 0.45 µm nitrocellulose membrane (Millipore), and concentrated to 50% and diluted in gel filtration buffer to reduce the imidazole content. Finally, the protein was concentrated to an approximate concentration of 2 mg/ml using a 10 ml Amicon Ultra concentrator with a 10 kDa molecular weight (Mw) cutoff (Millipore) at 4 °C. The protein was then loaded onto a Hi-load 16/60 Superdex 200 (GE Healthcare) at a flow rate of 1 ml/min at 4 °C using gel filtration buffer. 1.5 ml fractions were collected, and fractions in the peak corresponding to 70 kDa were pooled.

3.4.1.5 Adenovirus knob purification –second His-Trap chromatography

To obtain a homogenous protein sample, uncleaved and cleaved proteins were separated with a second His-Trap affinity chromatography run. The column was equilibrated in gel filtration buffer, and the sample was loaded onto the column, all using an ÄKTA™ (GE Healthcare) system at a flow rate of 1 ml/min at 4 °C. The

recombinantly expressed Ad knob protein bound unspecifically to the Ni-NTA matrix, and was eluted using the lysis buffer containing 50 mM imidazole. The protein eluted in approximally 4 ml at a concentration ranging from 1 mg/ml to 6 mg/ml. A small sample of protein was freeze-tested before storing it at 4 °C. If the protein precipitated in the freeze-test, it was stored at 4 °C. Otherwise, it was stored at -80 °C. In both cases, the concentration was adjusted with gel filtration buffer to 2 mg/ml prior to storage.

3.4.1.6 Thrombin cleavage

Cleavage of the N-terminal His tag was performed in the elution buffer containing approximately 250 mM imidazole, in a total volume of 30-50 ml. For cleavage, 10 U of Thrombin were used for each milligram of recombinant protein.

3.4.2 CD46 purification

The following purification procedure explains the purification of CD46 SCR1-SCR2 but the very same protocol was also used for the CD46 SCR1-SCR4 purification. The protocol was adapted from the work performed by Jose Casasnovas (Casasnovas et al., 1999) and Mykol Larvie (Larvie, 2001). Detailed information about buffers used here can be found in the Materials section 2.7 of this thesis.

3.4.2.1 General - Concanavalin A Sepharose chromatography

Con A Sepharose™ is Concanavalin A coupled to Sepharose 4B with the cyanogen bromide method. Concanavalin A is a tetrameric metalloprotein isolated from *Canavalia ensiformis* that binds molecules containing α-D-mannopyranosyl or α-D-glucopyranosyl residues and similar structures. Sugar binding requires the presence of C-3, C-4 and C-5 hydroxyl groups, as present in the high mannose glycans in CD46.

3.4.2.2 CD46 purification - Con A Sepharose chromatography

CD46 SCR1-SCR2 was purified by first applying 1000 ml cell culture supernatant to the Con A Sepharose resin (GE Healthcare) at a flow rate of 1 ml/min at 4 °C. Unspecifically bound protein was removed by washing with 50 ml of Con A equilibration buffer. Bound protein was eluted using 100 ml of Con A Sepharose

elution buffer. Eluted protein was concentrated to 2 ml using a Centricon Plus -70 at 4 °C at 3500 g. The Con A elution buffer was exchanged to gel filtration buffer by concentrating the pooled fractions to 5 ml, followed by dilution to 25 ml in gel filtration buffer, repeated three times. The column was then washed using 50 ml of equilibration buffer followed by 50 ml of Con A Sepharose regeneration high pH buffer followed by 50 ml Con A Sepharose regeneration low pH buffer. The column was then stored in Con A Sepharose regeneration storage buffer, all according to the manufacturer's recommendations.

3.4.2.3 CD46 purification – size exclusion chromatography

Concentrated CD46 was applied to a Hi-load 16/60 Superdex 200 (GE Healthcare) using a 2.5 ml loop at a flow rate of 1 ml/min using the gel filtration buffer, collecting 1.5 ml fractions at 4 °C. Fractions containing the second peak, corresponding to CD46, were concentrated to 2 ml at 4 °C, and diluted in 7 ml in ion exchange buffer A in order to reduce the NaCl in the gel filtration buffer, thus enhancing binding to the ion exchange column.

3.4.2.4 General - ion exchange chromatography (IEC)

IEC separates molecules on the basis of differences in their net surface charge. The charged groups within a molecule that contribute to the surface charge possess different pK_a values depending on their structure, and chemical microenvironment. Since all molecules with ionizable groups can be titrated, their net surface charge is highly pH dependent. IEC chromatography takes advantage of the fact that the relationship between net surface charge and pH is unique for a specific protein. A protein that has no net charge at a pH equivalent to its isoelectric point (pI) will not interact with a charged medium. An IEC medium contains a matrix of particles with ionic groups that can be negative (cation exchange) or positive (anion exchange). When the entire sample has been loaded, conditions are altered in order to elute the bound proteins. Proteins are normally eluted by increasing the salt concentration of the buffer or, occasionally, by changing the pH. As ionic strength increases the bound proteins begin to elute.

3.4.2.5 CD46 purification – ion exchange chromatography (IEC)

The 5/50 MonoQ (GE Healthcare) column was equilibrated in three 10 ml steps; first 10 ml ion exchange buffer A, followed by 10 ml ion exchange buffer B and finally a second 10ml step with ion exchange buffer A, all at 4 °C. The protein was loaded onto the column at a flow rate of 0.8 ml/min. After washing with 20 ml of ion exchange buffer A (four column volumes) the protein was eluted in a linear gradient extending from 100% ion exchange buffer A to 100% ion exchange buffer B over 60 ml, collecting 0.5 ml fractions. CD46 elutes in three peaks, very close to each other, at 10-15% ion exchange buffer B. The three peaks contain different glycosylation forms of CD46 (see Results section 4.1.2.4). The first peak contains just one glycosylation form and the second and third peak contain a mixture of at least two forms. For CD46 SCR1-SCR2 only the first peak, consisting of a single glycoform, was pooled and stored at a concentration of 0.5-1.5 mg/ml at -80 °C. For CD46 SCR1-SCR4 no total separation of the glycoforms was possible (see Results section 4.1.2.3), so the purified protein is not entirely homogeneous. Here also only the first peak was collected. The CD46 proteins from the remaining peaks, which had a lower purity, were saved to be added in future purifications.

3.4.3 Formation of Adenovirus:CD46 SCR1-SCR2 complex

CD46 SCR1-SCR2 was incubated at a 1.2 fold molar excess, assuming a 1:1 binding (one Ad protomer binding one CD46 molecule), with Ad knob protein (e.g. Ad11, Ad35, and Ad21) in gel filtration buffer at 4 °C over night. The protein complex was then concentrated to 500 µl using a 4 ml Amicon Ultra concentrator (Millipore), filtered, and loaded on to a Superdex 200 10/30 column (GE Healthcare) using a 500 µl loop, at a flow rate of 0.5 ml/min at 4 °C. This procedure separated saturated Ad:CD46 SCR1-SCR2 complex from excess CD46 SCR1-SCR2. The uncomplexed CD46 SCR1-SCR2 was collected and saved for later preparations.

3.4.4 Deglycosylation of CD46

CD46 SCR1-SCR4 was declycosylated using EndoH (New England Biolabs) at 20 °C, rotating, over night in the supplied buffer. 20 U of EndoH were used for each µg of CD46. The proteins were then separated using gel filtration after setting up complex.

3.4.5 Determination of protein concentration

The protein concentration was measured using 5 µl of protein in 1 ml of BioRad protein Assay (Bradford, Bio-Rad) diluted 1:5. Concentrations were determined after measuring the absorbance at a wavelength of 595 nm. Before crystallization the protein concentrations was measured using A260 at a 1:100 and 1:50 dilution in gel filtration buffer to minimize pipetting errors. The concentrations were calculated using Eq. 1.

3.5 Affinity measurements

3.5.1 Isothermal Titration Calorimetry (ITC)

3.5.1.1 General - ITC

Isothermal Titration Calorimetry (ITC) is a thermodynamic technique for monitoring interactions between two molecules, A and B. In ITC, a syringe containing protein B is titrated into a cell containing a solution of protein A. When protein B is injected into the cell, the two proteins interact, and heat is released or absorbed in direct proportion to the amount of binding. As protein A becomes saturated with protein B, the heat signal diminishes, until only background heat of dilution is observed (buffer effect). The measurement of heat generated or absorbed allows a fairly accurate determination of binding constants (K_D), reaction stoichiometry (n), enthalpy (ΔH) and entropy (ΔS), thereby providing a complete thermodynamic profile of the molecular interaction (Pierce et al., 1999).

3.5.1.2 Experimental setup - ITC

For the ITC measurements, we used a MicroCal™ VP_ITC Microcalorimeter, with a reaction cell of a total volume of 1.4295 ml (ITC equipment located at Max Planck Institute for Developmental Biology, Tübingen). The reference cell was filled with filtered MQ-H_2O supplemented with 0.02% NaN_3. During the experiments, a reference power of 10 µcal/sec was used on both cells, at a temperature of 26 °C. The measurements were performed in gel filtration buffer (see Materials section 2.7) using a concentration of 2 µM protein (setup 1: Adenovirus knob, setup 2: CD46 SCR1-SCR2) in the reaction cell. Each dataset comprised over 30 equivalent injections, each 300 sec apart. At each data point, 4 µl of 25 µM protein solution were injected, over a total time of 8 sec. As a negative control the knob affinity for JAM-A (Junctional Adhesion Molecule A), which does not bind Ad knobs, was measured. All buffers and proteins were filtered through a 0.45 µM (Millipore) filter prior to each experiment. The experiments were set up assuming a 1:1 binding model and an nM affinity (assuming an affinity that is comparable to the Ad knob binding to CAR, 15 nM) (Kirby et al., 1999, 2000). To verify obtained affinities, the experiments were repeated twice and, for Ad11 and Ad7, repeated with the knob injected into CD46 with CD46/JAM-A in the reaction cell. Data were collected for Ad7, Ad11, and Ad11 mutant knobs (R279Q, R279S, R280G, I282L, N283S and D284S). The recorded data were analyzed using the Origin 7.0 software with the MicroCal™ ITC add-on.

3.5.2 Surface Plasmon Resonance (SPR)

3.5.2.1 General - SPR

The SPR technology is based on detecting a change of mass in an aqueous layer close to the sensor chip by monitoring the angular change of reflected polarized light (called refractive index). The centerpiece of the technology is a gold coated glass surface on which the interactions between two proteins are analyzed. The sensorchip contains the gold-coated surface and a matrix providing a stable hydrophobic surface onto which molecules can be coupled using, for example, amine coupling. In the flow cells, the protein A (analyte) flows

over an immobilized protein B (ligand). Binding alters the refractive index, which results in an angular change of reflected light on the surface, allowing calculations of kinetics and affinity (Torreri et al., 2005).

3.5.2.2 Experimental setup - SPR

All interaction assays between different trimeric Ad knob proteins and CD46 regions spanning domains SCR1-SCR2 and SCR1-SCR4 were performed at 25 °C using a BiaCore 2000 system. Knobs interacting with a relatively lower affinity (< µM affinity for CD46) had to be coupled by amine coupling to a CM5 chip since CD46 binds unspecifically to the Ni-NTA chip at µM concentrations. HBS-EP was used as running buffer (see Materials section 2.5.1) in CM5 based assays while in NTA based assays HBS-P containing 50 µM EDTA (Sigma) was used. All proteins were filtered through 0.2 µM filters (Millipore) before use. Kinetic analysis using a 50 µl/min flow rate was performed using Ad11-His as non-covalently immobilized ligand on a nickel coated NTA chip. Datasets were measured separately for CD46 SCR1-SCR2 and CD46 SCR1-SCR4 as soluble analytes. Where kinetic analysis was not possible due to very fast interaction rates leading to a "square-wave" profile a steady-state analysis approach was chosen. Steady-state affinity analysis at a 10 µl/min flow rate was performed by covalently immobilizing either knob on a CM5 chip via amine-coupling chemistry (Jason-Moller et al., 2006) and using either CD46 SCR1-SCR2 or CD46 SCR1-SCR4 as soluble analytes. In the performed assays, no surface regeneration was necessary since all interactions showed very rapid to moderate dissociation rates. However, the NTA chip was stripped of nickel/ligand complex after each interaction cycle using HBS-P stripping buffer (see Materials section 2.5.1), followed by new nickel coating of the NTA chip and ligand immobilization at the beginning of a new cycle. This was done to ensure a constant ligand level in each cycle of a single assay. Raw data were processed and analyzed with BIAevaluation software 4.1. Kinetic data was fitted using a '1:1 binding with mass transfer' model and steady-state affinity data with a model optimized for steady-state affinity (Jason-Moller et al., 2006; Torreri et al., 2005).

3.6 Functional studies of binding and infectivity

Functional studies were performed by Dr. Marko Marttila, in collaboration with the group of Dr. Niklas Arnberg at the Department of Virology at Umeå University. The obtained data were analyzed jointly.

3.6.1 Propagation of ^{35}S-labeled Adenoviruses

Adenoviruses can easily be amplified in cell culture infecting several types of cells (Defer et al., 1990). By amplifying virions under controlled conditions radioactive amino acids can be incorporated into the viral proteins. Addition of ^{35}S-methionine during the translation of viral proteins will result in slightly radioactive viral capsids. Radioactively labeled virions allow quantifying binding through radioactivity. ^{35}S-labeled virions (Ad11 and Ad7) were produced as previously described (Johansson et al., 2007). The identity of the virons was determined by digesting viral DNA with restriction enzymes and compared to established patterns for prototype strains (Adrian et al., 1986). Aliquoted virions were then stored at □80 °C.

3.6.2 Binding experiments

Binding experiments to test whether CD46 SCR1-SCR2 is sufficient for Ad11 binding were performed as follows. ^{35}S-labeled Ad11 virions were incubated with increasing concentrations of soluble CD46 SCR1-SCR2 or SCR1-SCR4. After incubation with constant agitation, the mixtures were added to A549 cells in a 96 well plate, washed, and the cell-associated radioactivity was measured (Segerman et al., 2003b).

For testing whether soluble Ad11, Ad7 or Ad14 knobs can block binding of ^{35}S-labeled Ad11 or Ad7 particles, the same experimental setup was used, with one exception; the soluble knobs were incubated with the cells.

3.6.3 Fluorescent Focus Assay (FFA)

In order to investigate whether the observed binding of Ad11 to A549 cells also resulted in a productive infection after blocking with soluble CD46, an FFA assay

was performed in collaboration (Marttila et al., 2005). Briefly, Ad11 virions were pre-incubated with increasing concentrations of soluble CD46 SCR1-SCR2 or SCR1-SCR4 fragments. After one hour of incubation, the mixtures were transferred to 24 well plates containing semi-confluent A549 cells; after one hour non-bound virus was removed by washing (3x in PBS). The cells were then incubated for 44 hours at 37 °C, fixed, and stained with anti-Ad11 rabbit serum. Incubation with a FITC-labeled swine anti IgG rabbit serum (Dakopatts, Glostrup, Denmark) allowed detection of newly synthesized viral proteins (Segerman et al., 2003a).

3.7 X-ray crystallography

3.7.1 Crystallization of proteins

For crystallization of recombinantly expressed proteins, both the hanging drop and the sitting drop method were used (Figure 11). For sitting drop crystallization, a Tecan liquid handling system was employed. The advantage of such a system is the low consumption of protein (300 nl protein+300 nl buffer solution / drop) in comparison with the hanging drop setup, which uses 2 µl to 10 µl drops in a 1:1 ratio of protein:buffer. A further advantage is the ability to reproduce crystallization conditions with high accuracy. Using both setups, the vapor diffusion continues until equilibrium has been reached in 2-4 days for salt solutions and in up to 25 days for PEG solutions. However, crystals are often obtained long after the theoretical equilibrium is reached (Bergfors, 1999). For very volatile crystallization precipitants, the hanging drop method is preferred due to the lower surface tension of the reservoir: protein mixture. Through vapor diffusion, the protein reaches supersaturation where specific aggregates are formed, which later form crystals (Figure 12A) (Messerschmidt, 2007). As the protein crystallizes, the concentration of free protein in solution decreases and the solution enters the metastable region, in which crystal growth is favored (Figure 12B). The rate of vapor diffusion can be controlled by changing the temperature or by addition of a thin oil layer onto the reservoir solution. For initial crystallization conditions Crystal Screens 1 and 2 (Hamton Research) and Wizard Screens 1 and 2 (Emerald Biosciences) were used (Cudney et al., 1994; Jancarik and Kim, 1991). These screens are sparse matrix screens designed to sample a large number of

conditions. They are biased towards previously successful crystallization conditions for macromolecules published in the Protein Data Bank (PDB). The plastic material used for crystallization was obtained from Hampton Research (24 well plates) and Art Robbins Instruments (96 well plates).

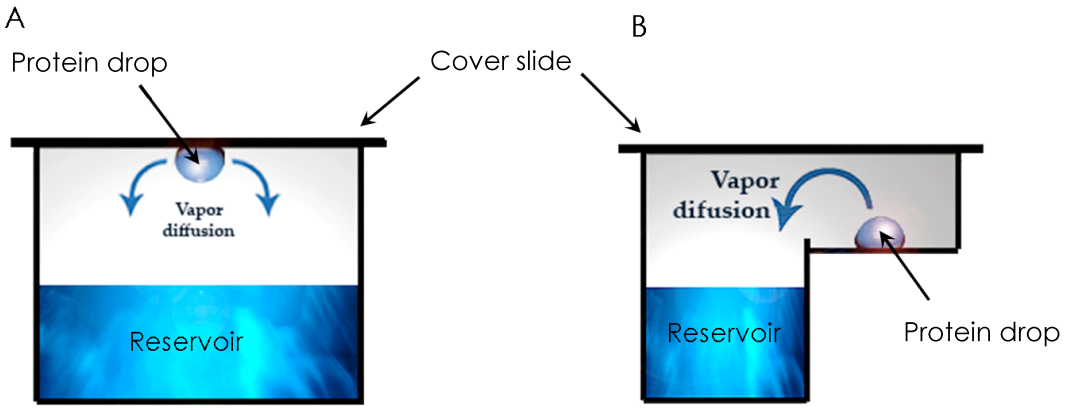

Figure 11. Schematic drawing of A) hanging drop and B) sitting drop crystallization setups. In both cases, the protein solution is mixed with reservoir solution containing precipitant and buffer. Water will diffuse from the protein drop by vapor diffusion to equilibrate with the reservoir solution, which contains a higher concentration of precipitant.

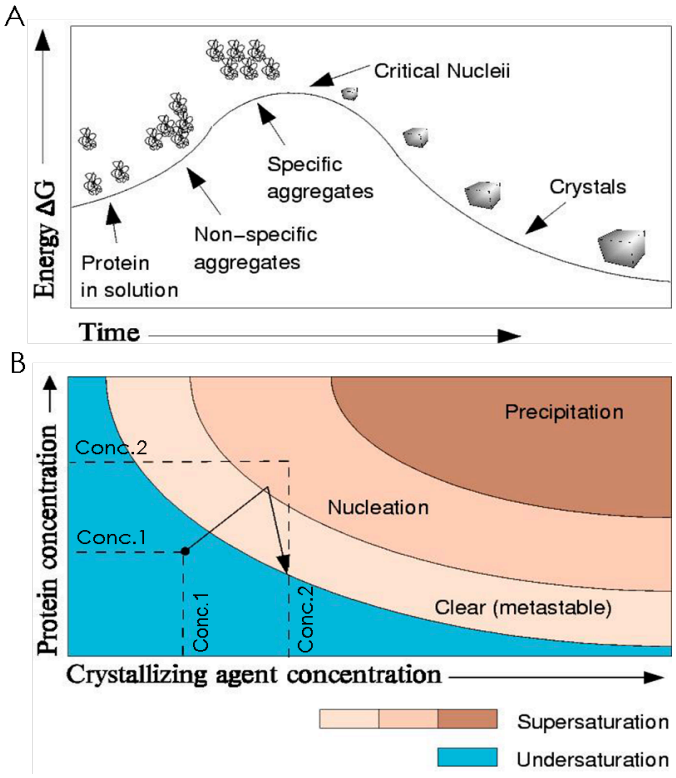

Figure 12. Energy and phase diagram for crystallization. (A) Energy diagram for crystallization. As vapor diffusion occurs, the increase in protein concentration forces the protein to form nonspecific aggregates that, if organized into specific aggregates, overcome the energy barrier and start to form crystals. (B) Phase diagram showing phases for crystal nucleation, growth and precipitation. As the protein and precipitant conc-entration increases and the energy barrier is passed, the protein reaches the nucleation point, where the protein is ordered in small crystals. At this point, the protein concentration in solution decreases and the drop enters the metastable phase, where crystal growth occurs. This continues until the setup is fully equilibrated (McCoy, 2005).

3.7.2 Crystals - the composition of the unit cell

A crystal is defined by the presence of repeating units of the "unit cell" in three dimensions. The crystal lattice falls into one of 14 Bravais lattices (McPherson, 2003). Crystals can belong to 230 space groups, which are mathematical descriptions of the symmetry of the crystal packing (McPherson, 2003). However many spacegroups can be eliminated since they do not appear for protein crystals due to symmetries such as mirror planes that are absent in proteins. The smallest possible element of the unit cell, based on mathematical symmetry operators, is called the asymmetric unit (ASU).

3.7.3 Crystal freezing

Crystals are usually frozen prior to data collection in liquid nitrogen, at -180 °C, or by moving them into the nitrogen cold stream at the x-ray system. This minimizes radiation damage but requires addition of a cryogenic solution to avoid ice formation, which can severely damage the protein crystal. In order to prevent ice formation one usually adds a cryogenic liquid (glycerol, glucose, 2-methyl-2,4-pentanediol, PEG) in sufficient concentrations to the reservoir solution. The crystals are then transferred in three steps, slowly increasing the concentration of the cryoprotectant. In each step the concentration increases with 5-10% (w/v), depending on the starting content of cryogenic solution. For the crystal transfer a depression well (Hampton Research) is used. Finally the crystal is fished up using a fine fiber loop connected to a magnetic base (Hampton research) (Figure 13) (Messerschmidt, 2007) *(Carter, 1997)*. When a crystal is exposed to X-rays, the majority of photons hitting the protein are absorbed by the crystal. A very low percentage of these generate the diffraction pattern, whereas the rest interacts with the solvent, generating the background noise, or losing energy in scattering events that form radicals (Garman and Owen, 2006). These radicals interact with the protein, breaking bonds, thus creating "radiation damage" in the protein (O'Neill et al., 2002). The first bonds to be broken are disulfide bridges followed by carbon-nitrogen bonds. The radiation damage caused in crystals is directly proportional to the energy of the incoming x-ray beam (Sliz et al., 2003).

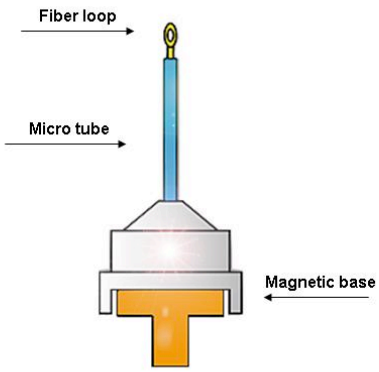

Figure 13. Schematic drawing of a loop used for crystal measurements. The crystals were fished into the fiber loop after incubation in a reservoir solution supplemented with cryoprotectants. The crystals were frozen in liquid nitrogen and measured at -180 °C.

3.7.4 X-rays

X-rays, or Röntgen rays, are a form of electromagnetic radiation with wavelengths ranging from 0.1 to 100 Å. They were discovered in 1895 by Wilhelm Conrad Röntgen and named after him (Stanton, 1895). X-rays used in X-ray crystallography are usually generated with a rotating copper anode or with synchrotron radiation sources. The rotating copper anode generates X-rays by focusing electrons onto a copper cylinder in a vacuum, resulting in K_α transitions of excited electrons in copper atoms. The K_α transition has a wavelength of 1.54178 Å (Blow, 2002). The focusing of electrons onto the anode generates heat, and the anode has to be rotated and cooled to distribute the heat over a larger surface. The second form of X-ray radiation is generated when charged particles are accelerated and injected into a curved storage ring. When particles, electrons or positrons, travels at high speed in such rings, they emit radiation in form of X-rays. The emitted X-rays cover a wavelength range of 0.1-4 Å, but radiation with a 1 Å wavelength is usually used.

3.7.5 Diffraction of X-rays at a lattice

The layers of a crystal act like reflecting mirrors for the X-rays. Only if the path difference of the reflected X-rays is a multiple of 2π does constructive interference occur. This is described by Bragg's Law (Eq. 2). If two reflected beams with a wavelength of λ travel the same distance from a common lattice point, they are exactly in phase. This appears if the lattice plane (A) acts as a mirror, or if the distance between the two planes are equal to the wavelength, but as that is normally not the case a portion of the X-rays will be reflected at this

point. Some will travel to the next lattice plane (B), at the distance d (Figure 14). After diffraction at plane B the reflected X-rays will travel a larger distance for reaching the target, the detector, in a different phase (the extra path equals 2d sin θ). The diffracted X-rays from point A and B will thus cancel each other out, partially or completely, or add up to each other (interference), depending on the distance. As the same reflection pattern occurs in each unit cell the signal is amplified in the crystal.

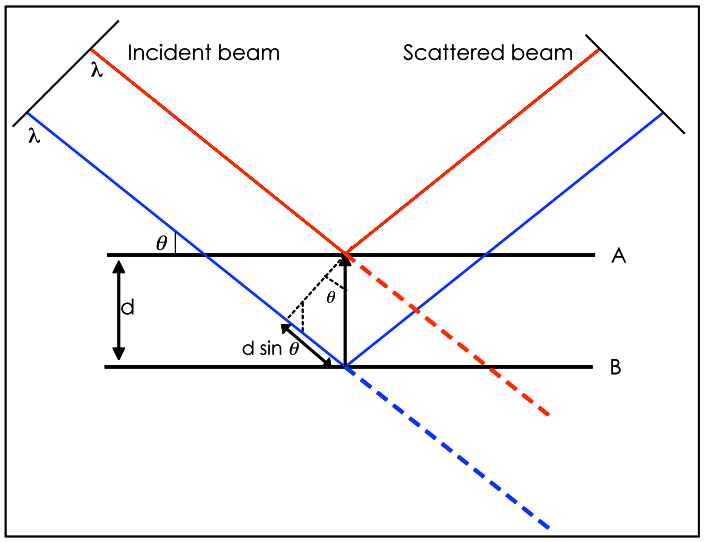

Figure 14. Bragg´s Law. X-rays scattered at a pair of parallel planes. The extra path for X-rays scattered at the second plane is 2d sin θ.

$$2d \sin\theta = n\lambda$$ Equation 2

Where:
d= the spacing between two planes
θ= angle between incoming beam and plane
λ= wavelength of incoming beam
n=any integer number

3.7.6 Data collection

X-ray data were usually first collected at our home source system, a Rigaku MicroMax™-007 HF microfocus X-ray generator (Rigaku) equipped with a MAR345 detector (MAR research). As a second step, measurements at the Swiss Light Source (SLS, Villigen, Switzerland, Beamline X06SA) or at the European

Synchrotron Radiation Facility (ESRF, Grenoble, France, Beamline ID23-1) were performed. At the synchrotron facilities, Charge Coupled Device (CCD) detectors (MARccd-225 detector at SLS, ADSC Q315 detector at ESRF) and recently the Pilatus pixel based detector (Pilatus 6M at SLS) (Bech et al., 2008; Schleputz et al., 2005) were used for data collection. Final data sets were always collected at a wavelength of 1 Å at 100 K using synchrotron radiation facilities. A complete summary of data collection statistics and refinement statistics can be found in Appendix 7.3.

3.7.7 Data processing

3.7.7.1 Indexing and integration

For data indexing and integration two programs were used. Initially the HKL software package (Otwinowski, 1997) was used for processing data collected at our home source, SLS, or at the ESRF. Due to incompatibility problems between HKL and the Pilatus pixel detector, the XDS package (Kabsch, 1993) was used to process these data. During the indexing procedure, the dimensions of the unit cell are determined. During integration, all spots are given an intensity value and an h, k, l value (i.e. reciprocal space "coordinates"). DENZO, the integration software in the HKL package, allows the user to follow the integration visually over the entire data range. This routine subtracts background from a box around the integrated spot. The user has the ability to determine the spot shape, but the same shape is used over the entire defined group. After refining all parameters for one frame, the entire dataset can be run automatically in batch mode, writing out files that contain an hkl value and intensity for each reflection for each image.

The program XDS works similarly, with two minor exceptions; XDS writes out one file, INTEGRATE.HKL, containing all reflections over the entire data range, and the background is determined from the overall background over a range of images (defined as coherent pixels higher then the background). XDS also reads refined settings saved in files from previous subroutines, allowing the user to rerun just the integration step, which can be an advantage since it saves computer time.

3.7.7.2 Scaling

The primary functions of scaling are to 1) scale together data recorded on several images (called partials), 2) scale up each image to the same level, and 3) to reduce the data, merging symmetry related reflections. The difference in symmetry related equal reflections are used for calculating R_{sym} (sometimes called R_{merge}), which is a measure of data quality (Eq. 3). In the set of reflections let N stand for at least two symmetry partners that have been measured. R_{sym} is the mean deviation of intensity of these N reflections:

$$Rsym = \frac{\sum_h \left\lfloor \hat{I}_h - I_{h,i} \right\rfloor}{\sum_h \sum_i^{n_h} I_{h,i}} \times 100\% \quad \text{and:} \quad I_h = \frac{1}{n_h} \sum_i^{n_h} I_{h,i} \quad \text{Equation 3}$$

Where:
$\hat{I}$= mean intensity of all the measurements
h= reflection
i= the symmetry related reflection to h
I= Intensity
n_h= multiplicity

The R_{sym} can be considered as the mean error of a measured intensity, compared to the mean intensity, averaged over a chosen group of reflections (Blow, 2002).

An R_{sym} can only be calculated if, (i) a given reflection has been collected at least twice, or (ii) if two symmetry related reflections have been collected. As more reflections are collected several times, the redundancy of the dataset increases, and the R_{sym} becomes more reliable. R_{sym} is somewhat flawed because it depends on the redundancy of the data. R_{sym} is written our by both the XDS and HKL package.

The introduction of R_{meas} has solved the problem of redundancy dependence; however the problem that more redundant reflections affect the overall R_{meas} is not considered (Eq. 4). The multiplicity of the reflections might be distributed differently in various datasets. Therefore the R_{meas-I} was introduced.

The $R_{meas\text{-}I}$ is equal for high and low redundancy datasets at different resolutions (Eq. 5) (Diederichs and Karplus, 1997).

$$Rmeas = \frac{\sum_h \sqrt{\frac{n_h}{n_h - 1}} \sum_i^{n_h} \left| \hat{I}_h - I_{h,i} \right|}{\sum_h \sum_i^{n_h} I_{h,i}} \times 100\% \quad \text{and:} \quad I_h = \frac{1}{n_h} \sum_I^{n_h} I_{h,i} \qquad \text{Equation 4}$$

$$Rmeas - I = \frac{\sum \left| I_{h,p} - I_{h,Q} \right|}{0.5 \times \sum I_{h,p} + I_{h,Q}} \times 100\% \qquad \text{Equation 5}$$

Where: $I_{h,p} = \frac{1}{n_{h,p}} \sum_{I_{\varepsilon,p}}^{n_{h,p}} I_{h,i}$ and: $I_{h,Q} = \frac{1}{n_{h,Q}} \sum_{IQ}^{n_{h,Q}} I_{h,i}$

Where:
P= dataset one
Q= dataset two
$I_{h,p}$= partially averaged estimates of true intensity for reflection h in dataset P
$I_{h,Q}$= partially averaged estimates of true intensity for reflection h in dataset Q

The R-factors, independent of which of the three calculations are used, should increase with higher resolution as the recorded reflections are less intense and thus have higher measured errors. An R-factor higher then 0.6 is essentially random. R_{meas} and $R_{meas\text{-}I}$ are only calculated in scaling using XDS.

3.7.7.3 I/σ

As the intensities (I) of the integrated reflections are listed for each resolution bin, a calculated statistical error for each intensity and each bin is also given. From this, the I/□ is calculated, displaying how much the integrated reflections at a certain resolution stand out above background. An I/□ of less than one indicates an error higher than the measured intensity; thus, no information can be extracted concerning the structure of the protein. These data normally also have high values of R_{sym}. To use such data would merely introduce error into the final 3D-model, therefore a reasonable I/□ cutoff between 1.5 and 2.0 is applied to the data.

3.7.7.4 Wilson plot

A Wilson plot is a plot of reflection intensities against the resolution (Wilson, 1949). For data collected from protein crystals, a characteristic maximum can be observed at 6 Å generated from the many 6 Å spacings between atoms in α-helices or β-sheets. From this point, a linear decrease can be seen beyond 3 Å. From this linear part of the Wilson plot, the overall temperature factor (B-factor) of the crystallized protein can be estimated as the negative slope of the linear gradient. This has implications for later refinement strategies as the B-factors determined during refinement should match the value from the Wilson plot.

3.7.8 Structure determination and truncation of data

When exposing a protein crystal to X-rays of a given wavelength, amplitude and phase, the photons on the path to the detector are absorbed and diffracted by hitting electrons in the protein crystal. To reconstitute the structure of the protein, a Fourier transformation (Blow, 2002) of the collected data is performed. Unfortunately, the phase information is lost during the experiment since the detector can only measure the amount of photons hitting it, i.e. intensities. Initially the intensities (I) are converted to structure factors amplitudes (F) (French and Wilson, 1978) using XSCALE (Kabsch, 1993) or TRUNCATE (CCP4, 1994). The structure factor equation represents the sampling of the reciprocal space lattice at points, hkl (Eq. 6):

$$\overline{F}(hkl) = \sum_{j=1}^{N} f_j \exp 2\pi i(hx_j + ky_j + lz_j) \qquad \text{Equation 6}$$

Where:
$\overline{F}$ = structure factor
hkl= indices of a reflection
f_j = diffraction contribution from atom j in position xyz.
N= all atoms in the lattice

This can be rewritten as (Eq. 7):

$$\overline{F}(hkl) = |F(hkl)| \exp(i\alpha(hkl)) \qquad \text{Equation 7}$$

Where:
$\overline{F}(hkl)$ = structure factor
$|F(hkl)|$= structure factor amplitude
$e^{i\alpha(hkl)}$= the phase component of the structure factor

The intensity, I, of the collected reflection (hkl) is given by (Eq. 8):

$$I(hkl) = k \times F(hkl)^2 \qquad \text{Equation 8}$$

Where:
$I(hkl)$= measured intensity
k= constant
$F(hkl)$= structure factor amplitude

3.7.9 The phase problem

In order to calculate an electron density map for model building, the phase of each reflection has to be determined. This section explains the method used in this thesis, molecular replacement. We first have to introduce how the phase can be excluded from the structure factor equations (Eq. 6) by mathematical conversions (Patterson, 1934).

3.7.9.1 Patterson methods

The intensity of the diffracted X-ray beam is proportional to the square of the amplitude of the corresponding wave (see Eq. 8). The Patterson function is essentially a Fourier transformation of the intensities rather then the structure factors. Thus it can be calculated using structure factor amplitudes alone, which is phase independent (Eq. 9). This function can be used to perform molecular replacement.

$$P(u,v,w) = \frac{1}{V_{EZ}} \sum_{h=-\infty}^{\infty} \sum_{k=-\infty}^{\infty} \sum_{l=-\infty}^{\infty} |F(hkl)^2 \times \exp\left[-2\pi i(hu + kV + lW\right]| \qquad \text{Equation 9}$$

Where:
V_{EZ}= Volume of the unit cell
$F(hkl)$=*structure factor amplitude of reflection hkl*
u,v,w = position vectors in the unit cell

3.7.10 General - molecular replacement

In Molecular replacement, one uses a homology model for phasing the collected data. Central to molecular replacement is the Patterson map, which is a map of cross vectors between all atoms in the molecule. The Patterson map is calculated without any phase information according to equation 9. The Patterson map for molecule A is rotated and translated onto the Patterson map for molecule B (Figure 15). The search is performed within a user defined sphere. After the search, the solutions with the highest correlation are listed. Good solution should have high correlation coefficients and low R factors (between collected and calculated data, i.e. search model) (see Eq. 10 and 11). Each tested position can be defined by the three angles of rotation and the three translation vectors. The search model is reoriented in space to the position giving the highest correlation and lowest R-factors. The model, in its new orientation, is used for calculating phases that can be used for refinement. These calculations are easier in reciprocal space than real space.

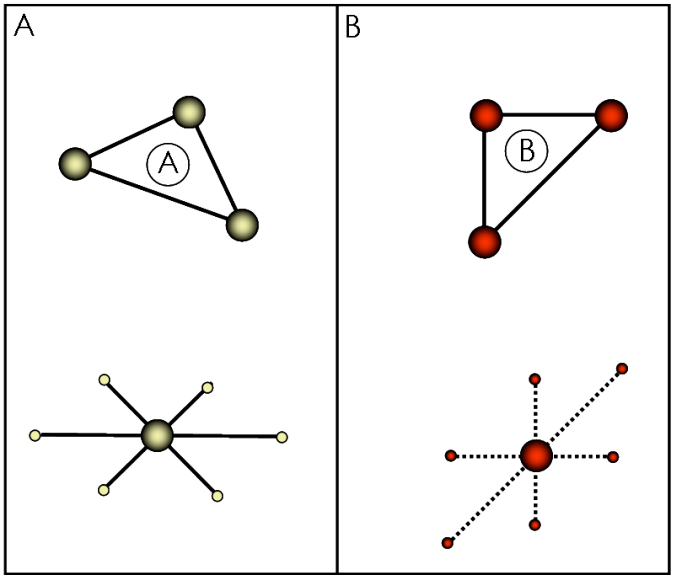

Figure 15. A simple known molecule (A) and an unknown, homologous molecule (B) and their corresponding Patterson maps.

$$Cc = \sum_{hkl} (\Delta \mid F_{obs} \mid \times \Delta \mid F_{calc} \mid) \times \sqrt{\sum_{hkl} \Delta \mid F_{obs} \mid^2 \times \sum_{hkl} \Delta \mid F_{calc} \mid^2}$$ Equation 10

With: $\Delta \mid F \mid = \mid F \mid - \mid \langle F \rangle \mid$

Where:
F_{obs}= observed structure factor amplitude (Eq. 6)
F_{calc}= calculated structure factor amplitude for the model (Eq. 6)
$|F|$= structure factor amplitude search model (Eq. 6)
$<F>$= structure factor amplitude collected data (Eq. 6)

$$R_{f\,actor} = \frac{\sum_h \left\| F_{obs} \right| - \left| F_{calc} \right\|}{\sum_h \left| F_{obs} \right|} \times 100\%$$ Equation 11

Where:
F_{obs}= measured structure factor amplitude
F_{calc}=calculated structure factor amplitude
h= reflection

3.7.10.1 Molecular replacement – rotation/translation functions

In this work, exclusively AMoRe (Navaza, 1994) and Phaser (Read, 2001) were used for molecular replacement. Phaser was always used in a completely automated way, and AMoRe was used when the rotation (ROTING subroutine) and translation (TRAING subroutine) functions had to be run independently to pick up the correct solution. Both programs compute the structure factor directly from the initial model after applying the rotation matrix and the translation vector, which moves the search model to the new position.

AMoRe includes routines to run a complete molecular replacement search by carrying out rotation and translation functions against various targets. Euler angles define the rotation part of the solution and fractional shifts, the translation part of the solution. The search is followed by an automatic rigid body refinement. The AMoRe cross-rotation function calculates a correlation coefficient between the observed and calculated Patterson functions. Good

solutions should give high correlation coefficients between observed and calculated Patterson functions well as low $R_{factors}$. The software contains routines for calculating structure factors from the model in a P1 cell (Navaza, 1994).

The maximum likelihood molecular replacement program Phaser combines the anisotropy correction, likelihood enhanced fast rotation function, likelihood enhanced fast translation function, packing and refinement modes for multiple search models and a set of possible spacegroups to automatically solve a structure by molecular replacement. The signal-to-noise ratio is judged using the Z-score. A score above three is considered a solid solution, which is computed by comparing the log likelihood gain (LLG) values from the rotation or translation search with LLG values for a set of random rotations or translations. The mean and the root mean square (RMS) deviation from the mean are computed from the random set, then the Z-score for a search peak is defined as its LLG minus the mean, all divided by the RMS deviation (McCoy et al., 2007).

3.7.11 General - structure refinement

For structure refinement the CNS (Brunger et al., 1998) and REFMAC5 (CCP4, 1994) software packages were used. During the refinement, the model is converted to structure factor amplitudes (F_{calc}) by a reverse Fourier transformation. These are compared to the measured intensities (F_{obs}) according to Equation 11. The aim during the entire refinement is to minimize the difference between F_{obs} and F_{calc} (Eq. 11) by refining xyz coordinates and B-factors. To avoid biasing the model, a random selected "test-set" of reflections is excluded (R_{Free}) , containing a minimum of 5% of the total reflections, to be used for cross-validation. The percentage of reflections used for the test set is set to contain enough reflections for a statistical relevance in the resolution bins. As one spot of the diffraction image contains information about all the atoms of the model, a good model should predict the intensities of the reflections of the test set. This is assessed by the use of free R factors, an R factor calculated between F_{obs} and F_{calc} using the free set of reflections that is not used in the refinement (Brunger, 1992). The R_{factor} should be carefully monitored during refinement, and an improvement of the working model should reduce both R-factors in a similar way. Refinement includes several approaches:

3.7.11.1 Rigid body refinement

After molecular replacement, it is sensible to perform a rigid body refinement, where the orientation of the entire molecule in relation to the unit cell axis is refined. During rotation and translation, several rigid bodies can be defined from one single molecule, e.g. two domains can be rotated independently. Even though both REFMAC5 (CCP4, 1994) and CNS (Brunger et al., 1998) allow rigid body refinement, the rotation and translation performed by CNS is much more powerful. Rigid body refinement is normally performed using data between 12 Å and 3 Å. The 3 Å resolution cutoff gives a higher radius of convergence given that the smallest details observed are 3 Å apart, like for example the strands in a β-sheet. This allows a movement of the molecule over larger distances in one cycle, e.g. higher radius of convergence.

3.7.11.2 Restrained refinement

During restrained refinement, known stereochemical parameters like planarity, bond distances and angles, torsion angles etc. are used for improving the model. The geometric parameters are weighted against the crystallographic terms by the programs with a factor. In CNS is this factor automatically set and in REFMAC5 several factors have to be tested, and the user determines which one to use based on the refinement statistics written out with each factor.

3.7.11.3 B factor refinement

During refinement one should also refine the B-factors. At 3 Å resolution, or worse, the slope in the Wilson plot is normally poorly defined and overall B-factors are refined giving all amino acids the same B-factors. With better data the B-factors can be refined in groups, where for example different domains in the model are given the same B-factors. The third type of B-factor refinement is called individual B-factor refinement. During this refinement the B-factors can be refined either, (i) isotropically, defining the B-factors as a sphere, or (ii) anisotropically. Anisotropic refinement requires a resolution of better then 1.6 Å. The B-factors are then defined as an ellipse that allows different movement in each of the 6 dimensions.

3.7.11.4 Calculation of electron density maps

The refinement is normally run over several cycles. Density maps are calculated based on the newly refined model (Eq. 12). The map routine calculates maps only at grid points, in order to save computer time during the Fourier transformation (Blow, 2002). The grid is normally set to 1/3 of the resolution.

$$\rho(xyz) = \frac{1}{V}\sum_{h=-\infty}^{\infty}\sum_{k=-\infty}^{\infty}\sum_{l=-\infty}^{\infty} F(hkl)\exp -2\pi i(hx+ky+lz) \qquad \text{Equation 12}$$

Where:
$\rho(xyz)$= the density of the unit cell at position (xyz)
V= the volume of the unit cell
$F(hkl)$= structure factor amplitude

3.7.11.5 Density modification- averaging

For some of the structures presented in this work, density modification was exploited due to the presence of non-crystallographic symmetry (NCS), i.e. symmetry that applies locally but not throughout the crystal. If the asymmetric unit contains n molecules of one type (n>1), one can make the assumption that these molecules are close to identical, and average the electron density for these molecules in order to improve the electron density map (Figure 16). For using averaging as a powerful tool, one has to be certain that the NCS is really present and that the rotation matrices and translation vectors are exact, otherwise the averaged density will be unclear. Prior to averaging, a mask has to be created surrounding the molecule to be averaged. If no initial model exists, averaging can be defined by a sphere or box around a given coordinate, i.e. a heavy atom position. In both cases an accurate transformation matrix from area A to area B has to be determined. As the electron density for molecules A and B are averaged, noise generated from measuring errors is reduced. The result will be a cleaner map, which facilitates the tracing of chains (Blow, 2002). This process can be run iteratively.

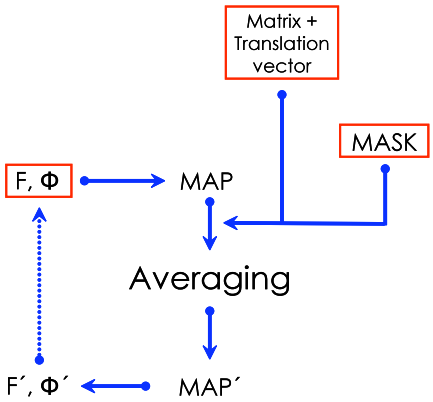

Figure 16. Schematic drawing of an averaging procedure. The red boxes indicate input to be supplied for averaging (F, θ= initial amplitude and phase; F´, θ´= improved amplitude and phase). The cycle can be repeated until convergence is reached, e.g. structure factor amplitude and phase changes become minimal in each cycle ("dotted arrow").

Averaging can be performed using the CCP4 package (MAPMASK, MAPAVE, LSQKAB) (CCP4, 1994) or the RAVE package (AVE, MAMA, MAPMAN, IMP) (Jones, 1992; Kleywegt, 2001). In this work, both packages were used.

3.7.12 The Matthews coefficient

The work performed by Matthews (Matthews, 1968) has become a useful statistical tool for crystallographers. Matthews statistically studied crystallized proteins, more specifically the solvent content in known protein structures. He showed that proteins have a Matthews parameter (V_m) ranging from 1.9-4.2 Å^3/da. Protein molecules have a rather constant density of 1.33 g/m^3 that corresponds to a volume of about 1.3 Å^3/ da. The V_m describes the density, or volume occupied by protein, within the crystal. Protein crystals do not show a constant density because of their solvent content (Eq. 13).

$$V_m = \frac{Vol}{(M * n_{asym} * n_{mol})} \qquad \text{Equation 13}$$

Where:
Vol= Unit cell volume (Å^3),
M= Molecular weight of the protein in Daltons
n_{asym}= number of asymmetric units
n_{mol}= number of molecules in the asymmetric unit.

By solving n_{mol} one is able to obtain an estimation of how many molecules are present in the unit cell in the crystal. This is useful information when one wants to determine a structure.

4 Results

4.1 Protein purification

Detailed information about all the buffers used in the protein purification can be found in the Materials section 2.7.

4.1.1 Adenovirus knobs

The purification for all recombinantly expressed Ad knobs followed the same protocol, with the total yields ranging from 1.5 mg/l (Ad11) to 50 mg/l (Ad35). All knobs could be purified to high purity. The mutant knobs precipitated upon freezing and were consequently stored at 4 °C and not -80 °C.

4.1.1.1 HisTrap affinity chromatography

The HisTrap chromatography was performed according the Methods section 3.4.1.2. The first peak, eluting at about 100 mM, contained some recombinant protein but mostly impurities and was discarded. The second peak, eluting at 250 mM imidazole, contained mainly pure protein. This peak was used for further purification (Figure 17).

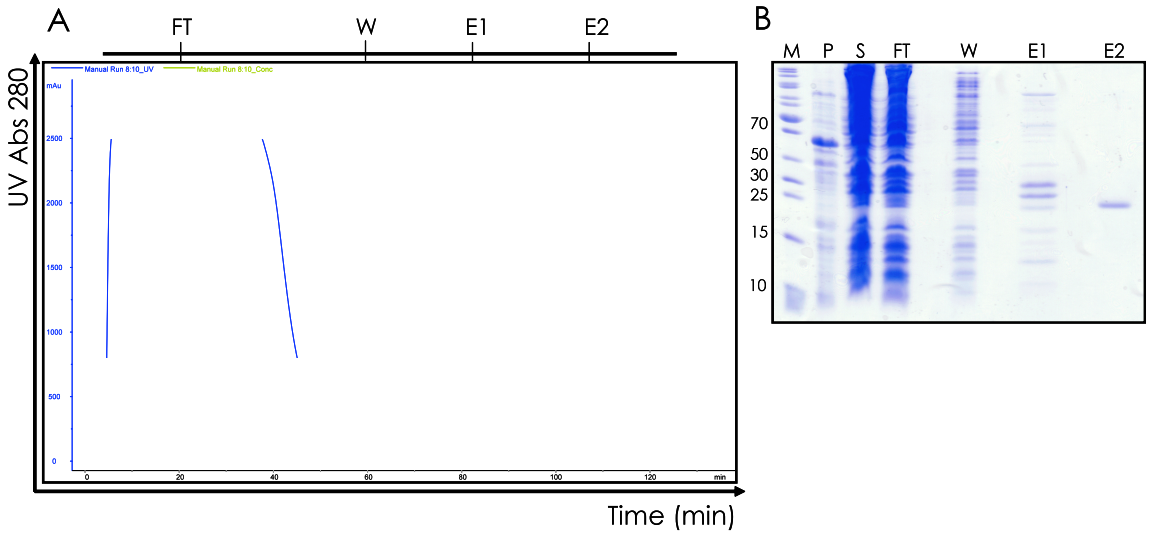

Figure 17. Affinity column chromatography of the Ad11 knob using a HisTrap column. (A)The recombinantly expressed protein elutes at a concentration of 250 mM imidazole. (B) The corresponding 12% SDS-PAGE with P= pellet, S= soluble fraction, FT= flow through, W= wash, E1= elution peak 1 and E2= elution peak 2. Molecular weight markers (kDa) are shown on the left (lane "M").

4.1.1.2 Cleavage of N-terminal hexa-histidine (His) tag

During thrombin cleavage, some protein precipitated if the total amount of protein exceeded 20 mg. Addition of 15% glycerol improved the yield significantly without affecting the cleavage efficiency (data not shown). The cleavage was performed in 50 ml tubes rotating at 20°C for 16 hrs (Figure 18). Cleaved protein was concentrated to about 50% volume, and diluted in gel filtration buffer to reduce the concentration of imidazole. Finally, the protein was concentrated to 2 mg/ml (measured using Biorad Protein Assay; Bradford) before gel filtration.

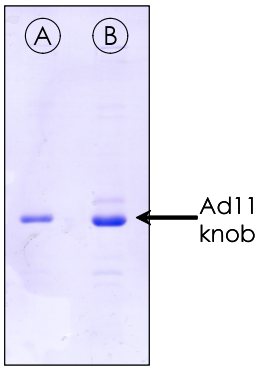

Figure 18. Thrombin cleavage of the Ad11 knob. Lane A uncleaved and and lane B, cleaved knob. Thrombin contains some impurities.

4.1.1.3 Size exclusion chromatography

The gel filtration was performed according to Methods section 3.4.1.4. The Ad knobs eluted as trimers, as expected. All knobs form dimers of trimers (Figure 19) over time, which can be separated on a Superdex 200. The dimer is not caused by disulfide bridges as a non-reducing gel gave the same result (data not shown). The dimerization can be avoided by storage at -80 °C. During gel filtration, some aggregation was also observed (Figure 19).

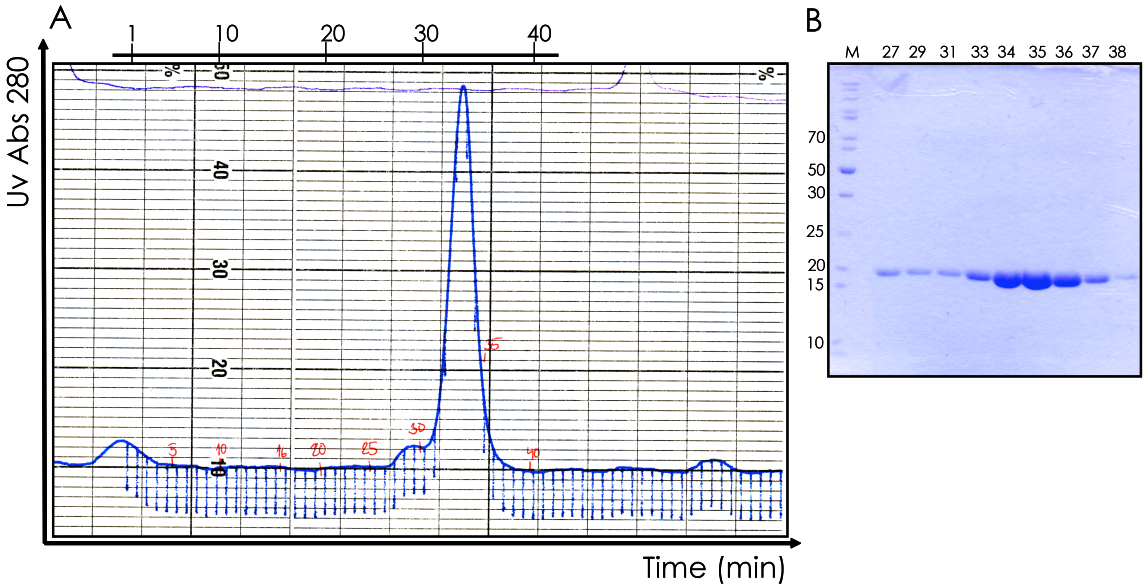

Figure 19. Gel filtration chromatography of the Ad11 knob. (A)Some aggregation is observed close to the void volume of the column (peaks at fraction 1). The protein elutes in a very symmetric peak at the corresponding size. (B) A 12% SDS-PAGE of the peak fraction. First, the dimer of trimer appears, due to its larger size. In fraction 35 the normal trimer is seen. Molecular weight markers (kDa) are shown on the left (lane "M").

4.1.1.4 Second HisTrap affinity chromatography

After gel filtration, the protein sample is pure, but not homogenous since the cleavage efficiency is never 100%. To remove remnants of His-tagged protein a second HisTrap chromatography has to be used for separating the two protein species prior to crystallization trials. The chromatography run was performed according to Methods section 3.4.1.5. All the knobs described in this thesis bound unspecifically to the column. The interaction is very weak, and untagged protein could be eluted using lysis buffer (50 mM imidazole) in one sharp peak at high concentration (Figure 20). The uncleaved protein was eluted using HisTrap elution buffer and discarded.

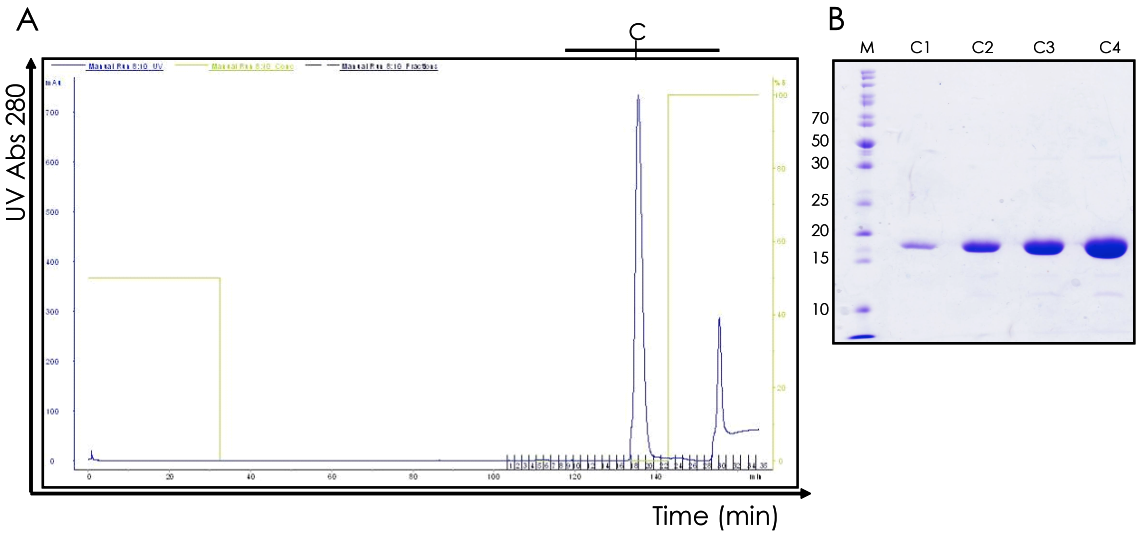

Figure 20. Second HisTrap chromatography of Ad11 knob. (A) Chromatogram. (B) The purified protein was run in increasing amounts, on a denaturing 12% SDS-PAGE. The size corresponds to a protomer (C1-C4 = increasing amounts of Ad11 knob, in each step double the amount). Molecular weight markers (kDa) are shown on the left (lane "M").

4.1.2 Purification of CD46 constructs

CD46 SCR1-SCR2 and CD46 SCR1-SCR4 proteins were expressed in CHO (Chinese Hamster Ovary) Lec 3.2.8.1 cells (Stanley, 1989). The purification for the two forms of CD46 follows the same protocol and will be presented together.

4.1.2.1 Concanavalin A Sepharose- affinity chromatography

The purification was performed using peristaltic pumps, and elution was monitored by SDS-PAGE (Figure 21). CD46 SCR1-SCR4 was analyzed using a 12% SDS-PAGE, whereas the smaller CD46 SCR1-SCR2 was analyzed by a 15% SDS-PAGE.

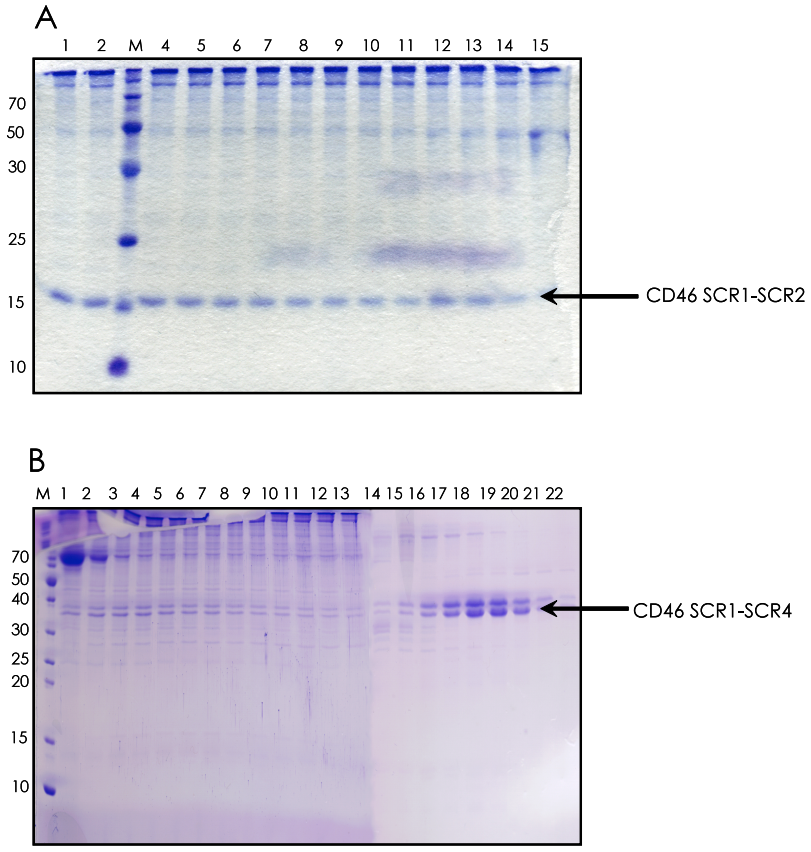

Figure 21. SDS-PAGE confirming elution of both forms of CD46 from Con A Sepharose. (A) CD46 SCR1-SCR2 was analyzed on a 15% SDS-PAGE and (B) CD46 SCR1-SCR4 on a 12% SDS-PAGE. Both proteins elute over a total volume of 100 ml. Molecular weight markers (kDa) are shown on the left (lane "M").

4.1.2.2 Size exclusion chromatography

CD46 was next applied to a gel filtration column (see Methods section 3.4.2.3). The first peak in the elution profile is most likely heavily glycosylated FCS components, since the height of the peak varied with the FCS content in the loaded cell supernatant (data not shown) (Figure 22 and Figure 23). A total separation of the FCS components and CD46 was never possible, and some CD46 had to be sacrificed for purity. The retention times of the two proteins were as expected (Figure 22A and Figure 23A). The collected fractions (in total about 10 ml) were loaded on a SDS-PAGE for analysis (Figure 22B and 23B). CD46 SCR1-SCR4 runs as two bands, which are likely two forms of glycosylation.

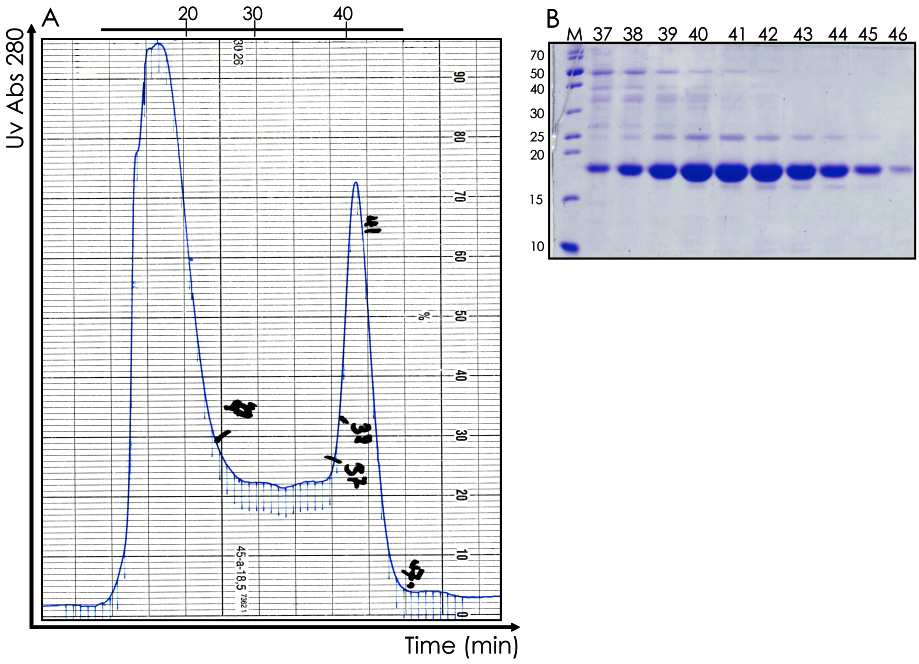

Figure 22. Size exclusion chromatography of CD46 SCR1-SCR2. (A) Gel filtration chromatogram and (B) the corresponding SDS-PAGE. Molecular weight markers (kDa) are shown on the left (lane "M").

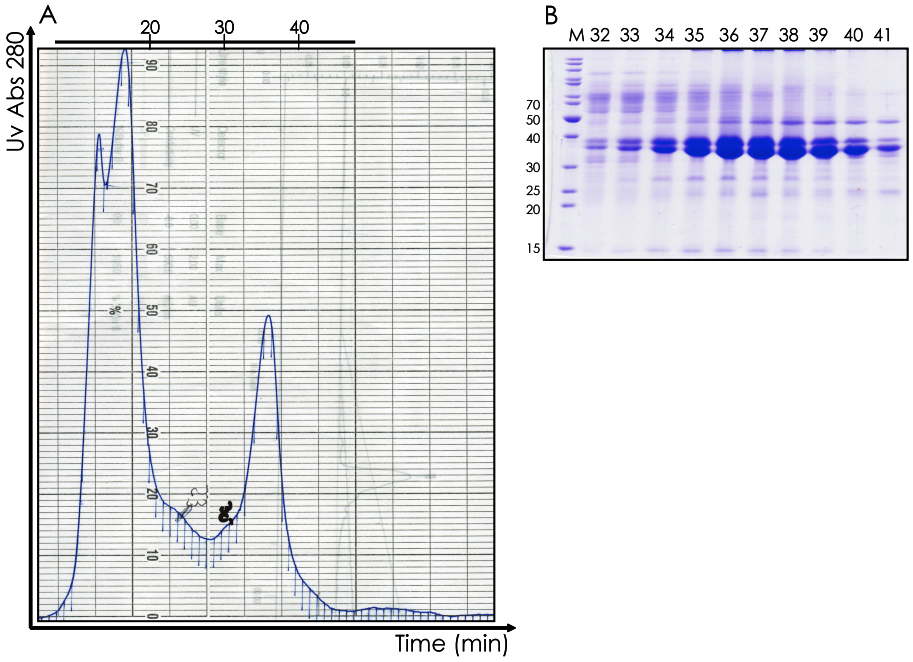

Figure 23. Size exclusion chromatography of CD46 SCR1-SC4. (A) Gel filtration chromatogram and (B) the corresponding SDS-PAGE. Molecular weight markers (kDa) are shown on the left (lane "M").

4.1.2.3 *Ion exchange chromatography*

In order to obtain highly homogeneous protein, ion exchange chromatography (IEC) was employed (IEC details in Methods section 3.4.2.5). For CD46 SCR1-SCR2, a highly pure homogeneous, protein was obtained, whereas for the longer construct pure CD46, in at least two different glycosylation forms, was obtained (Figures 24 and 25). Initially, no crystallization trials were planned using an Ad knob in complex with CD46 SCR1-SCR4, so the protein was considered to be homogeneous enough in that form. Both forms bind Ad knobs, independent of glycans (data not shown).

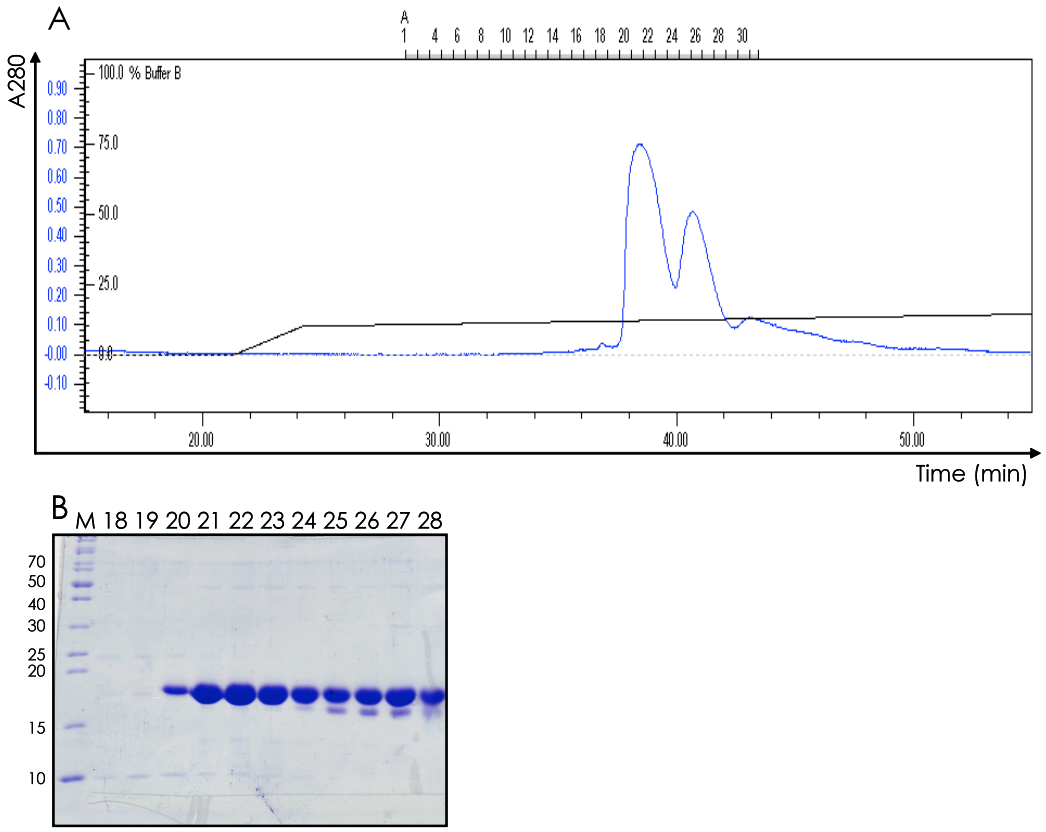

Figure 24. Analysis of IEC run of CD46 SCR1-SCR2. (A)The IEC chromatography allowed a separation of the two glycosylation forms. The first peak (fractions 20-23) contains only one glycoform. The second peak (fraction 24-28) contains both glycoforms, and was saved for later purifications. (B) 15% SDS-PAGE with the peak fractions. Molecular weight markers (kDa) are shown on the left (lane "M"). The mismatch between the fractions in the gel and in the chromatogram is due to the deadvolume between the UV-cuvette and fraction collector.

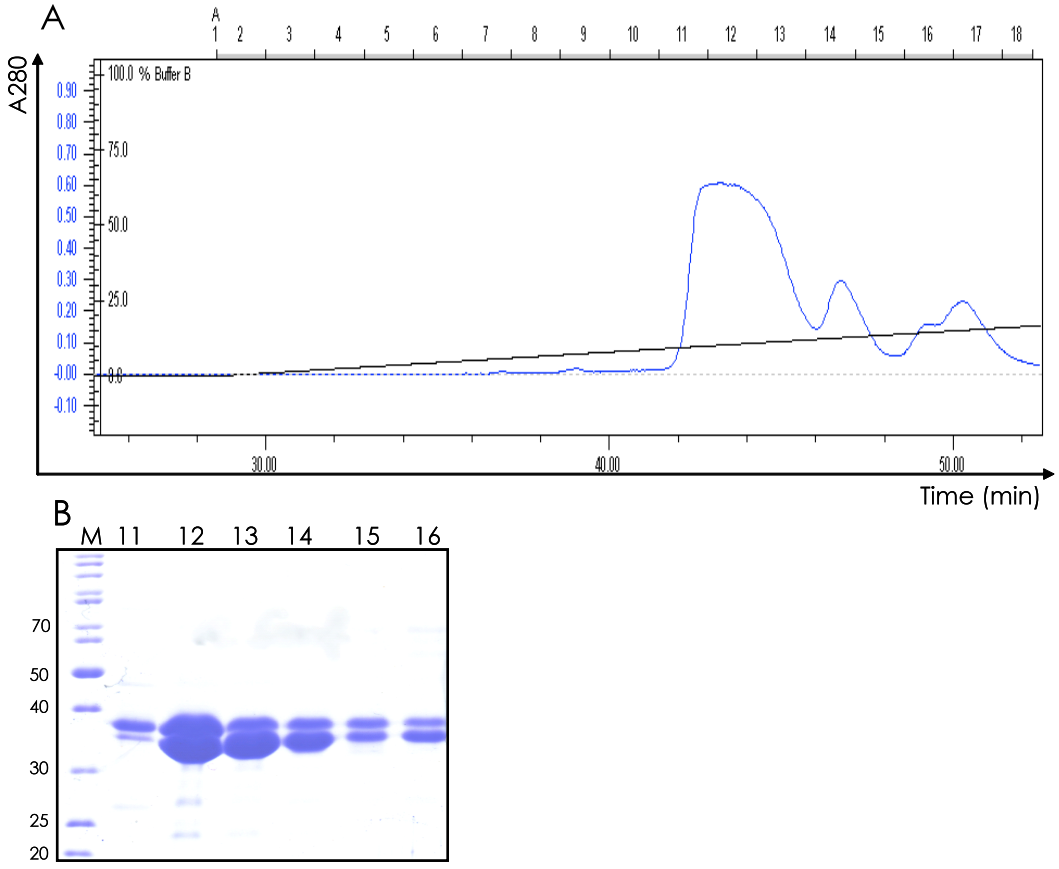

Figure 25. Analysis of IEC run of CD46 SCR1-SCR4. (A) Chromatogram of an IEC run separating several impurities from CD46. (B) 12% SDS-PAGE of CD46 SCR1-SCR4. The peaks contain several glycosylation forms. Molecular weight markers (kDa) are shown on the left (lane "M"). The mismatch between the fractions in the gel and in the chromatogram is due to the deadvolume between the UV-cuvette and fraction collector.

4.1.2.4 Deglycosylation of CD46

Deglycosylation of CD46 SCR1-SCR4, using EndoH (details in Methods section 3.4.4), results in one band. This confirms that the two bands seen in the gel are both CD46, in different states of glycosylation. A large amount of EndoH was used (Figure 26).

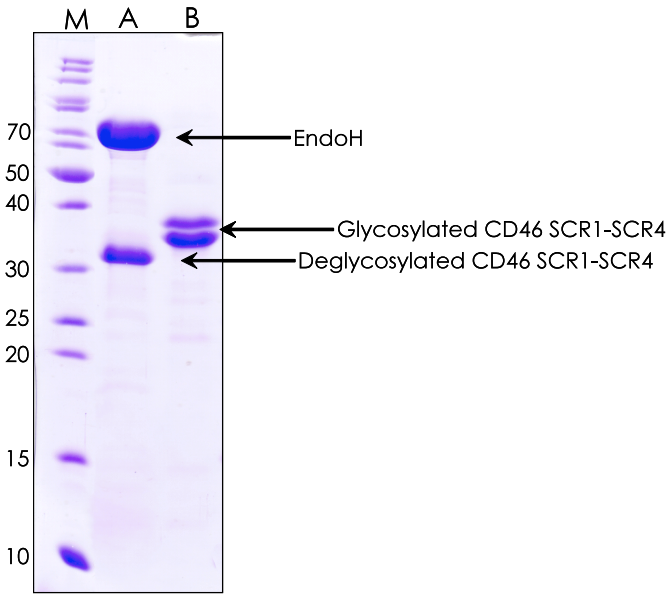

Figure 26. EndoH digestion of CD46 SCR1-SCR4. The two species of CD46 are cut and shifts to the same size supporting two glycosylation forms of the protein. Molecular weight markers (kDa) are shown on the left (lane "M").

4.1.3 Complex formation

4.1.3.1 CD46 SCR1-SCR2:Adenovirus knob

The separation of saturated complex and excess CD46 was performed using gel filtration (see Methods section 3.4.3). The complex elutes at a molecular weight corresponding to 140 kDa, whereas excess CD46 SCR1-SCR2 eluted at about 20 kDa. The excess CD46 was saved for later complex formations. The gel shows a nice separation between the complex and CD46, as expected (Figure 27) by their large size difference.

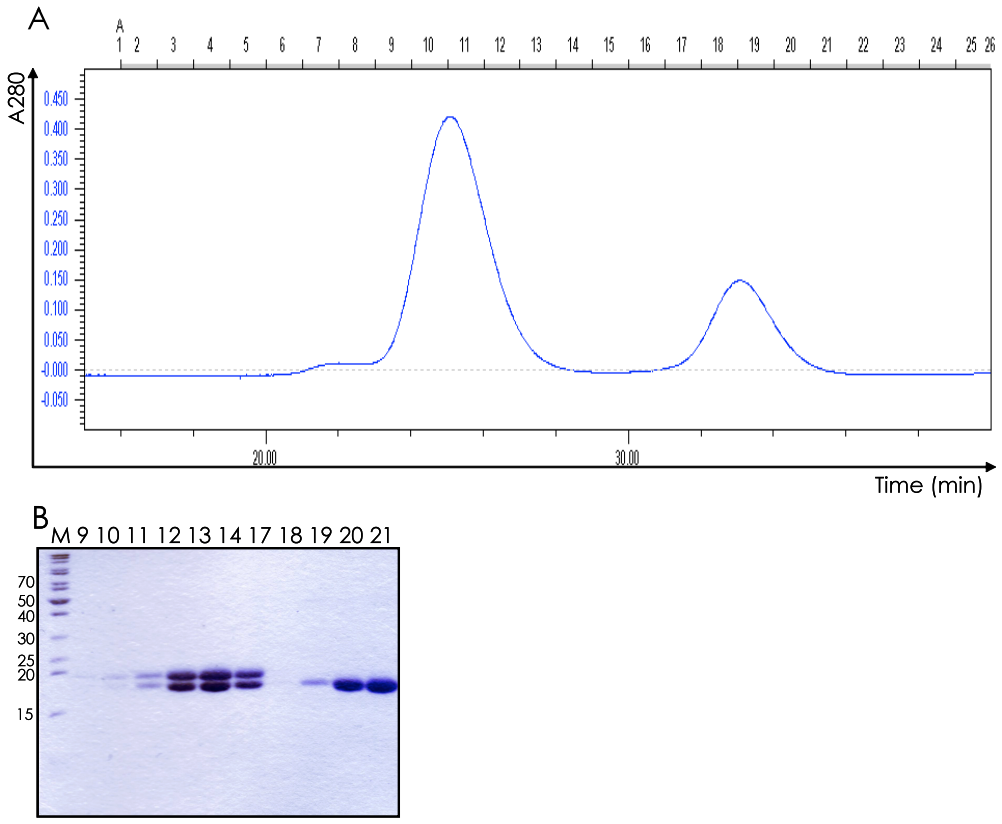

Figure 27. Gel filtration of the Ad11:CD46 SCR1-SCR2 complex. (A) The gel filtration run separated saturated complex (left peak) from the excess CD46 (right peak). (B) the 12% SDS-PAGE, from both peaks. Molecular weight markers (kDa) are shown on the left (lane "M"). The mismatch between the fractions in the gel and in the chromatogram is due to the deadvolume between the UV-cuvette and fraction collector.

4.1.3.2 CD46 SCR1-SCR4:Adenovirus knob

Isolation of the CD46 SCR1-SCR4 complex was done in a similar way to the CD46 SCR1-SCR2 complex (see Methods section 3.4.3) (Figure 28).

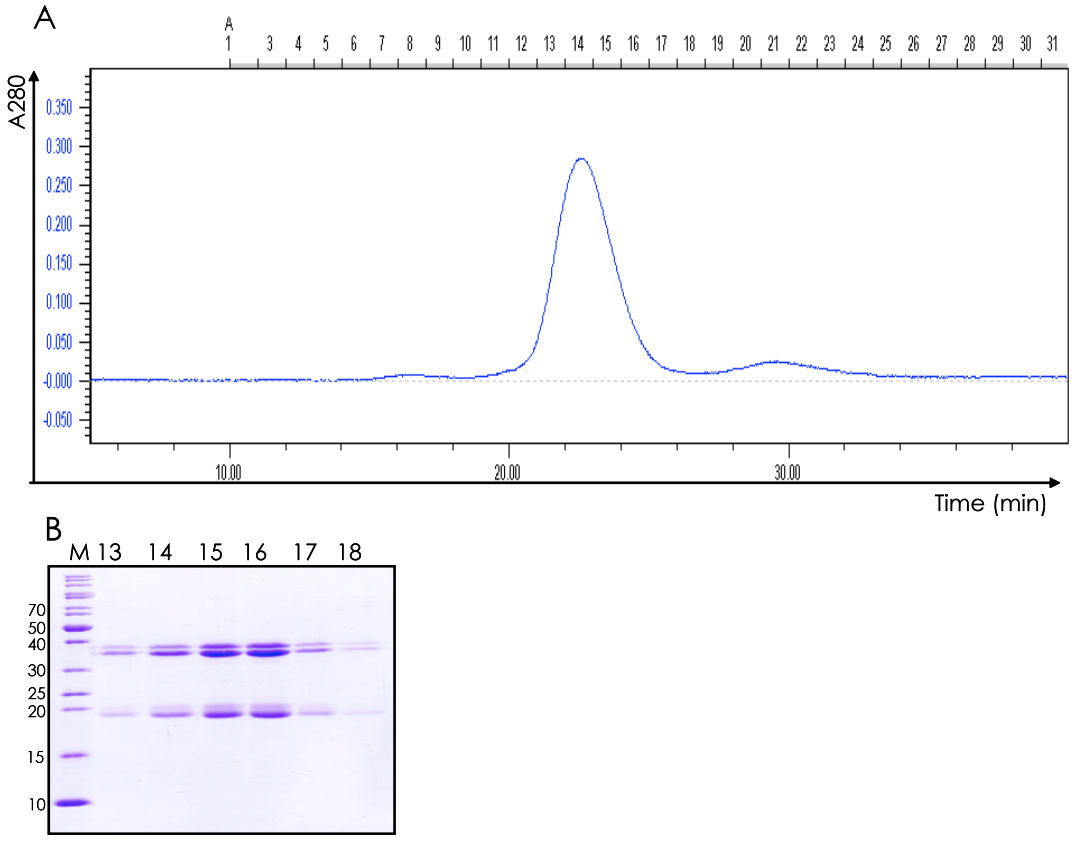

Figure 28. Gel filtration of the Ad11:CD46 SCR1-SCR4 complex. (A) The gel filtration run separated saturated complex (left peak) from the excess CD46 (right peak). (B) 12% SDS-PAGE showing only fractions from the larger peak. Molecular weight markers (kDa) are shown on the left (lane "M"). The mismatch between the fractions in the gel and in the chromatogram is due to the deadvolume between the UV-cuvette and fraction collector.

4.2 Crystallization and structure determination

4.2.1 The Ad11 knob

4.2.1.1 Crystallization of the Ad11 knob

In order to provide a structural basis for the Adenovirus interaction with CD46, we first determined the crystal structure of the unliganded Ad11 knob. The purified knob was crystallized using the hanging drop method, with 2 µl drops (1:1 ratio reservoir:protein), a protein concentration of 8 mg/ml, and a temperature of 20 °C. Well diffracting crystals were obtained after initial screening in 12 hrs over a reservoir containing 18% (w/v) PEG 6000, 0.1 M Hepes pH 7.0 (Figure 29). The

crystals allowed us to determine the structure at 1.45 Å resolution with excellent statistics (Table 2, Appendix 7.3).

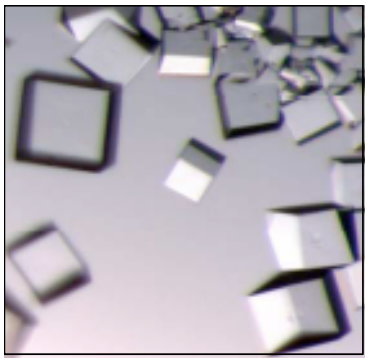

Figure 29. Crystals of the Ad11 knob grown using the hanging drop method. The largest crystals had a size of about 150 x 150 x 150 µm.

4.2.1.2 Structure determination of the Ad11 knob

The crystals were flash frozen in a cryogenic solution supplemented with 20% PEG600 to avoid ice formation. X-ray data were collected at the Swiss Light Source (SLS, Villigen Switzerland) beamline X06S using a MarCCD detector (Mar research). The data were indexed, integrated and scaled using the HKL package (Otwinowski, 1997). The protein crystallized in the cubic space group I23, with one monomer in the asymmetric unit, placed on the three fold rotation axis of the diagonal of the unit cell. Initial phases were obtained by molecular replacement in AMoRe (CCP4, 1994) using the Ad3 knob (PDB accession number 1H7Z, 49.5% homology). The sequences were aligned and amino acids in close proximity to gaps/insertions were removed. Remaining amino acids were mutated to the Ad11 sequence using COOT (Emsley et al., 2004). Molecular replacement search using AMoRe, in a resolution range between 12-3.5 Å using a 30 Å sphere, gave one solution that refined well in CNS (Brunger et al., 1998) (Table 2).

Table 2. Essential crystallographic statistics for the structure determination of the Ad11 knob. More detailed statistics can be found in Appendix 7.3.

Data quality	
Space group	I23
Unit cell dimensions (Å)	a=100.6
Resolution range (Å)	40-1.45 (1.45-1.50)
Completeness (%)	99.9 (100.0)
Redundancy	6.0 (5.4)
R_{Sym}(%)[1]	4.5 (38.8)
I/□	13.2 (1.56)
Refinement statistics	
R_{Work}(%)[2]	18.8
R_{Free}(%)[2]	21.6

Highest-resolution shell is shown in parentheses.

1-Defined in the Methods section 3.7.7
2-Defined in the Methods section 3.7.10
Free set contains 5% of reflections (see Methods section 3.7.10)

4.2.1.3 Overall structure of the Ad11 knob

Each Ad11 knob protomer folds into an eight-stranded anti-parallel □-sandwich, and three of these assemble into a propeller-like trimer with an extensive interface (see Introduction; Figure 4). Although the Ad11 knob is homologous in sequence to knobs from other serotypes, it differs in loop regions that define the receptor interactions, especially in the AB-, HI- and IJ-loops. Mutational studies have indicated that an epitope responsible for the interaction with CD46 is located around Ad11-R279, in the N-terminal part of the HI-loop. By constructing chimeras between the Ad7 knob, which was thought not to bind CD46, and the Ad11 knob the region responsible for CD46 binding was identified as region 279-283 (Gustafsson et al., 2006). The N-terminal 10 amino acids are disordered and not visible in our structure.

4.2.2 Structure of the CD46 SCR1-SCR2:Ad11 knob complex

4.2.2.1 Crystallization of the complex

To define the interactions of Ad11 with its receptor CD46 at the atomic level, we solved the structure of the complex between the N-terminal two SCR domains (SCR1-SCR2) of CD46 and the Ad11 knob. Crystallization was performed at room temperature using the hanging drop method (2 µl drops in a 1:1 ratio between reservoir solution and protein) at a protein concentration of 8 mg/ml. 100 x 60 x 30 µm crystals were obtained at 20 °C after initial screening in one week over a reservoir containing 35% (w/v) PEG200, 200 mM $CaCl_2$, 100 mM Tris pH 8.0 (Figure 30). Crystals were harvested, flash frozen in liquid nitrogen, and measured at the SLS (Villigen, Switzerland) using a MAR CCD detector (Mar research). Since the crystallization condition contains such a high concentration of PEG200, no additional cryoprotectant was needed.

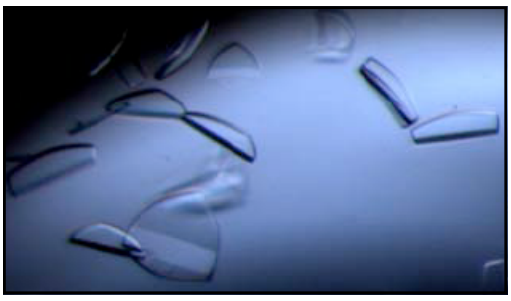

Figure 30. Halfmoon shaped crystals of the Ad11: CD46 complex.

4.2.2.2 Structure determination of the Ad11 complex

Data were collected from several crystals, and images were integrated and reduced using the HKL package (Otwinowski, 1997). The structure was solved by molecular replacement as implemented in AMoRe (CCP4, 1994) using the crystal structure of the unliganded Ad11 knob and, separately, the SCR1 and SCR2 domains of CD46 (Casasnovas et al., 1999) (PDB code 1CKL). After placement of the two Ad11 knobs, the SCR1 and SCR2 domains of CD46 could be placed unambiguously. After several rounds of refinement using CNS (Brunger et al., 1998) and model adjustments using Coot (Emsley et al., 2004), convergence was achieved. The final structure has R-factors of 23.4% (working set) and 28.7% (free set), for all data between 40 and 2.85 Å (Table 3).

The asymmetric unit of the crystals contains two Ad11 knob chains and two CD46 SCR1-SCR2 chains. These chains belong to two different trimers that are generated by crystallographic 3-fold symmetry axes located at the origin and the center of the P3 unit cell. Non-crystallographic symmetry restraints were used throughout the refinement, excluding loop residues and termini. The N-terminal ten residues of each monomer in the Ad11 knob are disordered in both copies. Therefore these residues are not included in the final model. All structural features, and especially all details of the Ad11 knob-CD46 interaction, are identical in both copies of the complex.

Table 3. Essential crystallographic statistics of the crystallized complex between Ad11 and CD46 SCR-SCR2. More detailed statistics can be found in Appendix 7.3.

Data quality	
Space group	P3
Unit cell dimensions (Å)	a=b=106.14 c=68.32
Resolution range (Å)	40-2.85 (2.85-2.95)
Completeness (%)	93.2 (83.0)
Redundancy	4.1 (4.0)
R_{Sym}(%)[1]	5.9 (32.5)
I/□	7.23 (2.64)
Refinement statistics	
R_{Work}(%)[2]	23.4
R_{Free}(%)[2]	28.7

Highest-resolution shell is shown in parentheses.

1-Defined in the Methods section 3.7.7
2-Defined in the Methods section 3.7.10
Free set contains 10% of reflections (see Methods section 3.7.10).

4.2.2.3 The overall structure of the Ad11: CD46 SCR1-SCR2 complex

The Ad11 knob binds three CD46 molecules. Each CD46 unit lies diagonally across an interface between two Ad11 knob protomers, making contacts with both (Figure 31A). The SCR domains of CD46 form □-barrels with a small hydrophobic core and two disulfide bonds, sealing each domain at the top and the bottom. The SCR1-SCR2 repeats of CD46 adopt an almost linear, rod-like

conformation. The CD46 fragment used here carries two glycans. Although only a portion of one glycan (at Asn80 in SCR2) is clearly visible in our electron density maps, the position of the second glycan (at Asn49 in SCR1) can be inferred from weak electron density. Both glycans face away from the virus-binding surface and do not interact with Ad11 knob.

The Ad11 knob-CD46 interface is extensive with the Ad11 knob covering almost the entire length of the glycan-free side of the receptor, from the mid-section of SCR1 to the base of SCR2, occluding an area of 1670 Å^2 (calculated using Contact (CCP4, 1994) from solvent. The interface features a strong complementarity in shape, with many direct protein-protein contacts and few water molecules mediating interactions (Figure 31B).

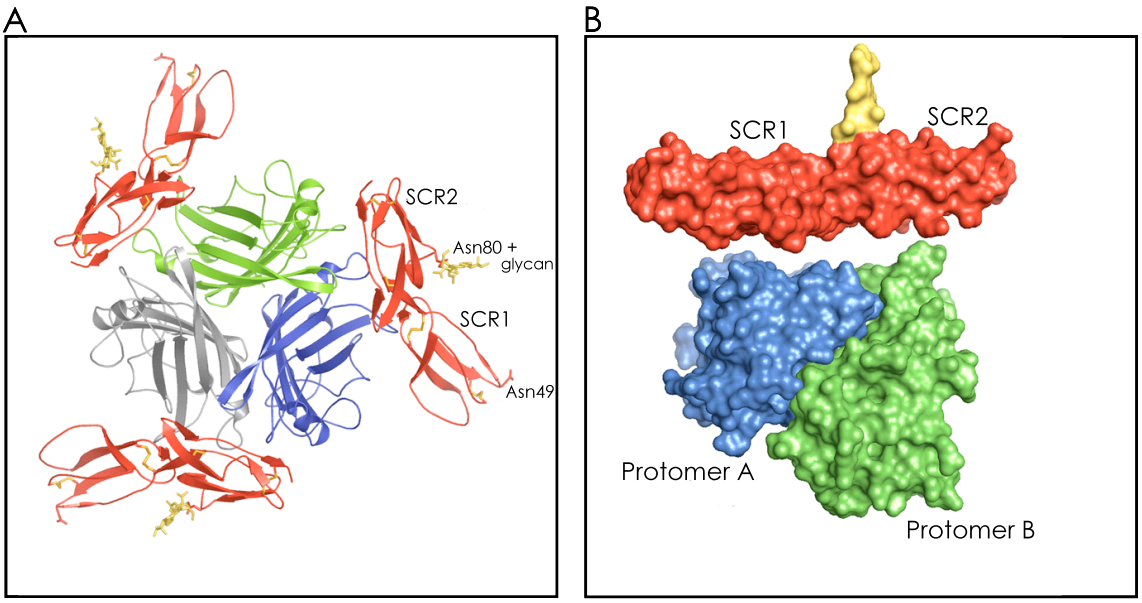

Figure 31. Structure of the Ad11 knob in complex with CD46 SCR1-SCR2. (A) Ribbon drawing of the complex. The three subunits forming the Ad11 knob are shown in blue, green and grey; bound CD46 SCR1-SCR2 is in red, with Asn49 and Asn80 shown in red and the glycans attached to Asn80 shown in yellow. The glycan attached to Asn49 is poorly ordered in the crystals and was not modeled. Disulfide bonds are shown in yellow. The view is along the three-fold axis. In this view, the Ad11 fiber shaft (and hence the virus particle) would be located below the plane of the paper; the cell bearing CD46 would be above it. (B) Surface representation of the complex. The two Ad11 knob monomers that contact CD46 are shown in blue and green, bound CD46 SCR1-SCR2 is in red, and the glycan attached to SCR2 is in yellow. To highlight the striking shape complementarity between the interfaces, CD46 has been translated away from the Ad11 knob by about 5 Å. The color code is the same as that used in panel A. Figures made in PyMOL (DeLano, 2002).

4.2.2.4 The binding interface

The majority of contact residues are contributed by a single Ad11 knob protomer (blue in Figure 31B), which interacts with SCR1 and with the SCR1-SCR2 interface. A second Ad11 knob protomer (green in Figure 31B) provides additional contact points with the base of SCR2. Although they cover a continuous surface, the contacts between the Ad11 knob and CD46 can be divided into three distinct regions (Figure 32A). The first region is centered at the HI-loop of Ad11 knob and residues at the side of SCR1 (Figure 32B). A large contact that helps to define shape complementarity is contributed by Tyr36 of CD46, which interacts tightly with the main chain of the Ad11 knob HI-loop. Additional contacts in this area include several hydrogen bonds between main chain atoms, as well as a salt bridge between Asp284 of Ad11 knob and His43 of CD46. The second region involves the HI- and DG-loops of Ad11 knob, which make extensive contacts with the SCR1-SCR2 interface (Figure 32C). A key residue here is Arg280 of the Ad11 knob, which forms a bi-dentate salt bridge with Glu63 of CD46. The hydrophobic portion of Arg280 docks against the Phe35 side chain in SCR1. Several additional polar and non-polar contacts strengthen the interactions in this region. The third contact is formed between the IJ-loop of a neighboring monomer of Ad11 knob and the lower portion of SCR2 (Figure 32D). Contacts in this region feature two hydrogen bonds, both involving the main chain of CD46. The relative position of the Ad11 knob and SCR1-SCR2 molecules in the complex indicates that regions missing in the two proteins (the N-terminal shaft of Ad11 fiber and domains SCR3-SCR4 of CD46) would face in opposite directions.

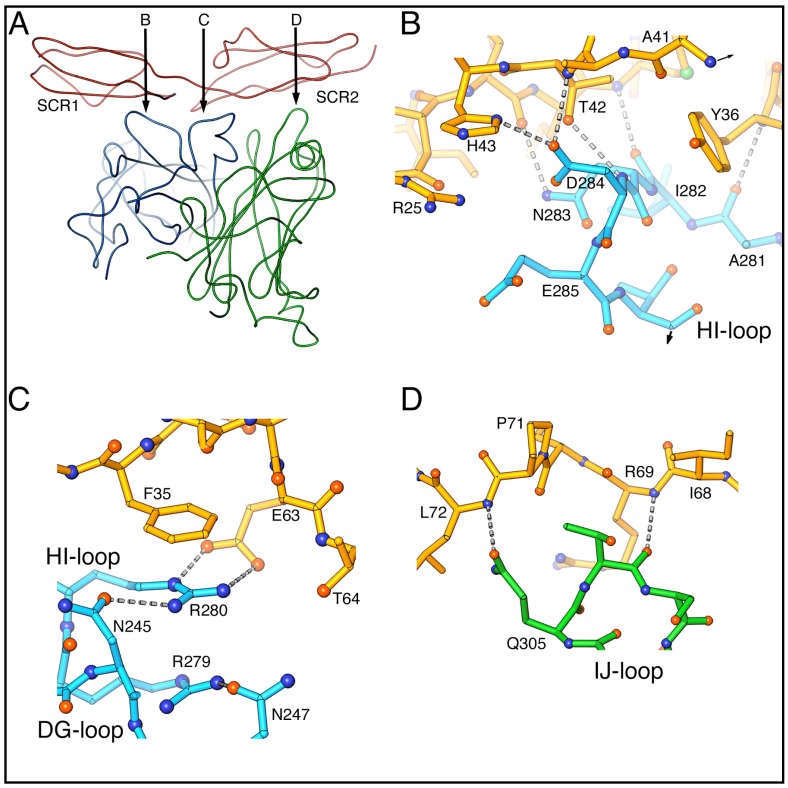

Figure 32. Interaction between Ad11 knob and CD46 SCR1-SCR2. Panel (A) shows a ribbon tracing of the complex using the color code from Figure 31. Panels (B) to (D) show detailed views of the three major contact regions involving the HI-, DG- and IJ-loops of Ad11 knob. The color scheme is based on that used in Figure 31: The two Ad11 knob monomers are in blue and green, respectively, and CD46 is shown in orange. Nitrogen and oxygen atoms of side chains are shown in blue and red, respectively. Hydrogen bonds and salt bridges (distance < 3.5 Å) are represented with dashed grey lines. Key residues are labeled using single-letter code. Figure made in Ribbons (Carson, 1997).

4.2.2.5 Binding and infectivity studies

To prove the hypothesis that the outer two domains of CD46 are sufficient for Ad11 binding, we performed a binding assay using ^{35}S-labeled Ad11 particles and a fluorescent focus infectivity assay (FFA). Recombinant soluble CD46 SCR1-SCR2 and CD46 SCR1-SCR4 fragments were incubated together with virus particles for one hour on ice before mixing with human respiratory epithelial cells (A549 cells). After washing, the cells were analyzed for the amount of bound radioactive particles. For the FFA the cells were grown for 48 hrs at 37°C before fixation and staining. Soluble CD46 SCR1-SCR2 and SCR1-SCR4 blocked binding and subsequent infectivity at nearly identical doses and with very similar kinetics (Figure 33).

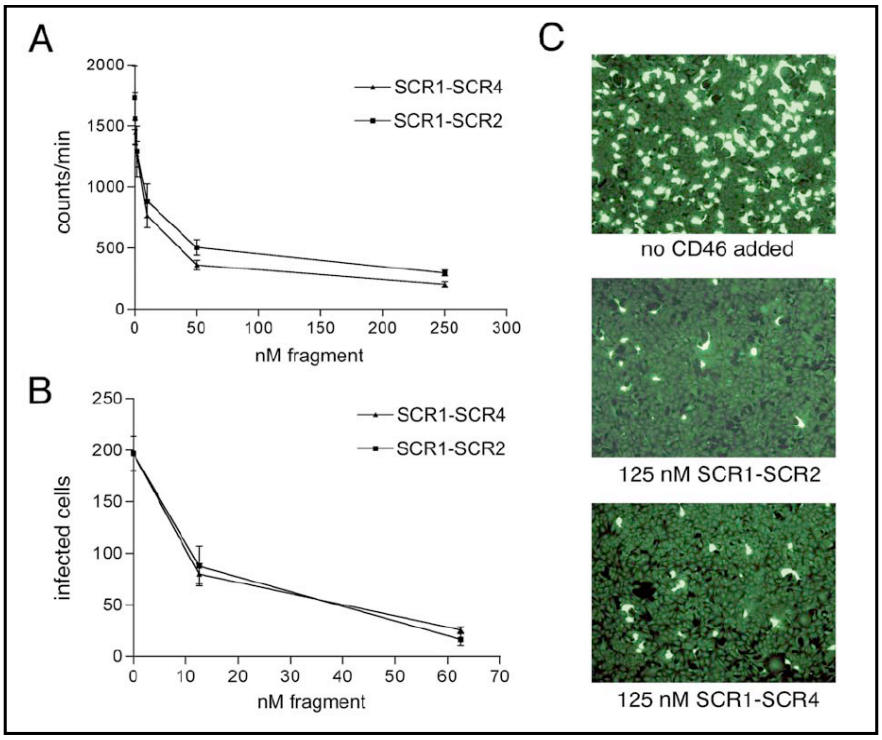

Figure 33. Fragments SCR1-SCR2 and SCR1-SCR4 of CD46 are equally efficient in preventing Ad11 from binding to and infecting A549 cells. Various concentrations of soluble SCR1-SCR2 or SCR1-SCR4 were incubated (A) with ^{35}S-labeled Ad11 and then allowed to bind to A549 cells on ice, or (B) with non-labeled Ad11 on ice and then allowed to infect A549 cells. Panel (C) shows infection of A549 cells with labeled Ad11, either adding no CD46 protein (top), purified SCR1-SCR2 (middle) or purified SCR1-SCR4 (bottom).

4.2.2.6 *Affinity measurements*

Number of contacts and extent of the binding surface indicate very tight binding. We decided to measure the Ad11 knob affinity for CD46 SCR1-SCR2 using isothermal calorimetry measurements (ITC). The reaction is exothermic and places the affinity of the Ad11 knob for CD46 SCR1-SCR2 around 2 nM (Figure 34) (see Methods section 3.5.1).

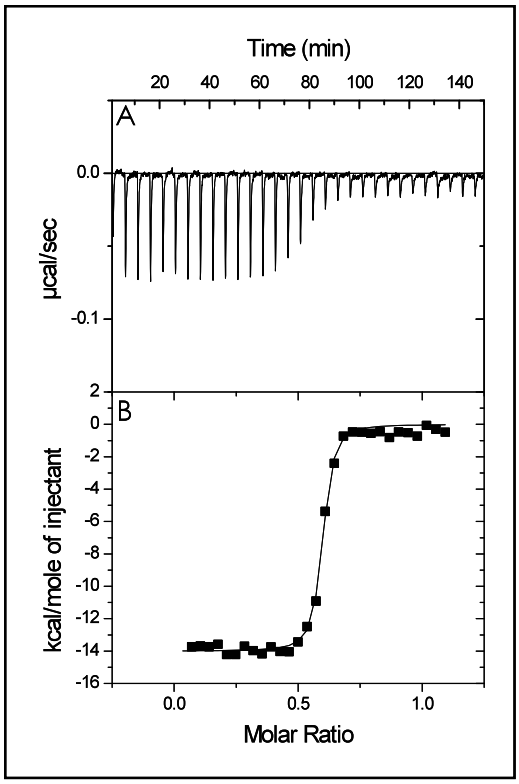

Figure 34. ITC measurements placed the Ad11 affinity for CD46 in the range of 2 nM. CD46 was injected into the reaction chamber containing Ad11 knobs. (A) Each of the 30 injections of CD46 results in a peak. The area under each peak corresponds to the heat released. (B) Integrated heat values plotted against molar ratio of ligand.

4.2.2.7 *The Ad11 knob alters the conformation of its cellular receptor CD46*

Perhaps the most striking feature of the Ad11 knob-CD46 complex is that the relative orientation of the two SCR domains of CD46, and thus the overall shape of the receptor, is dramatically changed from that seen in the unliganded structure (Casasnovas et al., 1999) (Figure 35A). We conclude, therefore, that Ad11 knob induces a profound conformational change in CD46 by realigning the two repeats and molding them into a rod-like segment. The change in conformation not only alters the relative orientation between Ad11-binding epitopes on SCR1 and SCR2 but also modifies the overall surface structure of CD46; exposing residues for binding that were hidden in the unliganded structure (Figure 35B; Figure 36).

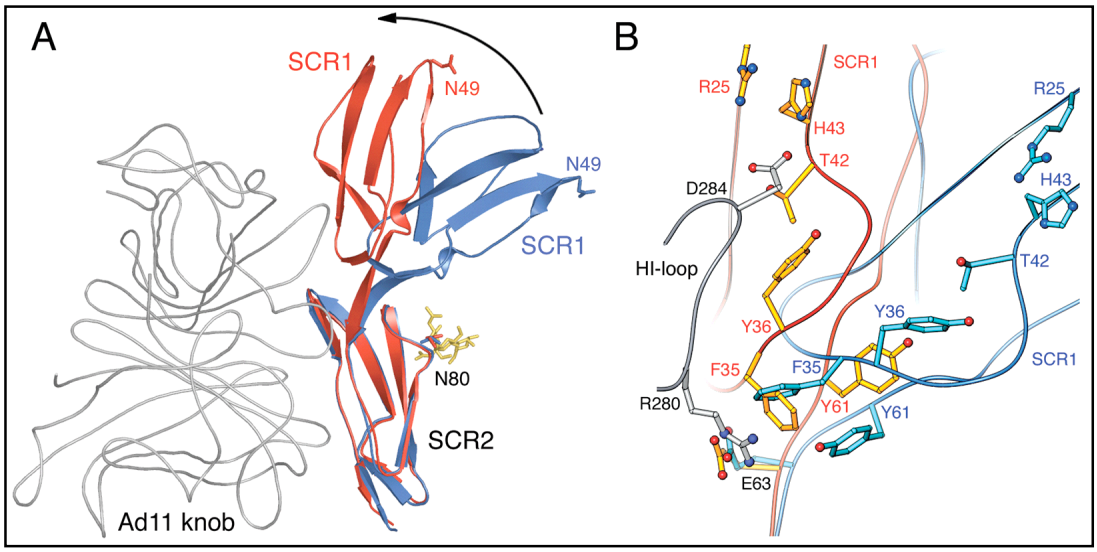

Figure 35. Ad11 knob induces a large conformational change in CD46. Shown here is a superimposition of the SCR2 domains of unliganded (Casasnovas et al., 1999) (blue) and liganded CD46 (red). The two Ad11 knob monomers that interact with CD46 are shown as grey ribbon tracings. (A) Overall structure. The arrow indicates the rearrangement of SCR1 upon binding to Ad11 knob. Asparagine side chains at positions 49 and 80 carry glycans. The glycan attached to Asn49 in the liganded structure is poorly ordered; glycans of the unliganded structure are not shown for reasons of clarity. (B) Close-up view of the interaction, using the same superposition and color code. Key amino acids of CD46 that take part in complex formation are shown in orange (CD46 bound to Ad11 knob) and light blue (unliganded CD46). Residues are labeled in single-letter code. Figure made in Ribbons (Carson, 1997).

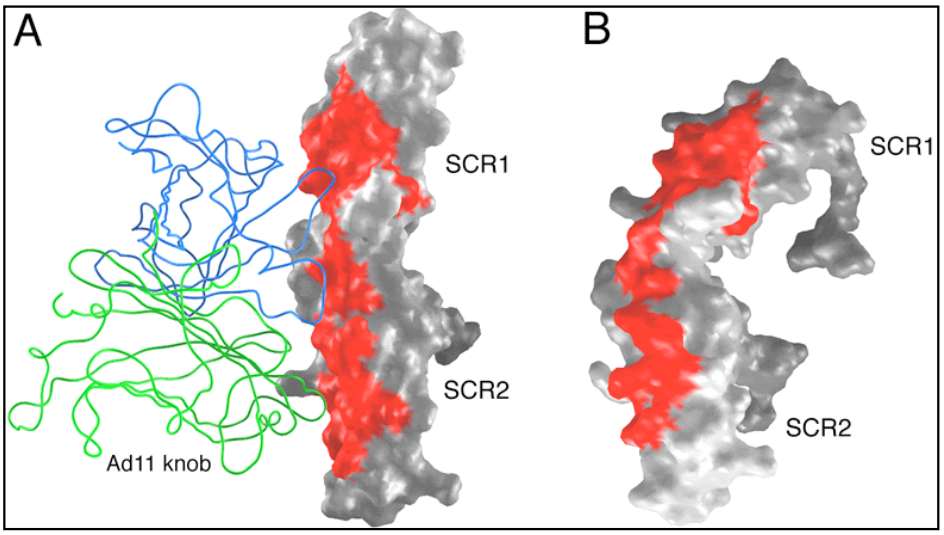

Figure 36. Ad11 knob alters the surface structure of CD46. (A) Surface representation of liganded CD46 SCR1-SCR2, with all residues that interact with Ad11 knob in the complex (distance < 4.5 Å) colored in red. Ribbon tracings of the two CD46-binding Ad11 knob monomers are shown in blue and green. (B) Surface representation using the structure of unliganded CD46 SCR1-SCR2 (Casasnovas et al., 1999). The same residues shown in panel A are highlighted in red. Figure made in GRASP (Nicholls et al., 1991).

Binding of Ad11 knob to CD46 can be severely impaired by introducing a single amino acid change, Arg279 to Gln (Gustafsson et al., 2006). Our structure shows that Arg279 is indeed a critical residue, although it does not directly interact with CD46. Arg279 is located in the second contact area. Its side chain lies directly beneath and parallel to the Arg280 side chain (Figure 32C). The Arg279 side chain thus forms a platform that helps to orient Arg280, allowing it to engage CD46 residues Glu63 and Phe35. Perhaps of equal importance, Arg279 also appears to help shape the surface structure of Ad11 knob by forming an intra-molecular hydrogen bond linking the HI-and DG-loops (Figure 32C). The proximity of Arg279 and Arg280 is somewhat surprising, as both side chains carry the same positive charge. In fact, Arg280 occupies a different position in the unliganded Ad11 knob structure and only swings next to Arg279 upon complex formation (Figure 37). While the amino acids in the DE- and IJ loops have similar conformations in the liganded and unliganded Ad11 knob structures, the HI-loop exhibits a significant rearrangement of residues that provide clues about the determinants of CD46 binding. The most profound conformational rearrangement is seen for the Arg280 side chain, which is defined by excellent electron density in both structures. In the Ad11-CD46 complex, Arg280 lies parallel to Arg279, with the two guanidinium groups stacked against each other (Figure 37A). The Arg280 guanidinium group faces towards CD46, forming a salt bridge with CD46 residue Glu63, whereas the Arg279 guanidinium group is hydrogen bonded to Ad11 residue Asn247. In the unliganded Ad11 knob, the Arg280 side chain has rotated about 170 degrees, now facing into the opposite direction and pointing away from Arg279 (Figure 37B). Its guanidinium group is now stacked against that of the Arg291 side chain. Thus, in both the unbound and bound structures, Arg280 is stacked against another arginine, albeit a different one on each case. In addition to Arg280, the Ad11 HI-loop residue Asp284 also undergoes a rotation as it engages His43 in CD46.

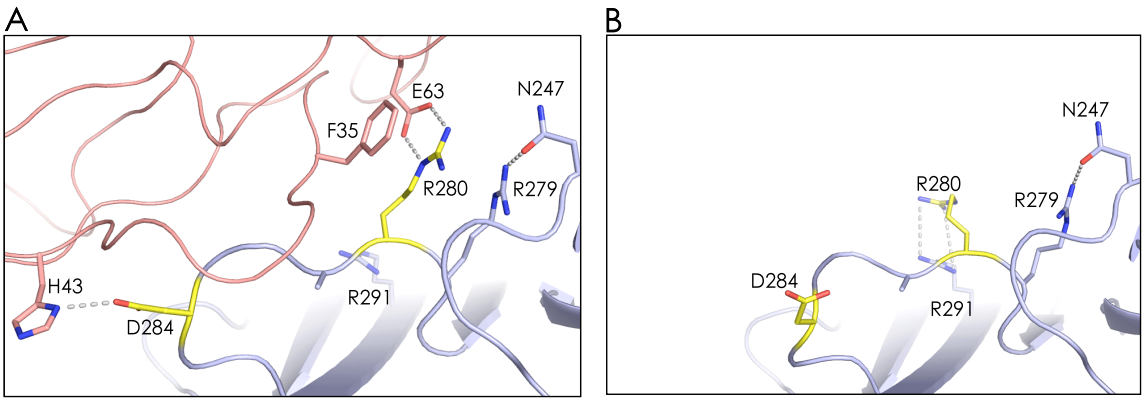

Figure 37. Comparison between complexed and uncomplexed Ad11 knobs. (A) Ad11 knob (blue) complexed with CD46 (red). Amino acids colored yellow are changed upon binding to CD46. (B) Ad11 knob uncomplexed. Figure made in PyMOL (DeLano, 2002).

4.2.3 The Ad7 and Ad14 knob

4.2.3.1 Crystallization of the Ad7 and Ad14 knob

The knobs of Ad11, Ad14 and Ad7 differ drastically in their ability to bind CD46. All three knobs bind better to CHO-CD46 cells than to regular CHO cells, indicating that all three knobs are able to interact with CD46 (Gaggar et al., 2003; Marttila et al., 2005; Segerman et al., 2003a). However, only Ad11 and Ad14 use CD46 as a receptor on human epithelial cells (Marttila et al., 2005), and Ad7 instead binds to a different, so far unidentified receptor (Tuve et al., 2006). Despite these functional differences, all three knobs are highly similar in sequence: the identity between Ad11 and Ad7 knob residues is 93.3 %, whereas the Ad11 and Ad14 knobs are 92.7 % identical, and the Ad7 and Ad14 knobs are 91.7% identical. Thus, these three knobs are ideally suited to define the determinants of CD46 binding of type B Ads.

In order to provide a structural basis for the observed differences in CD46 binding among the three knobs, we first determined the crystal structures of the unliganded Ad7 and Ad14 knobs. Both knobs were crystallized at 20°C using the hanging drop method at a concentration of 10 mg/ml protein. Well-diffracting crystals were obtained after 4-7 days (Figure 38A-B), diffracting to 1.75 Å and 1.8 Å resolution, respectively. After initial screening the final crystallization conditions are as follows: Ad7 knob: 23% (w/v) PEG 3350, 0.1 M Hepes pH 7.6; Ad14 knob: 20% (w/v) PEG 8000, 0.1 M CHES pH 9.0, 200 mM NaCl. The crystals were flash

frozen, in reservoir solution supplemented with 25% (w/v) glycerol, in liquid nitrogen and X-ray data were collected at the SLS (Villigen Switzerland) beamline X06SA using a MarCCD detector (Ad7 knob) and a Pilatus detector (Ad14 knob).

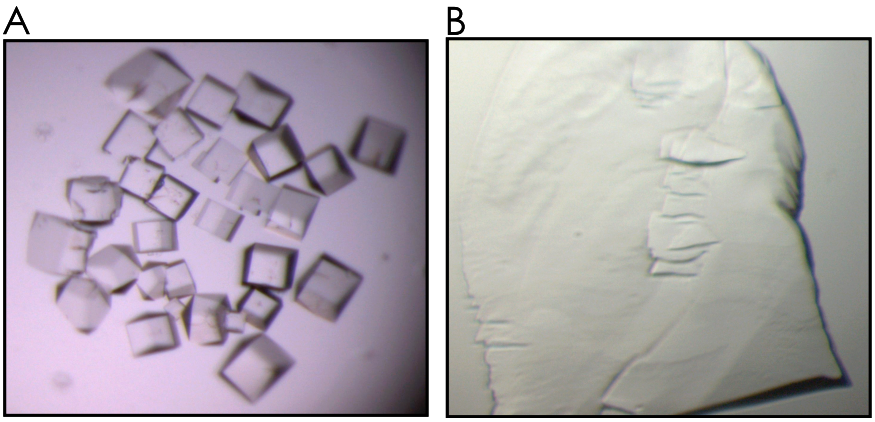

Figure 38. Crystals obtained from (A) Ad7 (about 100 x 100 x 100 µm in size) and (B) Ad14 (about 300 x 300 x 50 µm in size). Crystals were grown using the hanging drop method and flash frozen in liquid nitrogen prior to measurements at Beamline X06SA at SLS.

4.2.3.2 Structure solution of the Ad7 and Ad14 knob

Data for the Ad7 knob were integrated and scaled using the HKL package (Otwinowski, 1997), whereas the Ad14 knob data were processed with XDS package (Kabsch, 1993) due to incompatibility between the HKL package and the Pilatus detector. Initial phases were in each case obtained by molecular replacement using trimeric Ad11 knobs from the Ad11-CD46 complex structure (Persson et al., 2007) in PHASER (McCoy et al., 2007). Initial rigid body refinement of the solutions was performed with CNS (Brunger et al., 1998), and subsequent refinement was carried out in REFMAC5 (CCP4, 1994). In both cases the structures were refined to excellent R-factors converging at R_{work} of 19.2% and R_{Free} of 21.2% for Ad14 and R_{work} of 20.2% and R_{Free} of 23.8% for Ad7 (Table 4, Appendix 7.3).

Table 4. Essential crystallographic statistics of the crystallized Ad7 and Ad14 knob. More detailed statistics can be found in Appendix 7.3.

Data quality	**Ad7**	**Ad14**
Space group	$P2_12_12$	$P3_212$
Unit cell dimensions (Å)	a=83.31 b=88.05 c=79.17	a=b=83.31 c=311.71
Resolution range (Å)	79-1.75 (1.75-1.81)	47.4-1.8 (1.80-1.90)
Completeness (%)	99.1 (95.1)	99.1 (94.4)
Redundancy	5.1 (4.6)	11.9 (4.8)
R_{Merge}(%)[1]	5.0 (36.4)	7.8 (27.0)
I/□	10.17 (1.34)	11.91 (4.83)
Refinement statistics		
R_{Work}(%)[2]	20.2	19.2
R_{Free}(%)[2]	23.8	21.2

Highest-resolution shell is shown in parentheses.

1-Defined in the Methods section 3.7.7
2-Defined in the Methods section 3.7.10
Free set contains 10% of reflections (see Methods section 3.7.10).

4.2.3.3 Alignment of the Ad7, Ad11 and Ad14 knobs

All three sequences can be aligned without gaps (Figure 39A), suggesting that differences among them are primarily a result of altered properties due to individually substituted amino acids, rather than larger conformational changes in surface loops (using T-coffee at www.ch.embnet.org) (Notredame et al., 2000). We therefore used the Ad11 structure to map substitutions in Ad7 and Ad14 onto its surface. Perhaps not unexpectedly, most substitutions are located along the CD46 contact area, clustering in the loops responsible for the contacts (Figure 39B). Arg279, which has been identified as a key determinant of CD46 binding, is replaced with Gln in both Ad7 and Ad14. Moreover, Asp284, which also contacts CD46 in Ad11, is also replaced in both Ad7 and Ad14.

A

```
Ad11  1- MTKRVRLSDSFNPVYPYEDESTSQHPFINPGFISPNGFTQSPNGVLTLKCLTPLTTTGGS
Ad14  1- MTKRVRLSDSFNPVYPYEDESTSQHPFINPGFISPNGFTQSPDGVLTLKCLTPLTTTGGS
Ad7   1- MTKRVRLSDSFNPVYPYEDESTSQHPFINPGFISPNGFTQSPDGVLTLKCLTPLTTTGGS

Ad11    LQLKVGGGLTVDDTNGFLKENISATTPLVKTGHSIGLPLGAGLGTNENKLCIKLGQGLTF
Ad14    LQLKVGGGLTVDDTDGTLQENIGATTPLVKTGHSIGLSLGAGLGTDENKLCTKLGEGLTF
Ad7     LQLKVGGGLTIDDTDGFLKENISAATPLVKTGHSIGLSLGPGLGTNENKLCAKLGEGLTF

Ad11    NSNNICIDDNINTLWTGVNPTEANCQIIMNSSESNDCKLILTLVKTGALVTAFVYVIGVSN
Ad14    NSNNICIDDNINTLWTGVNPTEANCQMMDSSESNDCKLILTLVKTGALVTAFVYVIGVSN
Ad7     NSNNICIDDNINTLWTGVNPTTANCQIIMASSESNDCKLILTLVKTGGLVTAFVYVIGVSN

Ad11    NFNMLTTHRNINFTAELFFDSTGNLLTRLSSLKTPLNHKSGQNMATGAITNAKGFMPSTT
Ad14    NFNMLTTYRNINFTAELFFDSAGNLLTSLSSLKTPLNHKSGQNMATGAITNAKSFMPSTT
Ad7     DFNMLTTHKNINFTAELFFDSTGNLLTSLSSLKTPLNHKSGQNMATGALTNAKGFMPSTT

Ad11    AYPFNDNSREKENYIYGTCYYTASDRTAFPIDISVMLNRRAINDETSYCIRITWSWNTGD
Ad14    AYPFNNNSREKENYIYGTCHYTASDHTAFPIDISVMLNQRAIRADTSYCIRITWSWNTGD
Ad7     AYPFNVNSREKENYIYGTCYYTASDHTAFPIDISVMLNQRALNNETSYCIRVTWSWNTGV

Ad11    APEVQTSATTLVTSPFTFYYIREDD -325
Ad14    APEGQTSATTLVTSPFTFYYIREDD -325
Ad7     APEVQTSATTLVTSPFTFYYIREDD -325
```

B

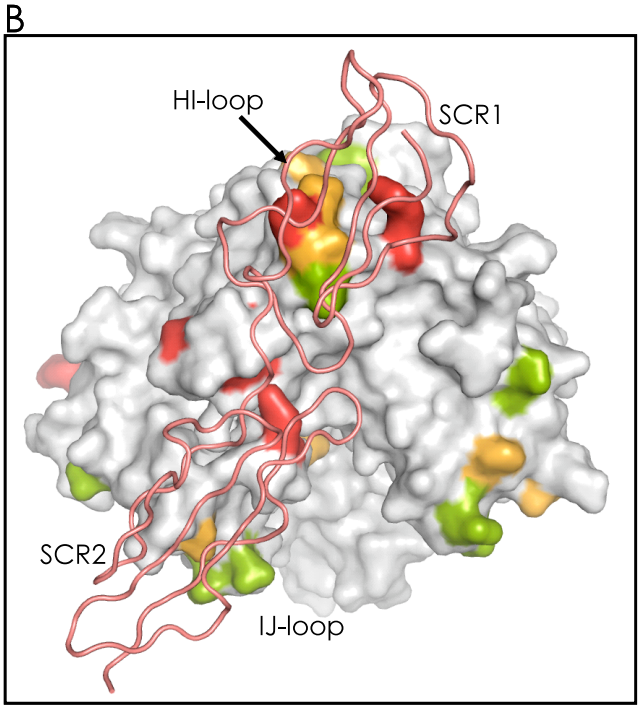

Figure 39. Comparison of Ad11, Ad14 and Ad7 knobs. (A) Alignment of Ad11, Ad14 and Ad7 fiber sequences. Amino acid substitutions are colored in red for substitutions in Ad14 and Ad7, orange for substitutions in Ad14 and green for substitutions in Ad7. The sequence of the shaft is colored gray and the loops involved in interactions with CD46 boxed in blue. (B) Mapping of the substituted amino acids upon the surface of Ad11 knob. Most of the interacting amino acids can be found along the binding epitope of CD46. For simplification, just one copy of CD46 is shown even though one Ad11 knob trimer binds three copies of CD46. Figure B made in PyMOL (DeLano, 2002).

4.2.3.4 *Structure comparison between the Ad7, Ad11 and Ad14 knobs*

As already suggested by the high sequence similarity, the overall structures of the three knobs are almost identical. Ad7 and Ad14 can be superimposed on Ad11 with an r.m.s. deviation of 0.3-0.4 Å using all Cα atoms (Ad7 protomer 0.218 Å and Trimer 0.296 Å; Ad14 protomer 0.445 Å and Trimer 0.387 Å). Differences are seen in surface exposed loops, with minor changes in the HI-loop (Figure 40A), DE-loop and IJ-loop, which also make contacts in the Ad11-CD46 complex structure. The HI- and DG-loops are bridged in Ad7 and Ad14 by a water molecule connecting Gln279 and Asn245, forming essentially the same structure as in the Ad11 knob. An interesting feature is the identical anti-parallel stacking of the Arg280-Arg291 pair in the Ad7, Ad11 and Ad14 knobs (Figure 40B-D).

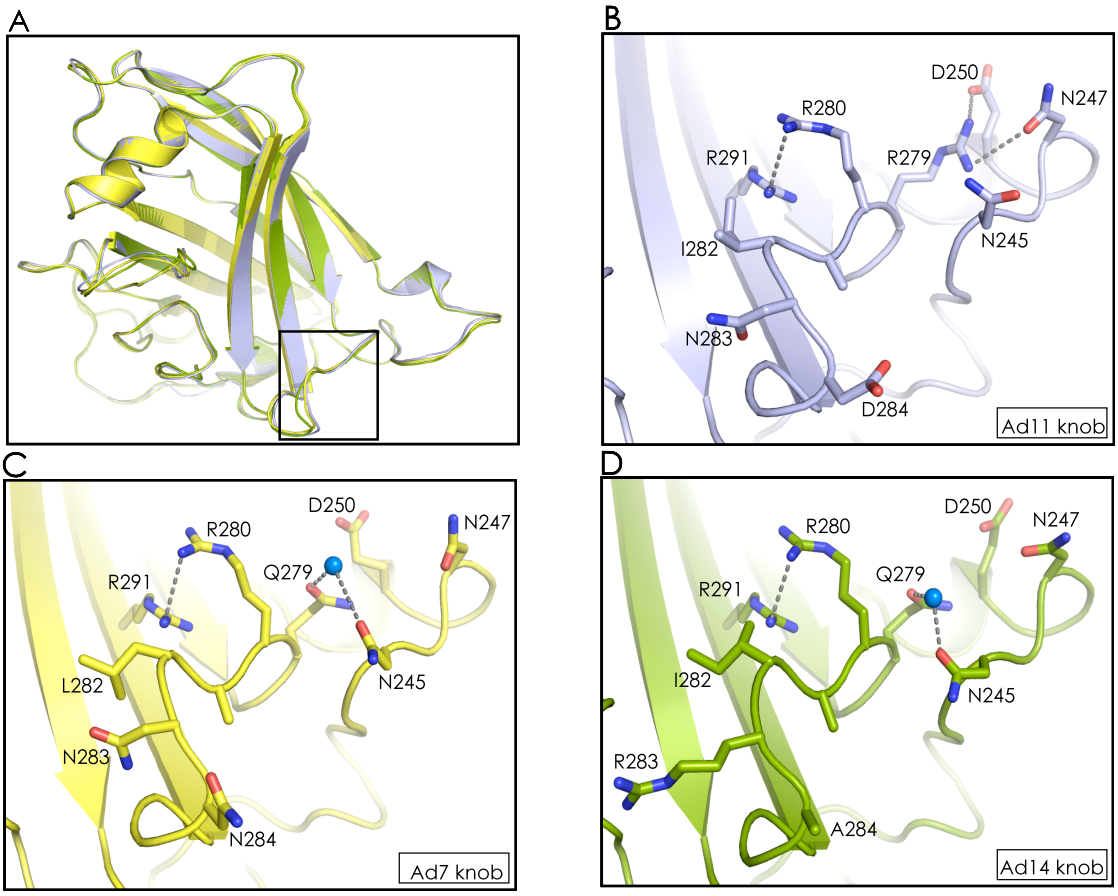

Figure 40. Comparison of the X-ray structures of the Ad11, Ad7 and Ad14 knobs. (A) Superimposition of the Ad11 (blue), Ad7 (yellow) and Ad14 (green) knobs. (C-D) Close-up views of the HI-loops of the Ad11, Ad7 and Ad14 knobs, respectively. Figure made in PyMOL (DeLano, 2002).

4.2.3.5 *Ad11 but not Ad7 and Ad14 block binding of S^{35}-labelled Ad11 particles*

Given their similarities in sequence, we performed a binding assay to determine whether each of the three knobs can compete for Ad11 binding to human respiratory cells. This assay was done at the University of Umeå in collaboration with Dr. Niklas Arnberg (see Methods section 3.6).

As expected, binding of ^{35}S-labeled Ad11 was substantially reduced upon preincubation with Ad11 knobs (Figure 41A). Interestingly, neither Ad7 nor Ad14 knobs were able to compete efficiently with binding of ^{35}S-labeled Ad11 virions. However, soluble Ad7 and Ad14 knobs efficiently blocked ^{35}S-labeled Ad7 particles (Figure 41B).

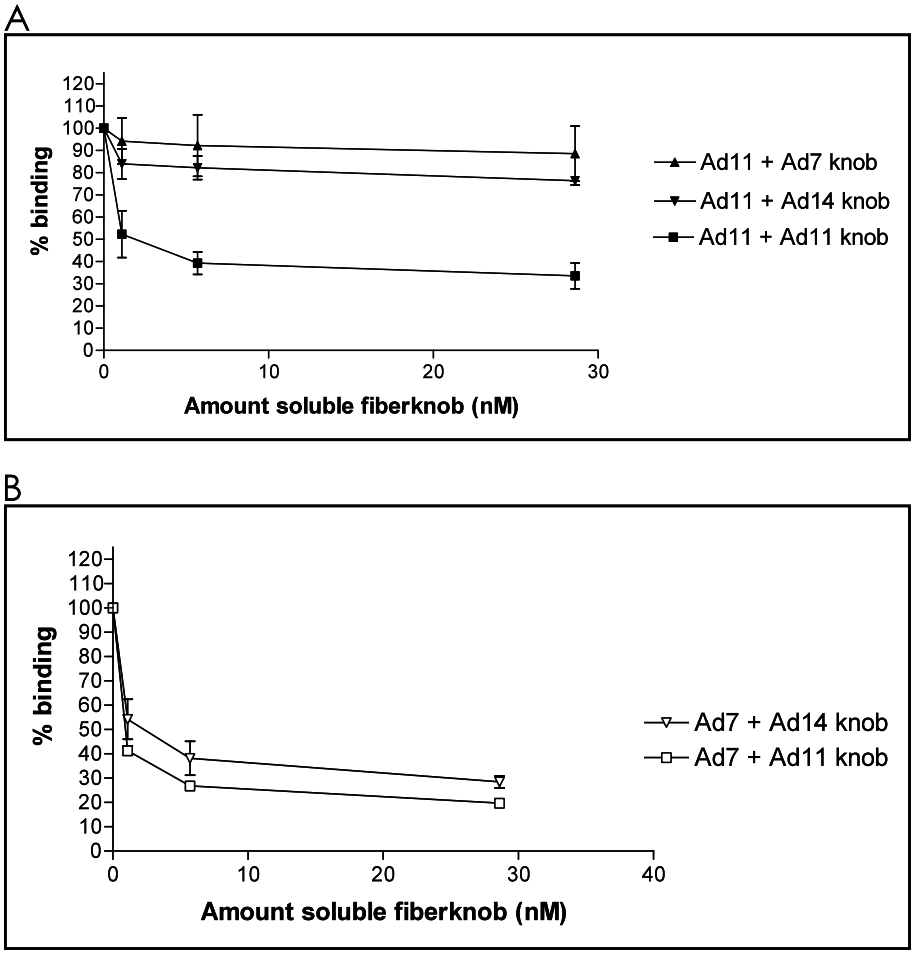

Figure 41. Binding experiments performed on A549 cells. Soluble knobs were incubated with A549 cells prior to addition of ^{35}S-labeled (A) Ad11 particles or (B) Ad7 particles. Values are given as percent of total CPM. Soluble Ad11 knobs blocks Ad11, Ad14 and Ad7 but neither Ad14 or Ad7 blocked Ad11. Interestingly, soluble Ad14 and Ad11 blocked Ad7. The data indicate that all tested knobs use similar epitopes on CD46 for binding.

4.2.3.6 *Ad7 and Ad14 knobs bind CD46 with a 3000-fold lower affinity compared with the Ad11 knob*

The binding experiments indicated that the Ad11 and Ad7/Ad14 knobs bind either different epitopes of, or have very different affinities for, CD46 (see Results section 4.2.3.5). In order to more precisely measure the affinities of all three knobs for CD46, we carried out SPR experiments using the BiaCore™ 2000 system. These experiments were performed by Steffen Müller (Interfaculty Institute for Biochemistry) and interpredet jointly. Each interaction was measured in duplicates followed by two control injections to verify a constant surface during the entire measurement. Kinetic constants could be extracted from the Ad11 knob data set (Figure 42A) but not for the Ad7 and Ad14 knobs due to their fast K_{on} and K_{off} rates (Figure 42B-C). Knob affinities were measured for both CD46 SCR1-SCR2 and CD46 SCR1-SCR4. The knobs had the similar affinities for CD46 SCR1-SCR2 and CD46 SCR1-SCR4, which were in the range of 12 nM for the Ad11 knob and 33 µM for the Ad7 and Ad14 knobs (Table 5). Thus, the Ad7 and Ad14 knobs bind to CD46 with a 3000-fold lower affinity. Since all knobs have a similar affinity for both CD46 fragments, our data confirm that only the SCR1-SCR2 region of CD46 interacts with the Ad knobs. At least for the Ad11 knobs, this is consistent with the structure of the complex with CD46, which is based on a binding surface formed by the SCR1-SCR2 region.

To elucidate if Ad11 and Ad7/Ad14 use the same epitopes for binding CD46 we designed a series of SPR experiments that were performed in solution (Adamczyk et al., 1998). A chip coated with the Ad35 knob, which previously had been shown to bind CD46 (Fleischli et al., 2005; Gaggar et al., 2005) (see Materials section 2.2.6 and Appendix 7.1), was used with a constant concentration of CD46 SCR1-SCR2 or CD46 SCR1-SCR4 as the analyte. The affinity of Ad11 and Ad35 knobs for CD46 is similar (see following section) Several datasets were collected using increasing concentrations of Ad11, Ad7 or Ad14 mixed with the constant concentration of CD46 competing with the Ad35 knobs on the coated surface for binding to CD46. As the concentrations of the Ad11, Ad7 or Ad14 knobs increased the RU signal diminished indicating similar binding epitopes between for example the Ad11 and Ad35 knobs. However, the signal for the Ad11 knob diminished faster than the one for the Ad7 and Ad14 knobs

due to the higher afnity for CD46. Multiple datasets allowed us to conclude that Ad11, Ad7 and Ad14 use partially overlapping or completely overlapping epitopes on CD46 for binding.

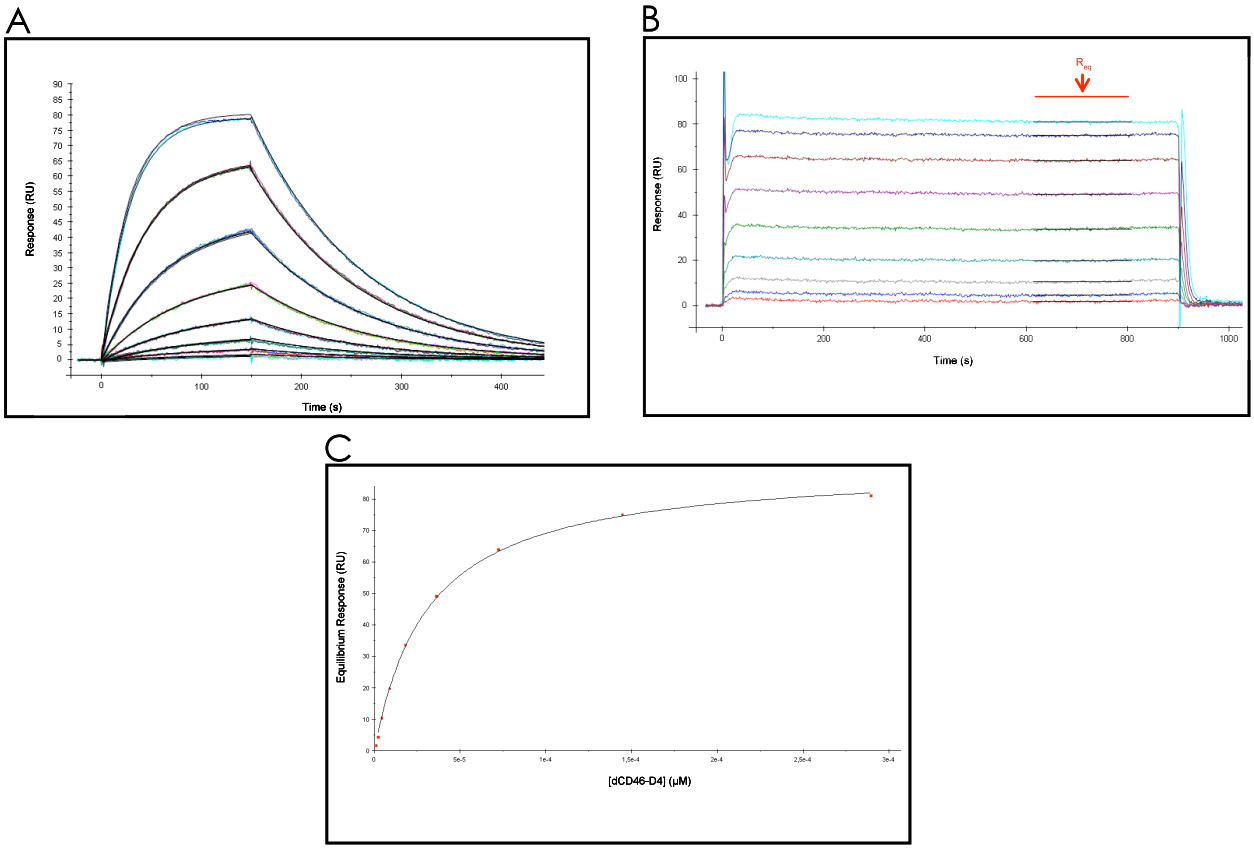

Figure 42. Examples of collected BiaCore data for (A) Ad11 binding to CD46 SCR1-SCR2, (B) Ad7 binding to CD46 SCR1-SCR2 and (C) concentrations of CD46 plotted against RU for the Ad7 dataset. The Ad11 affinity for CD46 SCR1-SCR2 was determined to 12 nM and the Ad7 affinity for CD46 SCR1-SCR2 to 33 µM. Experiments performed by Steffen Müller (Interfaculty Institute for Biochemistry, Tuebingen).

Table 5. Determination of Ad knob affinity for CD46 SCR1-SCR2 and CD46 SCR1-SCR4. Experiments performed by Steffen Müller (Interfaculty Institute for Biochemistry, Tuebingen).

Protein interaction		Steady-State-Analysis	Kinetic Analysis			Solution affinity Analysis
Immobilized knob	in solution	K_D [M]	K_D [M]	k_{on} [$M^{-1}S^{-1}$]	k_{off} [S^{-1}]	K_D [M]
Ad11	CD46 SCR1-SCR2	n.d.	11 e-09	1.3 e06	0.014	23 e-09
Ad11	CD46 SCR1-SCR4	n.d.	13 e-09	0.8 e06	0.009	19 e-09
Ad7	CD46 SCR1-SCR2	35 e-06	Not determined because of extremely high off rates.			58 e-06
Ad7	CD46 SCR1-SCR4	30 e-06				65 e-06
Ad14	CD46 SCR1-SCR2	27 e-06				73 e-06
Ad14	CD46 SCR1-SCR4	31 e-06				63 e-06

4.2.4 Mutation study of the CD46 SCR1-SCR2: Ad11 knob interaction

The major interactions in the complex between Ad11 and CD46 SCR1-SCR2 are located in the HI-loop, as previously described (see Results section 4.2.2.4). We characterized the interaction by introducing mutations using overlap extension PCR (see Methods section 3.1.1). Ad11 amino acids responsible for interactions with CD46 were mutated one by one, and the affinity was measured using ITC (see Methods section 3.5.1 and Appendix 7.2). To verify that the observed change in affinity was not due to major structural rearrangements of the epitope we also crystallized the mutant knobs. We mutated the amino acids as follows; N245S, R279Q, R279S, R280G, I282L, N283S and D284S (Figure 43). We also made a "rescue mutant" of Ad7 mutating Q279 to Arg, in order to restore the high affinity of the Ad7 knob for CD46.

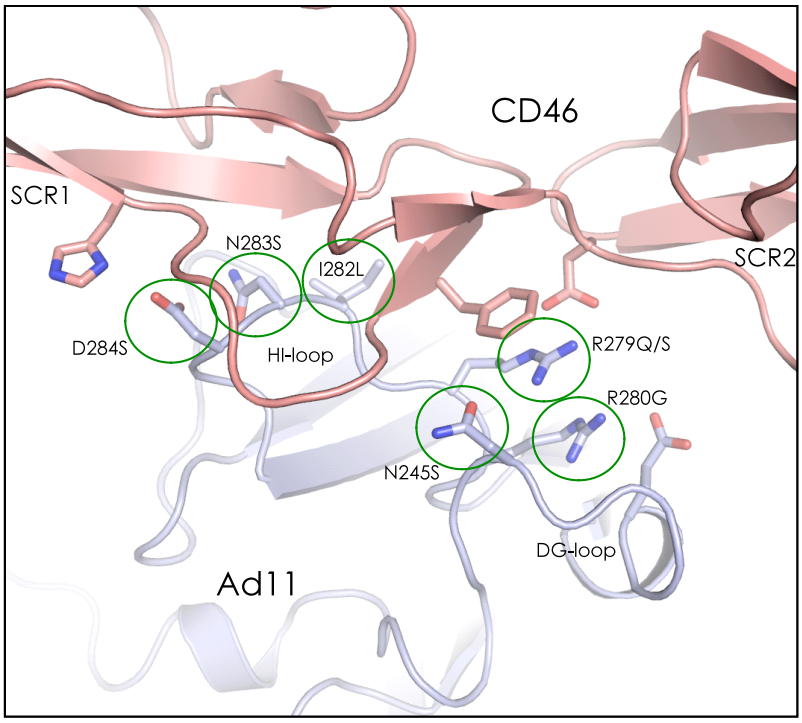

Figure 43. Cartoon representation of the Ad11 kno:CD46 complex. CD46 is shown in red and the Ad11 knob in blue. The green circles indicate amino acids of Ad11 that were selected for mutagenesis. Figure made in PyMOL (DeLano, 2002).

4.2.4.1 Affinity measurements

Initially, the mutants were screened for altered binding capacity to CD46 using our gel filtration assay (using analytical columns and a Smart system, GE Healthcare; data not shown); later, affinity was determined using ITC. However, some mutant knobs have also been measured using SPR due to the higher sensitivity of the method (Table 6). The mutant Ad11-N245S was just analyzed using the gel filtration assay. Previous observations have shown that mutating Ad11-R279 to Gln significantly reduces the knob binding to CD46 expressing cells (Gustafsson et al., 2006). Only a strong reduction was detected, and not a complete loss of binding. Gustafsson et al. also made the rescue mutant of Ad7 (Gln to Arg), which restored the binding to about 50%. We performed similar experiments, mutating the two amino acids, and measured the affinity for CD46 using ITC and SPR. Surprisingly, Ad11-R279Q, and Ad11-R279S, had no affinity for CD46 measured by ITC but a μM affinity in SPR. The affinity measured using SPR correlates with the published data for the Ad11 knob mutants as well as for the rescue mutant (Ad7-Q279R) (Gustafsson et al., 2006). The restored affinity is in the

higher nM, range indicating that Arg279 is the key for high affinity, but that the entire loop helps in building the tight interaction (Figure 44). In Figure 44, the Ad35 knob (see Results section 4.2.5) is also included as its affinity is almost identical to that of the Ad11 knob (Tuve et al., 2006).

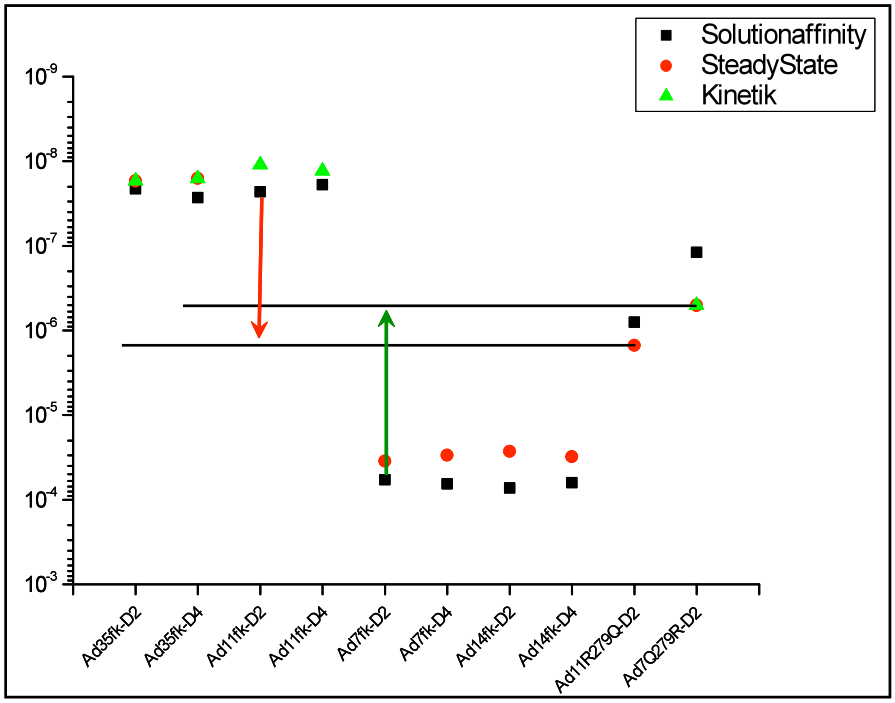

Figure 44. Evaluation of all available affinity data collected using SPR. The red arrow indicates loss of affinity for Ad11 upon mutation of Arg279 to Gln and the green arrow indicates increased affinity for CD46 upon mutating Ad7-Gln279 to Arg. The loss, or gain, of affinity is about 50%. Figure generously provided by Steffen Müller (Interfaculty Institute for Biochemistry, Tuebingen).

By mutating Ad11-I282L, a three-fold decrease in affinity for CD46 was observed using ITC. Thus, Ad11-R279Q/S and Ad11-I282L are the only mutations that displayed an altered affinity in our ITC setup. With the higher sensibility in SPR there could still be minor differences in affinity that we could not detect. The data indicate that the amino acid present at position 282 is the second most important, after position 279, for determining the affinity for CD46.

Table 6. Affinity of Ad11 mutants for CD46 measured using ITC and BiaCore. Experiments performed by Steffen Müller (Interfaculty Institute for Biochemistry, Tuebingen).

Protein interaction		BiaCore affinity	Solution affinity analysis	ITC affinity analysis	Structure determined
Knob	CD46	K_D [M]	K_D [M]	K_D [M]	Resolution (Å)
Ad11-N245S	CD46 SCR1-2	**n.d**	**n.d**	**n.d**	1.6
Ad11-R279Q	CD46 SCR1-2	1.5 e-06	0.8 e-06	None	2.55
Ad11-R279S	CD46 SCR1-2	**n.d**	**n.d**	None	**n.d**
Ad11-I282L	CD46 SCR1-2	**n.d**	**n.d**	6.8 e-09	1.8
Ad11-N283S	CD46 SCR1-2	**n.d**	**n.d**	1.8 e-09	1.72
Ad11-D284S	CD46 SCR1-2	**n.d**	**n.d**	1.8 e-09	**n.d**
Ad11-R280G	CD46 SCR1-2	**n.d**	**n.d**	None	**n.d**
Ad7-Q279R	CD46 SCR1-2	0.5 e-06	0.1 e-06	**n.d**	1.55

4.2.4.2 Crystallization of mutant knobs

During the crystallization trials not all mutants gave well-diffracting crystals. The mutated knobs for which crystals could be grown were crystallized using the hanging drop method at 20 °C, and crystals were obtained after one week. These knobs were crystallized over a reservoir solution as follows: Ad11-I282L 20% (w/v) PEG 3350 0.2 M Hepes pH 7.4, Ad11-N283S 30% (w/v) PEG3350 0.2 M Tris pH 7.0, Ad11-N245S 16% (w/v) PEG 6000 0.2 M MES pH 6.1, Ad11-R279S 25% (w/v) PEG3350 0.2 M Tris pH 7.0, Ad7-Q279R 26% (w/v) PEG3350 0.2 M Tris pH 8.0. Data for all the crystallized knobs were collected at beam line X06SA at SLS and refined to excellent statistics using Refmac5 (CCP4, 1994) after scaling and integration using the HKL package (Otwinowski, 1997) (Table 7 and Appendix 7.3).

Table 7. Essential crystallographic statistics for the five crystallized mutant knobs. More detailed statistics can be found in Appendix 7.3.

Data quality	**Ad11-I282L**	**Ad11-N283S**	**Ad11-N245S**	**Ad11-R279S**	**Ad7-Q279R**
Space group	I23	I23	I23	P32	$P2_12_12$
Unit cell Dimentions (Å)	a=102.63	a=101.41	a=101.66	a=b=148.65 c=74.44	a=83.13 b=87.8 c=79.1
Resolution Range (Å)	72.6-1.8 (1.8-1.86)	71.8-1.72 (1.72-1.78)	71.8-1.6 (1.6-1.66)	129-2.55 (2.55-2.64)	79.06-1.55 (1.55-1.61)
Completeness (%)	98.23 (86.2)	99.74 (99.4)	99.9 (100)	98.97 (98.1)	98.2 (95.8)
Redundancy	16.8 (1.66)	6.2 (2.7)	7.3 (7.1)	3.2 (2.9)	5.4 (5.3)
R_{Sym}(%)[1]	6.4 (38.2)	8.5 (38.2)	7.4 (44.0)	9.7 (38.9)	6.3 (38.9)
I/□	7.2 (5.7)	16.65 (1.22)	14.2 (1.8)	7.42 (1.2)	12.8 (1.4)
Refinement statistics					
R_{Work}(%)[2]	20.6	17.8	19.4	21.3	23.1
R_{Free}(%)[2]	23.8	22.2	22.0	23.6	25.4

Highest-resolution shell is shown in parentheses.

1-Defined in the Methods section 3.7.7
2-Defined in the Methods section 3.7.10
Free set contains 5-10% of reflections (see Methods section 3.7.10).

The overall folds of the mutant knobs are identical to that of the wt. The conformation of some loops differs slightly in the area close to the mutation, mostly around the HI- and DG-loops (Figure 45). Observed alterations in affinity can thus be connected to the mutated amino acid and not an altered overall conformation. In Figure 45, the mutations Ad11-N283S and Ad11-N245S are not included, since the loops were not significantly changed in comparison to the Ad11 knob.

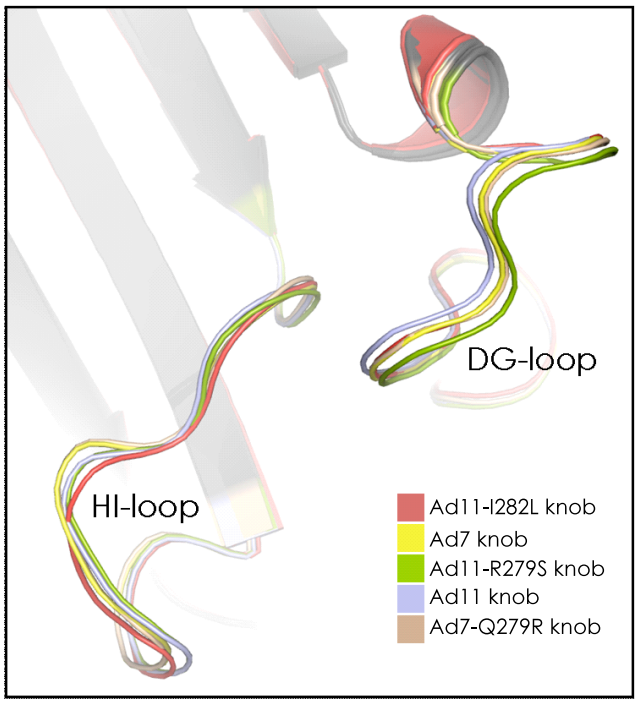

Figure 45. Close-up view of the HI-loop, with superimposed structures of knobs of Ad11 (blue), Ad7 (yellow), Ad11-R279S (green), Ad11-I282L (red) and Ad7-Q279R (wheat). All five proteins superimpose very well. Changes are seen in the distance between the two loops, suggesting that the mutations distort the overall shape of the epitope, thus affecting the affinity. Figure made in PyMOL (DeLano, 2002).

4.2.4.3 Ad11-I282L

The mutation Ad11-I282L places the amino acid of the corresponding Ad7 knob at position 282 (Figure 46A). Even though this amino acid of Ad11 is not directly involved in interactions to CD46, in our complex structure, it could be of importance due to its hydrophobic properties. The electron density is excellent in the entire loop.

4.2.4.4 Ad11-N283S

The entire loop has very well defined electron density (Figure 46B). By mutating Ad11-N283S, the hydrogen bond between CD46-H43 and Ad11-N283 should be abolished. This amino acid is conserved between the Ad11 and the Ad7 knob. This mutation will thus not indicate why Ad7 binds CD46 with a much lower affinity. It was made to define key residues of the interaction of the Ad11 knob with CD46. The overall fold of the knob is identical, with only minor alternations in the HI-loop.

4.2.4.5 Ad11-N245S

The Ad11-N245S mutants was analyzed based on the hypothesis that the hydrogen bonding between Ad11-N245 and Ad11-R279 would stabilize the position of the Arg, locking the DG- and HI-loop down and creating the crucial platform for CD46 binding. The density for the mutated amino acid is excellent, as well as for all other amino acids in close proximity (Figure 46C). The position of the loop is not altered and the affinity measured using ITC is identical to the wt knob.

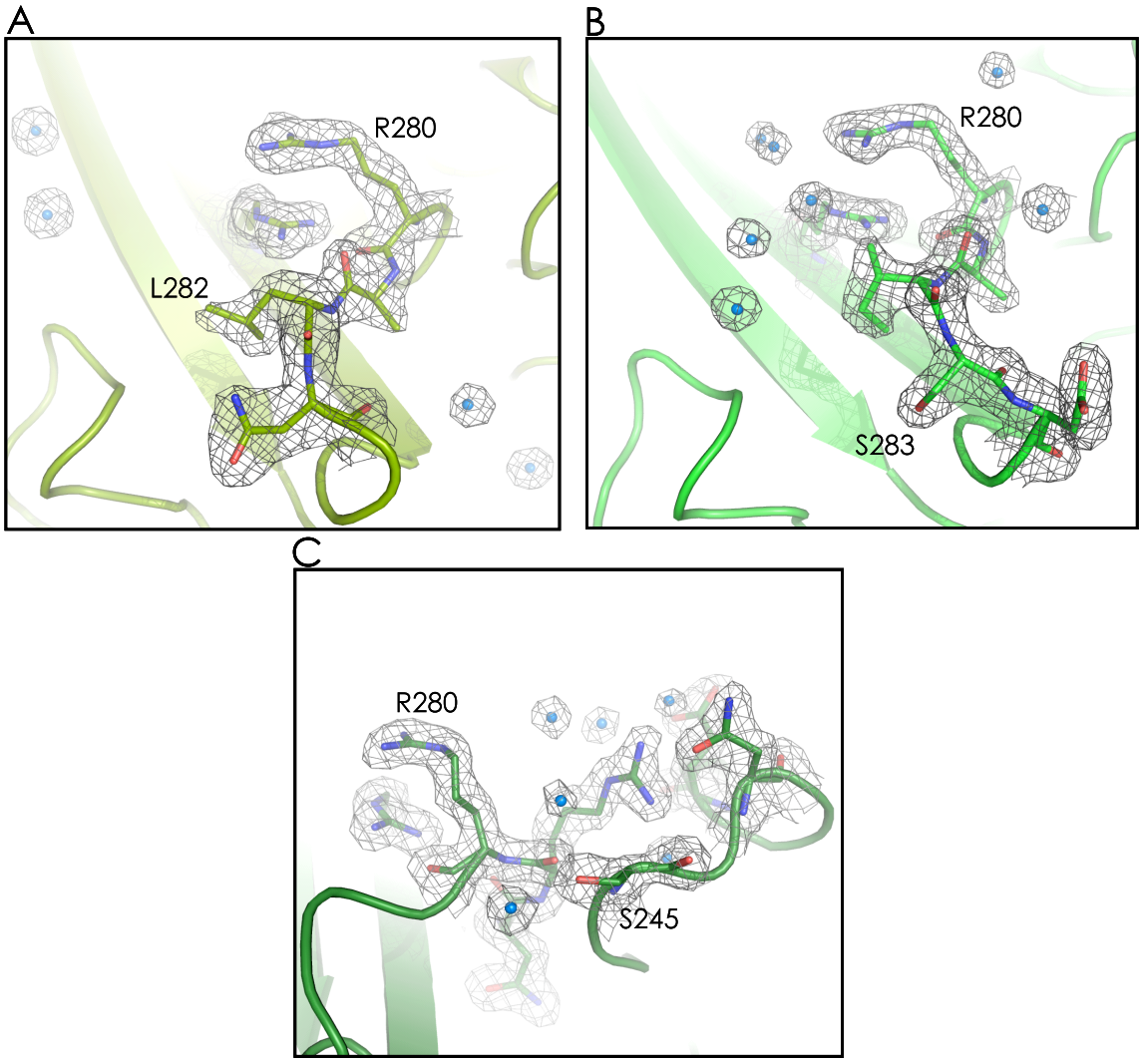

Figure 46. Close-up view of the HI-loop in (A) Ad11-I282L, (B) Ad11-N283S and (C) Ad11-N245S knobs, with the corresponding $2F_{obs}$-F_{calc} electron density maps at a contour level of 1 σ. Figure made in PyMOL (DeLano, 2002).

4.2.4.6 *Ad11-R279S*

The biggest impact on the relative orientation of the HI- and DG-loops was observed when Ad11-R279 was mutated to a Ser. The distance between the HI- and DG-loop is significantly increased. The mutation abolishes the interaction between the HI- and the DG-loop (Figure 47A and Figure 32C). Even though the mutant protein crystals diffracted less well, the structure is still reliable, with good statistics (Table 7 and Appendix 7.3) and clear electron density. Most likely, a high affinity interaction is not possible due to altered surface complementarity.

4.2.4.7 *Ad7-Q279R*

The structure of the "rescue" mutant of Ad7, which binds CD46 with high affinity, could be determined with excellent statistics (Table 6 and Appendix 7.3). In the crystal structure, the stabilization of the two loops is identical to the Ad11 wt knob (Figure 47B). Interestingly, the mutation of Ad7-Gln279 to Arg does not affect the orientation of the two loops, just the affinity for CD46.

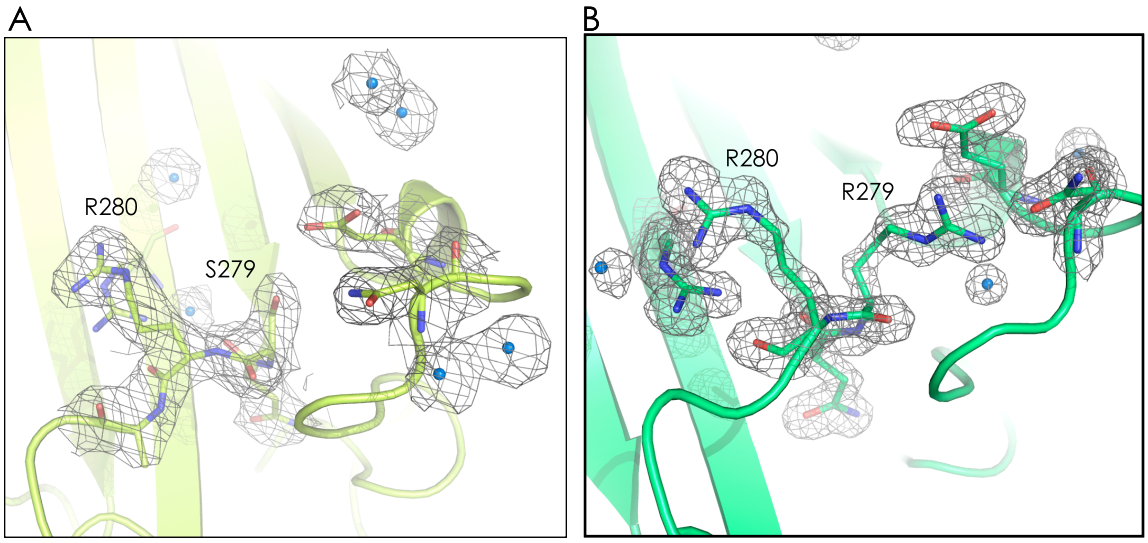

Figure 47. Close-up view of the HI-loop in (A) Ad11-R279S and (B) Ad7-Q279R with the corresponding $2F_{obs}$-F_{calc} electron density maps at a contour level of 1 σ. Figure made in PyMOL (DeLano, 2002).

4.2.5 Structural and functional characterization of Ad35 knobs

4.2.5.1 Expression of Ad35 knobs

The Ad35 and Ad35short knob proteins were expressed and purified as described in the Methods sections 3.3 and 3.4. Both knobs were functionally active as judged by the ability to bind CD46 in our gel filtration assay (data not shown).

4.2.5.2 Affinity studies of the Ad35 interaction with CD46

We measured the affinity between the Ad35 knob and both CD46 fragments using ITC and SPR. Our results show that the Ad35 knob affinity for CD46 is about 14 nM, the average of two measurements (Table 8 and Figure 44), and therefore similar to that of the Ad11 knob-CD46 interaction. As with the other knobs, the affinity does not differ between the two forms of CD46. Furthermore, epitope mapping experiments in solution indicate that the Ad35 knob-binding epitope of CD46 overlaps with the one used by the Ad11, Ad7 and Ad14 knobs. We therefore conclude that, like the other strains, Ad35 binds exclusively to the N-terminal two domains of CD46, SCR1-SCR2. This was also shown previously (Fleischli et al., 2005; Gaggar et al., 2005).

Table 8. Affinity measurements of the interaction between Ad35 knob and CD46. Experiments performed by Steffen Müller (Interfaculty Institute for Biochemistry, Tuebingen).

Protein interaction		Steady-State-Analysis	Kinetic Analysis			Solution affinity Analysis	ITC Affinity
immobilized	in solution	K_D [M]	K_D [M]	k_{on} [$M^{-1}S^{-1}$]	k_{off} [S^{-1}]	K_D [M]	K_D[M]
Ad35 knob	CD46-SCR1-2	n.d. 17 e-09	11 e-09 17 e-09	3.4 e06 1.5 e06	0,036 0,025	19 e-09	3.5e-9 4.5e-9
Ad35 knob	CD46-SCR1-4	n.d. 17 e-09	11 e-09 17 e-09	3.4 e06 1.5 e06	0,036 0,025	27 e-09	n.d

4.2.5.3 Crystallization of the Ad35 knob

The affinities of the Ad11 and Ad35 knobs for CD46 are similar. However, sequences of the two knobs are not especially well conserved, even in the area of the Ad11 knob that engages CD46. Still, the similar behavior of the two knobs with respect to binding CD46 suggests that some variation in sequence, and

possibly surface structure, of CD46-binding residues can be tolerated. We therefore set out to initiate structural studies of the Ad35 knob alone and in complex with CD46. We performed extensive crystallization trials with the longer Ad35 knob protein comprising amino acids 118-325 (see Methods section 2.2.6) at 20 °C as well as 4 °C, and several different crystal forms were obtained. Unfortunately, all crystal forms diffracted relatively poorly. The best crystals diffracted only to about 3.8 Å (Table 9). Although a structure determination at 3.8 Å resolution is possible, it was not pursued since the crystals had an extremely large unit cell that contained between 10 and 15 copies of the Ad35 knob trimers as estimated by the Matthews coefficient (Matthews, 1968). In the meantime, the crystal structure of an Ad35 knob was solved by others, to a resolution of 2.0 Å (Wang et al., 2007). Interestingly, this published crystal structure was obtained from a crystallization condition that is similar to one with which we also obtained crystals. However, our crystals did not diffract well, probably because our protein had five extra N-terminal amino acids that were not present in the protein crystallized by Wang et al. Very likely, these N-terminal amino acids impede crystallization.

4.2.5.4 Crystallization of the Ad35 knob:CD46 complex

In order to define the interaction between the Ad35 knob and CD46, we also pursued the crystallization of this complex. Purification was done using the approach described in detail for the purification of the Ad11 knob-CD46 complex in the Methods section 3.4.3. We performed extensive crystallization trials with the longer version of the Ad35 knob in complex with CD46 SCR1-SCR2, and obtained several crystal forms that all diffracted very poorly, to about 7 Å. However, once the crystal structure of a shorter version of the Ad35 knob was published (Wang et al., 2007), we decided to test whether using this construct would produce better-diffracting crystals of the complex with CD46. Unfortunately, while we were able to also produce crystals of the complex, they did not diffract beyond 7 Å and thus did not allow us to determine the structure.

Table 9. Essential crystallographic statistics for the Ad35 knob.

Data quality	**Ad35**
Space group	$P2_12_12_1$
Unit cell Dimentions (Å)	a=166.92 b=186.63 c=314.56
Resolution Range (Å)	40-3.8 (3.8-3.94)
Completeness (%)	94.2 (88.6)
Redundancy	6.9 (7.2)
R_{Sym}(%)[1]	12.9 (45.8)
I/□	6.22 (1.95)

Highest-resolution shell is shown in parentheses.

1-Defined in the Methods section 3.7.7

5 Discussion

5.1 Interactions of pathogens with CD46

Understanding the precise mode of interaction with cellular receptors is essential for revealing the mechanism of viral pathogenesis, and also for the development of novel antiviral agents as well as vaccines. Several groups of pathogens use CD46 as a cellular receptor. Measles virus binds to the two most membrane distant repeats, SCR1 and SCR2 (Casasnovas et al., 1999), while human herpes virus 6 binds to SCR2 and SCR3 (Greenstone et al., 2002). In addition, *Neisseria gonorrhoeae* pili bind to SCR3 and the STP region (Kallstrom et al., 2001), whereas the M protein from streptococci A strains binds to SCR3 and SCR4 (Giannakis et al., 2002). We used a combination of functional and structural studies to characterize the interaction between several species B Ads and CD46. We find that the interaction of CD46 with Ads is most similar to that reported for measles virus, as in both cases the same region of the receptor (domains SCR1 and SCR2) is used. The observed interactions could easily occur in the context of an entire virus particle and a cell surface bearing CD46. Both the measles virus hemagglutinin and the Ad fiber are large, multimeric proteins and thus interaction with the outermost, membrane-distal region of CD46 may be preferred in both cases. Thus, the results presented in this thesis have relevance also for the interactions of CD46 with other pathogens.

5.2 Structure of the Ad11 knob:CD46 complex

5.2.1 Implications of the structure

We solved the structure of the knob of Ad11, a member of the species B Ads, in complex with CD46 SCR1-SCR2 to a resolution of 2.85 Å by X-ray crystallography. CD46 binds two Ad knob protomers, making more extensive contacts with one of them. The area of CD46 that is recognized by the Ad11 knob is exposed and distant from the membrane, and could easily be engaged by an approaching knob. A striking feature in the complex is the surface complementarity, occluding

a total of 1600Å^2 from solvent. In the crystal structure of ligand-free CD46 SCR1-SCR2, an angle of ~60° was observed between SCR1 and SCR2. Since a similar angle was present in multiple copies of the protein and in two crystal forms, the bent shape is unlikely to be a crystallization artifact but rather represents the conformation of the unliganded protein at the cell surface. The Ad11 knob binds to the interface between SCR1 and SCR2 making contacts to both repeats, thus reshaping CD46 and causing it to adopt an elongated rod like shape (Persson et al., 2007). The Ad11 affinity for CD46 was measured using ITC and is in the range of 2 nM, and thus about 10 fold higher than the interaction between Ad5 and its receptor CAR (Kirby et al., 2000).

Interactions in the complex involve a large number of residues. About 50% of contacts are mediated through backbone atoms, hinting at a potential strategy that allows the virus to alter its surface structure through mutation without affecting its interaction with CD46. The long and flexible HI and DG loops are stabilized by hydrogen bonds between Arg279 and Asn247/Gln250 respectively, which form a platform for CD46 binding. A key observation is a parallel stacking of the guanidinium groups of Ad11 arginines Arg279 and Arg280, in the immediate vicinity of CD46 residue Phe35. The positioning of the two arginine side chains would be expected to be non-favorable as the two positively charged guanidinium groups would repel each other. However, non-covalent interactions, such as the Arg-Arg stacking, can be important in determining the structure and function of proteins. A similar interaction to the Arg-Arg stacking is the cation-π interaction, which is increasingly recognized as an important non-covalent interaction determining drug specificity and protein function (Gallivan and Dougherty, 1999). Energetically, a typical cation-π interaction can be stronger than a normal salt bridge (Zacharias and Dougherty, 2002), and it is often observed between guanidine groups of Arg and aromatic ring systems in, for example, tyrosines or tryptophans (Burley and Petsko, 1986). The delocalized electrons of the aromatic ring act as hydrogen bond acceptors, and can accept hydrogens from the $-NH_3$ group in the arginine sidechain (Flocco and Mowbray, 1994). The interaction has effects on the pK value of neighboring amino acids, thus altering the charge distribution. As the stacking

probably affecs the pK values in the direct environment it is plausible to assume that one of the two arginines is deprotonated even though the pk value for isolated arginines is very high (Flocco and Mowbray, 1994). Most likely, Arg279 is deprotonated as Arg280 directly interacts with Glu63 in CD46 and therefore likely keeps its charge.

Interestingly, an additional Arg-Arg stacking is observed in the structure of the uncomplexed Ad11 knob which we determined to high resolution. In this case, the guanidinium groups of Arg280 and Arg291 are stacked on top of each other. The stacking is anti-parallel and almost perfectly planar, with an average distance of 3.9 Å between atoms facing each other. The Arg-Arg stacking may act as a molecular switch. Arg280 is stacked against Arg291 in the unbound knob (off-position), whereas it is stacked against Arg279 in the structure of the Ad11 knob in complex with CD46 (on-position).

5.2.2 Comparison with the Ad35 knob

Ad11 and Ad35 both use CD46 as a receptor. The crystal structure of the Ad35 knob was recently published (Wang et al., 2007). Both structures superimpose very well, suggesting that a conserved mode of interaction with CD46 exists between Ad11 and Ad35 (Figure 48). The affinity of both knobs for CD46 is in the same range of 12 nM (measured using SPR). It is noteable, though, that the Ad35 knob lacks the Arg-Arg stacking observed in the uncomplexed Ad11 knob structure. The amino acid corresponding to Ad11 Arg280 is Arg279 in Ad35. This amino acid is already in the "on-position" and thus appears to be readily available for the cation-π interaction with CD46-Phe35. It appears that the "off-position" in Ad35 is not favored for Arg279 as there is no arginine equivalent to the Ad11-residue Arg291 in the Ad35 knob. We are currently working on the crystallization of CD46 in complex with the Ad35 knob in order to define the basis of interaction for this Ad type.

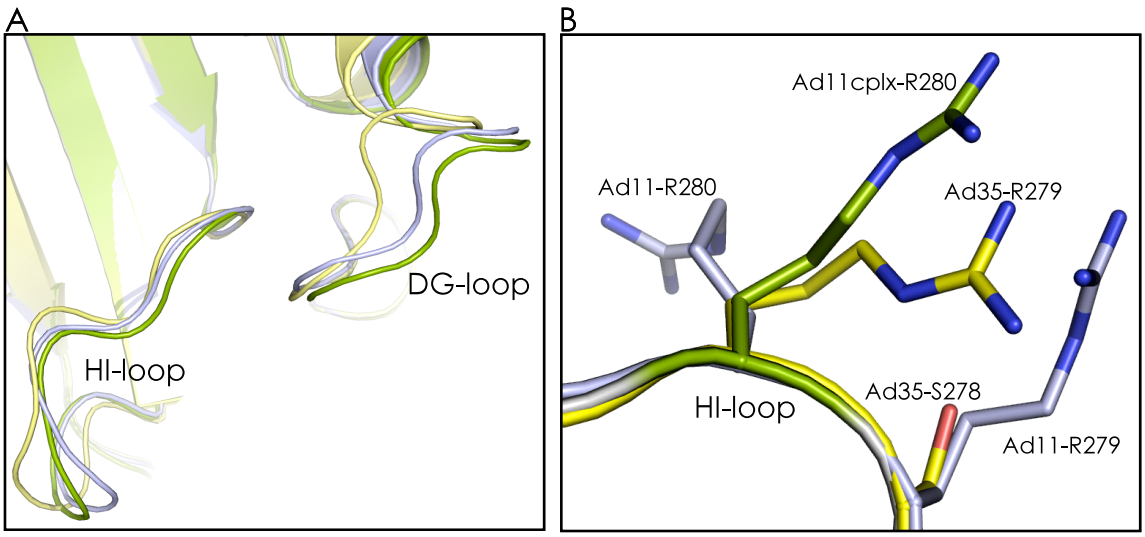

Figure 48. Comparison of the structures of the Ad11 knob, the Ad11 knob:CD46 complex and the Ad35 knob. (A) Superimposition of the unliganded Ad11 knob (blue), liganded Ad11 knob (green), and unliganed Ad35 knob (yellow). (B) Close-up view of the HI-loop using the same superposition.

5.2.3 Comparison with the Ad12-knob:CAR complex

The location and architecture of the CD46-binding surface is completely distinct from that used by other Ads to bind to CAR (Figure 49). The structure of the complex between the Ad12 knob and the N-terminal domain of CAR (CAR-D1) (Bewley et al., 1999) shows that CAR binds at a region near the AB-loop of the Ad12 knob. The AB-loop is located on a different face of the knob, almost exactly opposite from the site of CD46 attachment. Ads therefore appear to have evolved to bind different receptors not by subtly modifying one binding surface but by creating an alternative site while deconstructing the first. Non-CAR binding Ads typically carry an insertion in the AB-loop, which likely helps to prevent binding to CAR. Conversely, CAR-binding Ads have very short DG- and HI-loops, eliminating most of the possible contact points for CD46. Significantly, the mode of binding is different as well. The CAR-binding surface of Ad12 features several discrete, smaller contact points separated by large solvent-filled cavities (Bewley et al., 1999), whereas the CD46-binding surface of Ad11 knob is extensive, continuous, and devoid of solvent molecules.

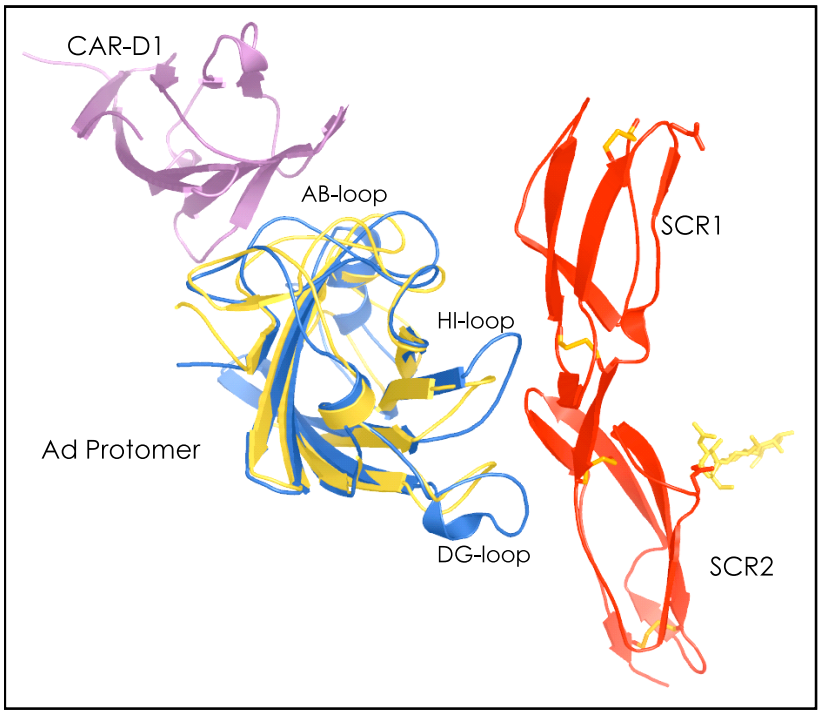

Figure 49. Comparison of the mode of interaction of Ad knobs with CAR and CD46. The structures of the Ad12 knob-CAR (Bewley et al., 1999) and Ad11 knob-CD46 complexes were superimposed using all corresponding Ad knob residues. Only one Ad knob monomer is shown in each case, although a second monomer also contributes some contacts in both complexes. The N-terminal domain of CAR (D1) binds to a surface that mostly involves the AB-loop of the Ad12 knob monomer, whereas CD46 lies across a platform that is formed by the DG- and HI-loops of Ad11 knob. CAR is drawn in pink, the Ad12 knob in yellow, the Ad11 knob in blue, and CD46 SCR1-SCR2 in red. The glycans and disulfide bonds of CD46 are shown in yellow.

5.2.4 Comparison with the Ad37-knob:sialic acid complex

The Ad37 knob has been reported to bind to CD46, CAR, as well as α2,3-sialic acid (Arnberg et al., 2000a; Burmeister et al., 2004). However, superimposition with the Ad11 knob indicates that if the Ad37 knob binds CD46, it must do so with different epitopes that those seen in the Ad11-CD46 complex. The HI- and DG-loops in the two proteins are rather different, with the HI-loop of the Ad37 knob having a drastically altered conformation that would preclude engagement of CD46 as we see it in the structure of the complex produced with the Ad11 knob. Interestingly, the shaft length of the fiber is shorter in the D-types that bind sialic acid (Ad9, Ad19 and Ad37), and also in the B types. Published data indicate that a high flexibility of the shaft is required for an interaction with CAR since CAR is a

component of tight junctions and thus may not be accessible by fibers with a more rigid, shorter shaft (Wu et al., 2003). The sialic acid binding knobs and the CD46 binding knobs could therefore share a common ancestor that had a shorter shaft and did not bind to CAR. From this ancestor, knobs binding sialic acid may have evolved by creating a positively charged region at the top of the knob that interacts with sialic acid, and knobs binding CD46 may have evolved towards forming a shorter HI-loop that would allow for interactions with CD46. This could also be one explanation for the observations that Ad37 binds CD46 (Wu et al., 2004), since some shared features could remain that under optimal conditions may allow an interaction with CD46, probably via a mechanism that is different from the one seen in the Ad11 knob complex.

5.3 Interactions of Ad7 and Ad14 with CD46

At the outset of our study, it was unclear whether Ad7 binds to CD46 or not. The literature on this topic is not conclusive as some authors reported that Ad7 does bind (Fleischli et al., 2007), whereas other studies reported that CD46 does not serve as a receptor for Ad7 (Marttila et al., 2005; Segerman et al., 2003b). We therefore decided to investigate if Ad7 can interact with CD46 using SPR and, secondly, if the binding can be blocked by soluble knobs in a binding assay using radioactive virions. At the same time we investigated the binding characteristics of Ad14, which is highly homologous in sequence to both Ad7 and Ad11. We find that both the Ad7 and Ad14 knobs bind CD46 with an affinity in the range of 30 μM. However, the interaction occurs in a very fast, square wave like mode. Although the affinity is well within the range for a productive interaction, the kinetics suggest that is it unlikely that these two knobs bind CD46 in vivo as the complexes form only transiently and fall apart quickly. The most likely explanation of this binding behavior is that key residues for a stable interaction are missing. The two molecules engage each other and dissociate from each other so quickly that there would most likely not be enough time for the secondary interaction with cell-surface integrin receptors that triggers uptake. It is certainly possible that CD46 functions as a cellular receptor for Ad7 and Ad14, on certain cell types and under optimal conditions. These conditions

could be hard to reproduce in an *in vitro* setup. In addition, CD46 could function as an adhesion-strengthening receptor that is either only engaged once the primary receptor, such as the receptor X described by Tuve et.al., 2006, is engaged, or that facilitates the engagement of receptor X. It is also possible that Ad7 binds to CD46 but fails to elicit the structural change between SCR1 and SCR2. Without this change, a high-affinity interaction can not occur as the surface of both SCR1 and SCR2 contribute residues to the interface with Ad knobs.

The blocking experiment indicates that the three types share the same epitope for binding to CD46. Soluble Ad11 knobs effectively blocked the binding of both radioactively labeled Ad11 and Ad7 particles. However, soluble Ad7 and Ad14 knobs did not block the attachment of radioactively labeled Ad11 virions. Even with high concentrations of Ad11 total blocking could never be observed, most likely due to unspecific binding or the engagement of a secondary receptor (Wickham et al., 1990). The amount of unspecific binding varies between cell types and virus strains. A more efficient inhibition can probably be achieved by measuring infectivity, where productive interactions alone are quantified. The observed much faster interaction between Ad7/Ad14 and CD46 could explain why Ad7 and Ad14 knobs do not block the binding of Ad11 particles. Due to the much higher turnover of the Ad7/Ad14 interaction, Ad11 particles will accumulate on the surface of the cell. During washing more of the Ad7/Ad14 knobs or particles will thus be washed away. The observed difference in the binding experiment between Ad11 and Ad7/Ad14 could be due to the experimental setup.

Our data indicate that all three knobs bind CD46 using partially, or completely, overlapping epitopes our results do not answer ithe question whether the Ad7 and Ad14 interaction with CD46 is physiologic, leading to replication of viral genes.

5.4 The crystal structures of the Ad7 and Ad14 knob

In order to define the structural basis for CD46 binding, structures of Ad7 and Ad14 knobs were determined. Both knobs are similar in sequence to the Ad11 knob but bind CD46 with drastically different affinities and kinetics. Both structures were determined at high resolution and thus possess high accuracy. The two structures superimpose very well with the unliganded structure of the Ad11 knob. The anti-parallel stacking of Arg280 and Arg291, which was observed in the unliganded Ad11 knob structure, is present in both Ad7 and Ad14. Thus, Arg280 is in the "off position" in all three unliganded knobs. Interestingly, Ad11 residue Arg279, which stabilizes the Arg280 side chain in the "on position" in the complex with CD46, is replaced with a glutamine in both Ad7 and Ad14 knobs. Since a glutamine is not charged and shorter than the arginine side chain, this residue may be the critical determinant of binding as suggested (Gustafsson et al., 2006). It would not be favorable for Arg280 to leave the "off position" in Ad7 and Ad14 as no productive interaction with Gln279 would be possible.

In order to test this hypothesis, a "rescue" mutant of Ad7 was constructed that carries an arginine at position 279. Interestingly, the affinity of the Ad7 knob for CD46 was drastically increased, to about 50% of that observed for the Ad11-CD46 interaction. This indicates that the Arg279 residue indeed serves as the major determinant of binding. Other, surrounding amino acids also contribute to stability of complex formation, but they are not major determinants of affinity. The key amino acid for a stable complex is therefore the arginine at position 279.

Taken together our data indicate that Ad7 and Ad14 interact with CD46 but probably in a different way than is seen with Ad11. Thus, the presence or absence of a single amino acid appears to determine whether CD46 can be bound with high affinity.

5.5 Mutations at the Ad11 knob:CD46 interface

In order to define the contributions of Ad11 knob residues for binding CD46, we performed a mutational study. Key amino acids of the Ad11 knob that were identified as interacting partners for CD46 were mutated to either serine or glycine, and in some cases to the corresponding amino acid in the Ad7 knob. Interestingly, with the exception of mutations of Arg279, very few mutations had significant effects on the overall affinity for CD46. The results from the mutational studies therefore strengthen our finding that Arg279 is the key determinant of binding to CD46.

5.5.1 Mutation of Ad11-R279S and Ad11-R279Q

As expected, the mutation of Ad11-R279 to Gln or Ser had a large effect on the affinity for CD46. The affinity of the Ad11 knob was reduced from 12 nM to 500 nM in both cases (measured using SPR), indicating that the presence of an arginine at position 279 is key to a very high affinity interaction. On the other hand, these data also show that additional residues are important for binding because an affinity of 500 nM can still be considered high. Several of these additional residues were mutated in subsequent experiments (see below). The affinity of the Ad11-R279S mutant for CD46 is still about 100 fold higher than those of the Ad7 and Ad14 knobs, which also lack the arginine at position 279. Finally, these results show that the same affinity is seen with a serine and a glutamine at position 279. This confirms that the type of amino acid (large or small) does not matter much and that the switch of Arg280 from the "off" to the "on" position is not simply prevented by steric blockage with the larger glutamine side chain. The serine side chain at position 279 is too small to block the switch, and Arg280 could easily fit next to it.

5.5.2 Mutation of Ad11-I282L

The isoleucine at position 282 faces towards CD46 residues Lys29 and Tyr36, making contacts with the hydrophobic portions of both. Mutation of Ile282 to a Leu reduced the affinity of Ad11 knobs for CD46, measured using ITC, five fold.

The most likely explanation is that, while Ile and Leu are both hydrophobic and have a similar molecular weight, the shape of the side chain matters in order to allow for a tight packing of both partners in the complex. Thus, the different overall shape of the leucine side chain likely affects the surface complementarity, thus lowering the affinity for CD46.

5.5.3 Mutation of Ad11-R280G

In the complex between Ad11 knob and CD46, the hydrophobic portion of the Arg280 side chain packs against the Phe35 sidechain of CD46. The guanidinium group of Arg280 forms a salt bridge with Glu63 of CD46. Moreover, the guanidium group also stacks next to the side chain of Arg279, forming an Arg-Arg sandwich as described above. The mutation of Ad11-R280 to glycine completely abolished binding to CD46, confirming the absolutely critical importance of this arginine for the interaction with CD46. In addition, the introduction of a glycine residue, could also have increased the flexibility of the HI-loop, which may have contributed to the complete loss of binding.

5.5.4 Mutation of Ad11-N283S

The Asn283 side chain forms a hydrogen bond with the backbone carbonyl atom of CD46-Y28. Mutating this residue to serine did not appreciably alter the affinity for CD46, which was measured using ITC. The mutation did probably not affect the affinity due to its position between the two solid interactions Ad11-D284 to CD46-H43 and Ad11-R280 to CD46-E63. The mutation would create a cavity in which a water molecule could bridge the contact, thus not changing the affinity. Affecting the affinity by a mutation at this position would require a large bulky amino acid that would produce clashes between the two proteins.

5.5.5 Mutation of Ad11-D284S

In the complex, Asp284 forms a hydrogen bond to CD46-H43 and seals off the binding interface at one end. The Ad7 knob has an Asn this position, which would be able to make a similar contact, although the salt bridge would be replaced with a hydrogen bond.. The Ad14 knob has an Ala in this position, which would not be able to contact the His. As Ad14 and Ad7 knobs bind CD46

with similar (low) affinity, position 284 does not seem to be a "hotspot" that defines the high-affinity interaction with CD46. However, the Ad11 knob D284 interaction with CD46-H43 was thought to at least contribute somewhat to the affinity. Surprisingly, the mutation did not affect the affinity in a measurable way (measured with ITC). A possible explanation is that a Ser at position 284 could also interact with the CD46-H43, perhaps via a bridging water molecule. The CD46-H43 side chain is fairly exposed, and modelling suggests that it could adopt an orientation that could engage the serine.

5.5.6 Mutation of Ad11-N245S

In the Ad11 knob-CD46 complex, Asn245 is engaged in a hydrogen bond with the guanidinium group of Arg280. This residue is located on the side opposite of that occupied by Glu63 of CD46, and it does appears to help fix the Arg280 side chain in place. However, this amino acid is conserved in Ad11 and Ad7, and thus probably not a major determinant for a high affinity interaction to CD46. As expected, mutating it did not alter the affinity of the Ad11 knob for CD46, indicating that this residue is not a determinant of binding to CD46.

5.5.7 Mutation of Ad7-Q279R

Mutation of the Ad7-Q279 to an arginine has been suggested to partially restore the binding capacity to CD46 (Gustafsson et al., 2006). If the presence of an arginine at position 279 is required to allow the Arg280 to switch from the "off"to the "on" position, then a mutation of Ad7-Q279R should result in relatively tight binding of the Ad7 knob to CD46. This was confirmed by our studies, wich show that the mutant Ad7 knob has nM affinity for CD46.

5.5.8 Summary of the mutational analyses

The interaction between Ad11 and CD46 covers an extensive interface, occluding a total of 1600 $Å^2$ from solvent. Many interactions are main chain interactions. These interactions can therefore not be probed through mutagenesis experiments. However, several side chains form contact points between the two proteins. Mutating these residues one at a time will in most cases result in only a small (or no) change. This is in keeping with the observation

that many contacts, together, provide the high affinity seen for the complex. Change of any one amino acid will perhaps reduce the affinity somewhat, but the many remaining contacts will be able to absorb this loss and still be able to bind CD46 tightly. The major exceptions are of course the Arg280 and Arg279 residues, both of which need to be present for a productive interaction with nanomolar affinity. Without Arg280 no interaction is possible at all, indicating that charge-charge interactions between Arg280 and CD46-residue Glu63 are a critical component of complex formation. Thus, the following scenario emerges from our studies. Charge-charge interactions cover a longer distance than hydrophobic interactions or hydrogen bonds. It is therefore conceivable that the Arg280 interaction with CD46 serves as the initial attraction force once the molecules are in closer vicinity– if it is not present the initial contact will not be made at all. Once the Arg280 has been engaged, the remaining contacts are made, providing additional energy through the fine-tuning of interactions of a hydrophobic (e.g., Ile282) or polar (e.g., Asn245, Asp283) nature. Because there are many of these secondary interactions, mutation of any one of them does not yield dramatic effects. The role of Arg279 is critical in that it stabilizes and orients Arg280 in a position (the "on"-position) so it can make this initial contact. In the Ad7, Ad11 and Ad14 knobs, the Arg280 side chain is in the off position prior to binding CD46. Very high affinity interaction with CD46 is possible only for Ad11 knobs, which do have an arginine at position 279. Without it, as in the Ad11-R279S mutant, the Arg280 probably does not want to leave its "off" position.

5.6 Comparison of ITC and SPR

In this work, we have presented affinity data obtained with both ITC and SPR. Initially, ITC was used to determine affinities as SPR equipment was not available. As measuring interactions using SPR became possible due to the purchase of a BiaCore 2000 system, we changed methods. Initially, this was done primarily in order to reduce the amount of required protein. However, as some proteins were remeasured using SPR the measured affinity did not agree fully with the ITC data. With high affinity data in the lower nM range a 10 fold higher affinity value was obtained using ITC, which can be considered as the same order of magnitude.

However, for lower µM affinities of the Ad7 and Ad14 knobs we did not observe any binding using ITC.

ITC relies on measuring heat that is generated or lost during an interaction (see Methods section 3.5). By contrast, SPR detects a change in mass close to the chip surface (see Methods section 3.5). In our experimental setup for ITC, we assumed a high affinity for the Ad11 knob interaction with CD46, and the same setup was later used for all the mutants as well as for Ad7 and Ad14 knobs. It is very likely that this setup does not allows a detection of the lower affinity, and that if the setup would be optimized some affinity could be measured. We did not alter the setup to detect this affinity since the consumption of protein would be too large. Measuring Ad11 knob affinities required about 2 ml of a 2 µM Ad11 knob solution and 350 µl of a 25 µM CD46 solution. In order to measure the much weaker-binding Ad7 and Ad14 knobs, we would have needed a >1000 fold higher concentration of CD46, which is not possible. Additionally, the mutations were designed to abolish favorable interactions in the complex, thus reducing the energy released to the system. This would have required even higher concentrations of proteins. For these reasons, we switched to SPR.

SPR offered several advantages: (i) we could use smaller volumes of protein with (ii) lower concentrations and did not have to (iii) rely on energy released but on detecting a change in mass. Binding could also be (iv) observed in real time, and the measurement could be interrupted in order to save protein if no binding was detected. We connected the Ad knobs to the chip to avoid measuring avidity, which occurs when several proteins on the chip interact with one protein molecule in the solution. Avidity makes the binding model fit less well, with a risk of biasing the data. We also used CM5 chips for covalently attaching the knobs, which made the setup more expensive but reduced nonspecific binding of CD46 in the flow cells. However, each experiment was always performed in duplicates. The affinity data recorded using SPR can also be cross-validated by using several experimental setups. We collected, in duplicates, affinity data using two different setups, solution affinity and steady state affinity. Our data correlate well and can be considered as reliable.

5.7 Conclusions

The structure of the Ad11 knob in complex with CD46 defined, for the first time, how CD46 is recognized by a pathogen. Many pathogens use CD46 for attachment, but the mode of interaction has so far remained elusive. Moreover, other receptors with a similar domain structure (CD21, CD55) also serve as viral receptors, but again no information is available on the modes of recognition. In addition, the structure shown here represents the very first example of a virus protein distorting the overall conformation of its receptor, and thereby the pattern of amino acids on the receptor surface. Known atomic-resolution structures of complexes between viral proteins and protein receptors include complexes between HIV gp120 and its receptor CD4 (Kwong et al., 1998), between a CAR-binding Ads (Ad12) and CAR (Bewley et al., 1999), between Epstein Barr Virus (EBV) glycoprotein 42 (gp42) and the MHC class II molecule HLA-DR1 (Mullen et al., 2002), and between Herpes Simplex Virus and HveA (Carfi et al., 2001). In addition there is a lower-resolution structure of human rhinovirus complexed with its receptor ICAM-1 (Bella et al., 1998). The structures of the complexes all share a common feature, with an interaction between the two components without any major conformational changes in the receptors. The cellular receptors are bound essentially as rigid bodies, and structural changes are limited to alteration of the orientation of very few side chains. In the structure presented here, we see a profound alteration of the receptor structure and its surface. Binding of the Ad11 knob to CD46 alters the relative orientation of the outer two domains, which adopt an elongated rod-like shape. It is intriguing to speculate that, perhaps, the changes in CD46 structure are linked to altered signalling behavior of this receptor. Recent data indicate that CD46 plays a role in signalling, and that its signalling properties can be modulated by ligation. Antibody cross-linking of CD46 has shown to alter polarization of T-cells, thus connecting ligand binding to cell signalling (Oliaro et al., 2006). In the crystal structure of CD46 SCR1-SCR2, the crystallized protein formed trimers that are believed to also occur at the cell surface (Casasnovas et al., 1999). These trimers were formed through interactions between SCR1 domains. It is tempting to speculate that Ad11 binding would disrupt trimerization, as the Ad11 knob

engages a surface of SCR1 that is also used for trimerization. In addition to determining the structural basis of Ad attachment to CD46, we also performed an analysis of the roles of each of the contact residues. This allowed us to postulate a binding mechanism that is primarily driven by two arginines that act in concert to engage the CD46 receptor. An unusual Arg-Arg stack is at the center of this interaction, and it remains to be seen if other viruses or pathogens use similar mechanisms to engage CD46 or related receptors. The measles virus hemagglutinin, for example, is also known to bind to a large surface on domains SCR1 and SCR2 (Casasnovas et al., 1999), and it is therefore likely to also engage in contacts with residues that interact with the Ad11 knob.

6 Outlook

Although several important results have been obtained in this thesis, many questions remain. It is for example not entirely clear how other B-type Ad knobs engage CD46. This is especially true for Ad35, whose knob is quite different in loop structure to that of Ad11, and its close homolog Ad21. We will initially try to solve the structure of a second complex, performing in parallel crystallization tirals with both the Ad35 knob as well as the Ad21 knob in complex with CD46. Additional efforts will focus on crystallizing Ad knobs in complex with a longer fragment of CD46 comprising SCR1-SCR4. The main motivation here is to obtain a structure of full-length CD46, which has so far remained unsuccessful. Isolated CD46 SCR1-SCR4 crystallizes but the crystals diffract poorly, indicating that flexibility is present in the CD46 molecule. In complex with Ad11, this protein will likely be less flexible and perhaps more amenable to crystallization. This structure will reveal the overall architecture of SCR3-SCR4, including properties of binding sites for other proteins that are located on these domains.

We have also started to investigate how other pathogens bind CD46, and to study the role of pathogen binding in cell signalling. Using SPR, we will map the binding sites for several pathogens in order to create a "pathogen map" of CD46. If several pathogens share a similar epitope, this epitope could be an important target for drug design. We will also repeat all ITC measurements using SPR, stepwise converting the HI-loop of Ad7 to Ad11 and thus mapping the contribution of each amino acid. The goal is to reach the Ad11 affinity for CD46 with a modified Ad7 knob. These experiments will help us complete the picture of the Adenovirus: CD46 interaction.

7 Appendix

7.1 Ad fiber sequences

Table I. Gene sequences for the expressed Ad knobs

Ad type	**Amino Acid number**	**Mutation**	**Construct Name**	**Genebank number**
Ad7	118-325		Ad7	AY594255
Ad7	118-325	Q279R	Ad7-Q279R	AY594255
Ad11	118-325		Ad11	AAN62521
Ad11	118-325	N245S	Ad11-N245S	AAN62521
Ad11	118-325	R279Q	Ad11-R279Q	AAN62521
Ad11	118-325	R279S	Ad11-R279S	AAN62521
Ad11	118-325	R280G	Ad11-R282G	AAN62521
Ad11	118-325	I282L	Ad11-I282L	AAN62521
Ad11	118-325	N283S	Ad11-N283S	AAN62521
Ad11	118-325	D284S	Ad11-D284S	AAN62521
Ad14	123-325		Ad14	AAW33140
Ad21	118-325		Ad21	AAA16493
Ad35	118-325		Ad35	AY271307
Ad35	123-325		Ad35short	AY271307

7.2 ITC data

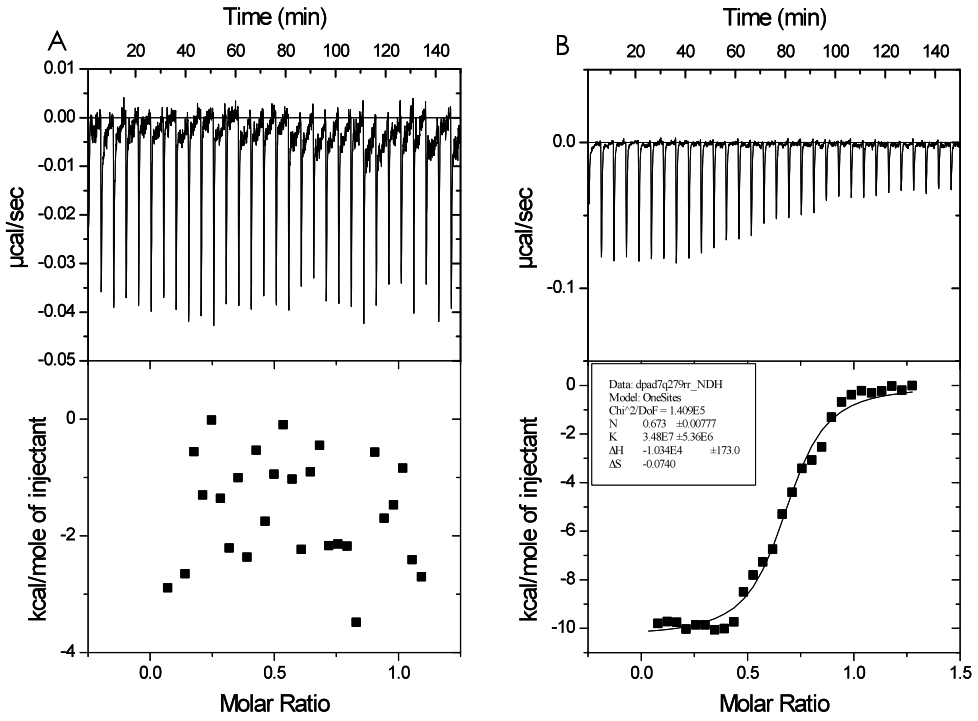

Figure A. ITC data for knob binding to CD46 SCR1-SCR2 (A) Ad7 (B) Ad7-Q279R

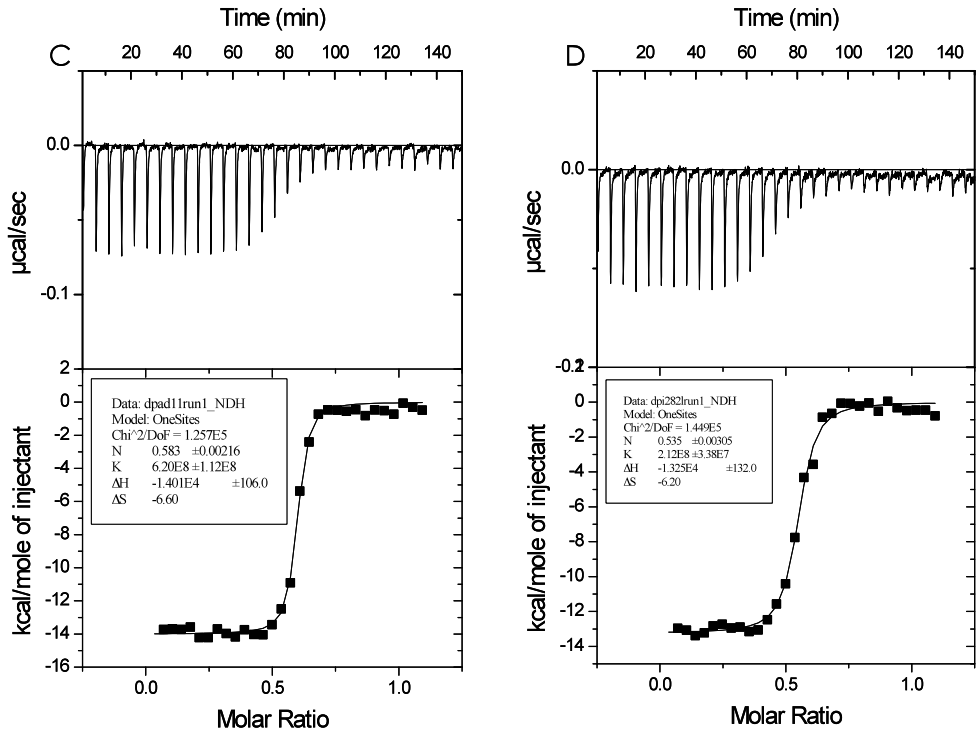

Figure B. ITC data for knob binding to CD46 SCR1-SCR2 (C) Ad11 (D) Ad11-I282L

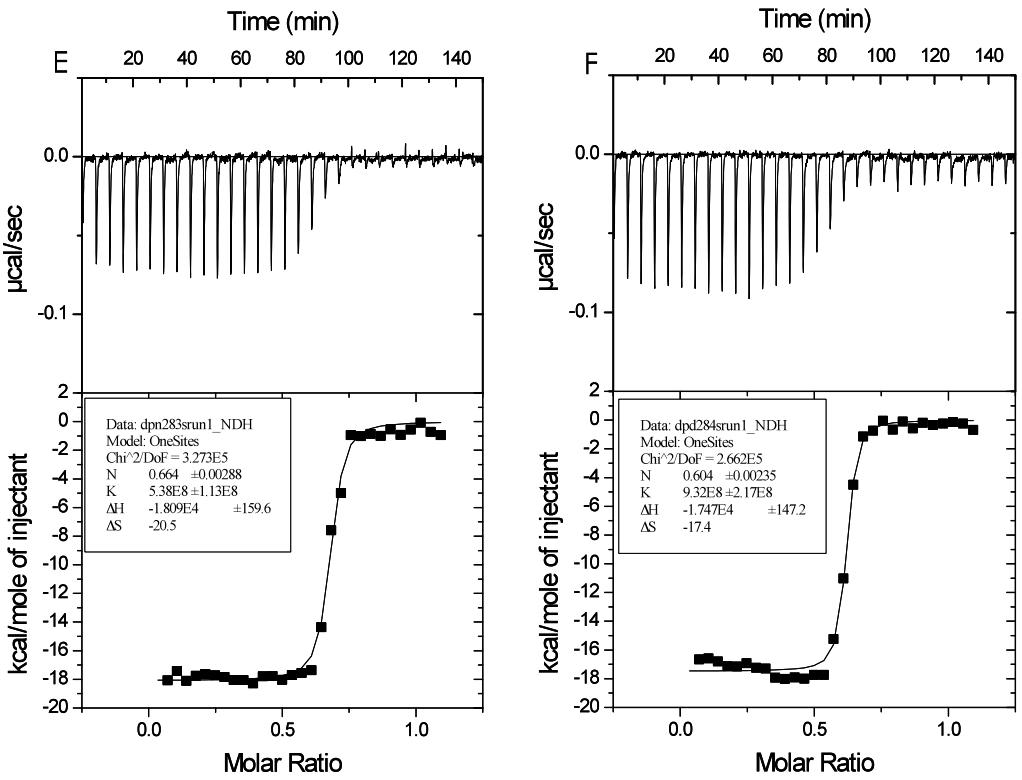

Figure C. ITC data for knob binding to CD46 SCR1-SCR2 (E) Ad11-N283S (F) Ad11-D284S

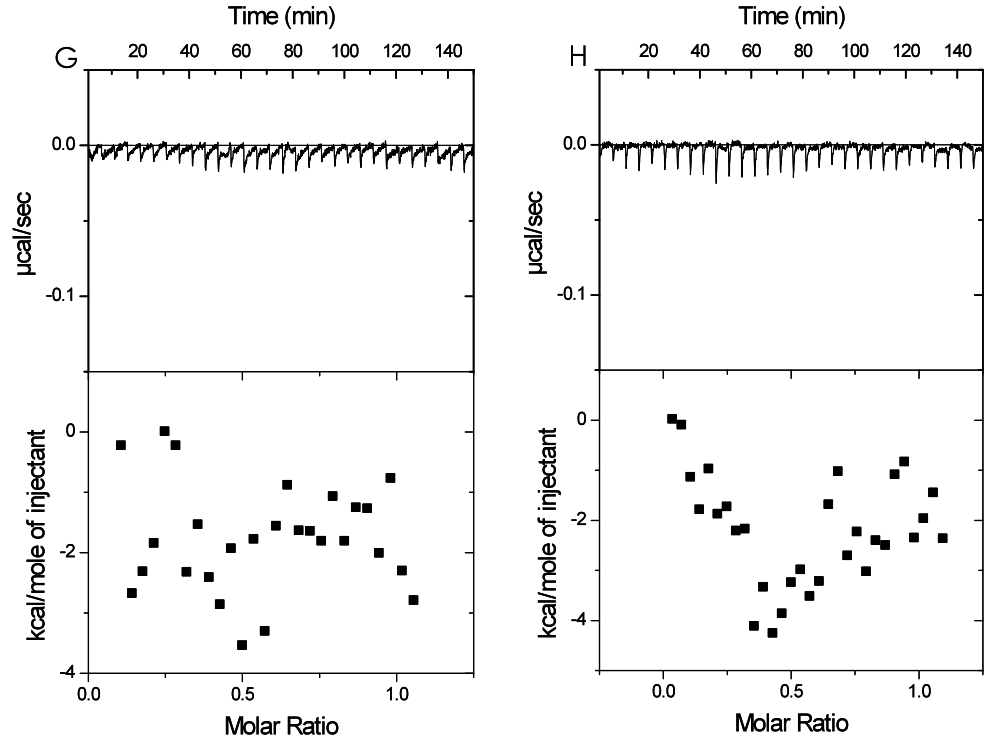

Figure D. ITC data for knob binding to CD46 SCR1-SCR2 (G) Ad11-R279Q (H) Ad11-R279S

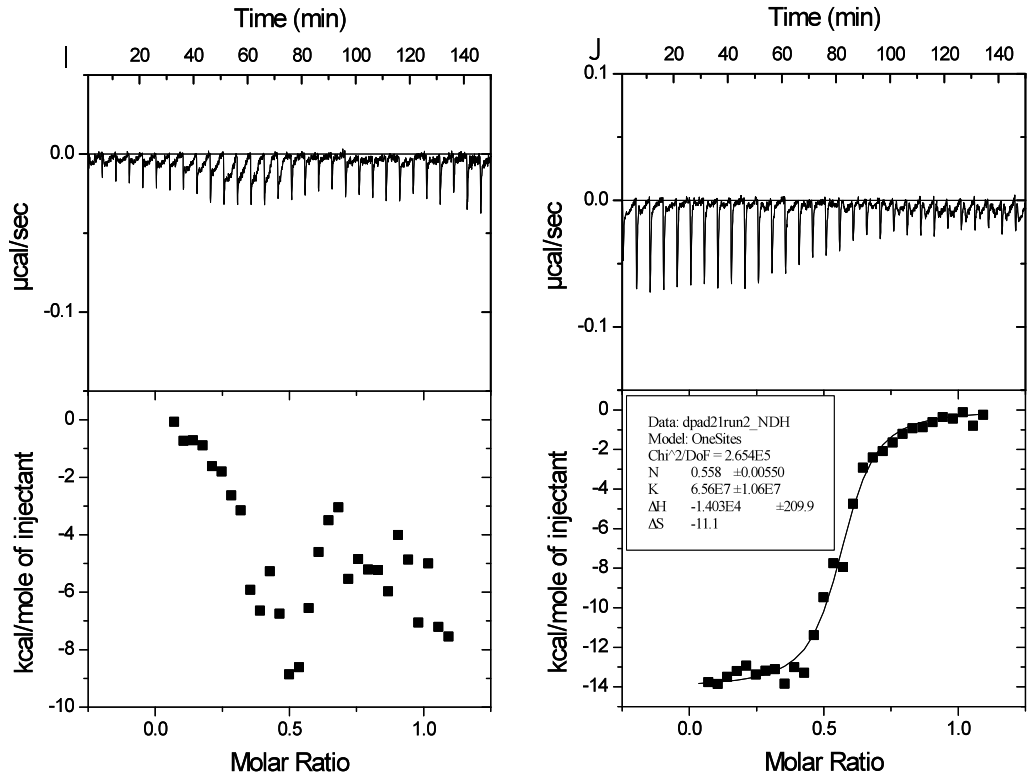

Figure D. ITC data for knob binding to CD46 SCR1-SCR2 (I) Ad11-R280G (J) Ad21

7.3 Crystallographic data statistics

Table II. X-ray crystallographic data for the Ad11, Ad7 and Ad14 knob

	Ad11 knob	Ad7 knob	Ad14 knob
Data collection			
Space group	I23	$P2_12_12$	$P3_212$
Cell dimensions			
a, *b*, *c* (Å)	100.6, 100.6, 100.6	83.31, 88.05, 79.17	106.47, 106.47, 311.71
α, β, γ (°)	90.00, 90.00, 90.00	90.00, 90.00, 90.00	90.00, 90.00, 120.00
Resolution (Å)	40-1.45 (1.45-1.50) *	79-1.75 (1.75-1.81) *	47.4-1.8 (1.80-1.90)*
R_{sym}	4.5 (38.8)*	5.0 (36.4)*	7.8 (27.0)*
I / σ	13.2 (1.6)*	10.17 (1.3)*	20.9 (5.2)*
Completeness (%)	99.9 (100.0)*	99.1 (95.1)*	99.1 (94.4)*
Redundancy	6.0 (5.4)*	5.1 (4.6)*	11.9 (4.8)
Refinement			
Resolution (Å)	40.0-1.45	79.06-1.75	40.0-1.8
No. reflections	30051	58882	185418
R_{work} / R_{free}	18.8/21.6	20.2/23.8	19.2/21.2
No. atoms	1754	5095	15979
Protein	1574	4626	13975
Ligand/ion/glycans			
Water	180	469	2004
B-factors (Å^2)			
Protein	13.7	21.8	19.0
Ligand/ion			
Water	24.9	36.6	24.4
R.m.s. deviations			
Bond lengths (Å)	0.005	0.008	0.006
Bond angles (°)	1.15	0.945	1.071

*Highest-resolution shell is shown in parentheses.

Table III. X-ray crystallographic data for the Ad11: CD46 SCR1-SCR2 complex

	Ad11:CD46 SCR1-SCR2
Data collection	
Space group	P3
Cell dimensions	
a, *b*, *c* (Å)	106.14, 106.14, 68.34
α, β, γ (°)	90.00, 90.00, 120.00
Resolution (Å)	40-2.85 (2.85-2.95) *
R_{sym}	13.8 (32.5)*
I / σ	7.23 (2.64)*
Completeness (%)	93.1 (83.0)*
Redundancy	4.1 (4.0)*
Refinement	
Resolution (Å)	40-2.85
No. reflections	18934
R_{work} / R_{free}	23.8/27.3
No. atoms	5249
Protein	5134
Ligand/ion/glycans	81
Water	34
B-factors (Å^2)	
Protein	45.8
Ligand/ion	58.2
Water	32.4
R.m.s. deviations	
Bond lengths (Å)	0.008
Bond angles (°)	1.5

*Highest-resolution shell is shown in parentheses.

Table IV. X-ray crystallographic data for crystallized mutant knobs

	Ad11-N245S	Ad11-R279S	Ad11-I282I	Ad11-N283S	Ad7-Q279R
Data collection					
Space group	I23	P32	I23	I23	$P2_12_12$
Cell dimensions					
a, *b*, *c* (Å)	101.66, 101.66, 101.66	148.65, 148.65, 74.44	102.63, 102.63, 102.63	101.41, 101.41, 101.41	83.13, 87.8, 79.1
α, β, γ (°)	90.00, 90.00, 90.00	90.00, 90.00, 120.00	90.00, 90.00, 90.00	90.00, 90.00, 90.00	90.00, 90.00, 90.00
Resolution (Å)	71.8-1.6 (1.6-1.66) *	129.1-2.55 (2.55-2.64) *	72.5-1.8 (1.80-1.86)*	71.8-1.72 (1.72-1.78)*	79.05-1.55 (1.55-1.61)*
R_{sym}	7.4 (44.0)*	9.7 (38.9)*	6.4 (38.2)*	8.5 (38.2)*	6.3 (38.9)*
I / σ	14.2 (1.8)*	7.42 (1.2)*	7.2 (5.7)*	16.65 (1.22)*	12.8 (1.4)*
Completeness (%)	99.9 (100)*	99.0 (98.1)*	98.2 (86.2)*	99.7 (99.4)*	98.2 (95.8)*
Redundancy	7.3 (7.1)*	3.2 (2.9)*	16.8 (1.66)	6.2 (2.7)	5.4 (5.3)
Refinement					
Resolution (Å)	71.8-1.66	129.1-2.55	72.5.0-1.8	71.8-1.72	79.06-1.55
No. reflections	21984	53384	14847	17590	74740
R_{work} / R_{free}	19.4/22.0	21.3/23.6	20.2/23.8	17.8/22.0	19.2/21.2
No. atoms	1670	14346	1668	1705	4922
Protein	1554	14033	1556	1554	4620
Ligand/ion/ glycans					
Water	116	313	112	151	302
B-factors (Å^2)	19.9	44.7	32.5	28.9	23.8
Protein	16.6	45.5	28.6	22.8	20.8
Ligand/ion					
Water	23.3	41.0	36.4	35.0	26.8
R.m.s. deviations					
Bond lengths (Å)	0.007	0.007	0.007	0.011	0.005
Bond angles (°)	1.4	0.783	0.713	0.908	0.897

*Highest-resolution shell is shown in parentheses.

8 Acknowledgments

Words can not express the feelings on this day. So many to thank, so little space for doing it…

I would like to thank Thilo Stehle for giving me the opportunity to obtain my PhD in his lab. I have to admit that when I first came here it did not look too promising. I asked myself: -"Will there ever be science done in these rooms". Today we know the answer to that question, luckily. I will for ever see you as a friend not as my old boss. We did it!

Niklas, without you I would not be here today. You took good care of me from day one, always listening to my ideas answering: -"Yes, we could do it like that…or let's do it like this…" You taught me how to work independently, how to get an idea into a working experiment, thank you. I will always be there for you whenever you feel like loosing some money in poker…

Min kära familj, vad skulle jag göra utan er. Ni finns alltid där för mig när jag behöver er. Livet är inte alltid enkelt, men det finns alltid en utväg. Jag är så oerhört stolt över att vara er son/bror och barnbarn. Utan er skulle jag inte stå här idag ni är mina idoler! Jag älskar er!

Alle unsere TA's. Danke für alles. Die besten TA's alle Zeiten…

A special thanks to Uli, my spare mum. You have always kept me in a good mood, giving me cakes at birthdays and homemade German food! You made sure that I did not starve to death, and that I had enough protein. BIG thanks, without your work I wouldn't be here today.

Nenne, min älskade vän. Tack för allt det stöd du get mig under dessa år. Livet är full av möjligeheter, vi får väl se vart våra liv tar oss nu. Älskar dig!

Jan och Lena Sandtröm, och OlleBull. Tack för allt, ni får mig alltid på bra humör . Jag kommer för alltid känna mig "hemma" med er... Visst är det roligt nästan jämt...

Great friends are not easy to find… Sebastian, thank you for all our unforgettable evenings, especially the bike ride after Risiko. You are right; it is more interesting when you do not know how the evening will end. Steffen; my organized friend, thank you for the nice "gaming-evenings" at your place. I am really looking forward to the Haggis, of course with the bagpipe ceremony, what happened with that by the way? Dirk our coffee-man. Thank you for sharing all your crazy ideas, one more insane than the other…

My feeding team Stefan and Richard: how would I have done this without you?

And all you others at the lab…thank you for everything. It is easy to come to a new country with friends like you… and all the lists… Keep them! Maybe my autograph will be worth something one day… =)

9 References

Adamczyk, M., Johnson, D.D., Mattingly, P.G., Moore, J.A., and Pan, Y. (1998). Immunoassay reagents for thyroid testing. 3. Determination of the solution binding affinities of a T4 monoclonal antibody Fab fragment for a library of thyroxine analogs using surface plasmon resonance. Bioconjug Chem 9, 23-32.

Adrian, T., Wadell, G., Hierholzer, J.C., and Wigand, R. (1986). DNA restriction analysis of adenovirus prototypes 1 to 41. Arch Virol *91*, 277-290.

Akiyama, H., Kurosu, T., Sakashita, C., Inoue, T., Mori, S., Ohashi, K., Tanikawa, S., Sakamaki, H., Onozawa, Y., Chen, Q., *et al.* (2001). Adenovirus is a key pathogen in hemorrhagic cystitis associated with bone marrow transplantation. Clin Infect Dis *32*, 1325-1330.

Angata, T., and Varki, A. (2002). Chemical diversity in the sialic acids and related alpha-keto acids: an evolutionary perspective. Chem Rev *102*, 439-469.

Arnberg, N., Edlund, K., Kidd, A.H., and Wadell, G. (2000a). Adenovirus type 37 uses sialic acid as a cellular receptor. J Virol *74*, 42-48.

Arnberg, N., Kidd, A.H., Edlund, K., Nilsson, J., Pring-Akerblom, P., and Wadell, G. (2002a). Adenovirus type 37 binds to cell surface sialic acid through a charge-dependent interaction. Virology *302*, 33-43.

Arnberg, N., Kidd, A.H., Edlund, K., Olfat, F., and Wadell, G. (2000b). Initial interactions of subgenus D adenoviruses with A549 cellular receptors: sialic acid versus alpha(v) integrins. J Virol *74*, 7691-7693.

Arnberg, N., Pring-Akerblom, P., and Wadell, G. (2002b). Adenovirus type 37 uses sialic acid as a cellular receptor on Chang C cells. J Virol *76*, 8834-8841.

Athappilly, F.K., Murali, R., Rux, J.J., Cai, Z., and Burnett, R.M. (1994). The refined crystal structure of hexon, the major coat protein of adenovirus type 2, at 2.9 A resolution. J Mol Biol *242*, 430-455.

Bai, M., Harfe, B., and Freimuth, P. (1993). Mutations that alter an Arg-Gly-Asp (RGD) sequence in the adenovirus type 2 penton base protein abolish its cell-rounding activity and delay virus reproduction in flat cells. J Virol *67*, 5198-5205.

Bangari, D.S., and Mittal, S.K. (2006a). Current strategies and future directions for eluding adenoviral vector immunity. Curr Gene Ther *6*, 215-226.

Bangari, D.S., and Mittal, S.K. (2006b). Development of nonhuman adenoviruses as vaccine vectors. Vaccine *24*, 849-862.

Bartha, A. (1969). Proposal for subgrouping of bovine adenoviruses. Acta Vet Acad Sci Hung *19*, 319-321.

Bebbington, C.R., Renner, G., Thomson, S., King, D., Abrams, D., and Yarranton, G.T. (1992). High-level expression of a recombinant antibody from myeloma cells using a

glutamine synthetase gene as an amplifiable selectable marker. Biotechnology (N Y) *10*, 169-175.

Bech, M., Bunk, O., David, C., Kraft, P., Bronnimann, C., Eikenberry, E.F., and Pfeiffer, F. (2008). X-ray imaging with the PILATUS 100k detector. Appl Radiat Isot 66, 474-478.

Bella, J., Kolatkar, P.R., Marlor, C.W., Greve, J.M., and Rossmann, M.G. (1998). The structure of the two amino-terminal domains of human ICAM-1 suggests how it functions as a rhinovirus receptor and as an LFA-1 integrin ligand. Proc Natl Acad Sci U S A *95*, 4140-4145.

Benkö, M., Elo, P., Ursu, K., Ahne, W., LaPatra, S.E., Thomson, D., and Harrach, B. (2002). First molecular evidence for the existence of distinct fish and snake adenoviruses. J Virol *76*, 10056-10059.

Benkö, M., Harrach, B., Both, G.W., Russell, W.C., Adair B.M, Ádám, É., de Jong, J.C., Hess, M., Johnson, M., Kajon, A., Kidd, A.H., Lehmkuhl, H.D., Li, Q.-G., Mautner, V., Pring-Akerblom, P. and Wadell, G. (2006). Index of Viruses - Adenoviridae (New Yourk, Columbia University), pp. ICTVdB - The Universal Virus Database.

Bergfors (1999). Protein Crystallization Techniques, strategies and Tips, A laboratory manual (La Jolla, International university line).

Bewley, M.C., Springer, K., Zhang, Y.B., Freimuth, P., and Flanagan, J.M. (1999). Structural analysis of the mechanism of adenovirus binding to its human cellular receptor, CAR. Science *286*, 1579-1583.

Blow, D. (2002). Outline of crystallography for Biologists (New Yourk, Oxfrod University Press).

Boros, G., Graf, Z., Benko, M., and Bartha, A. (1985). Isolation of a bovine adenovirus from fallow deer (Dama dama). Acta Vet Hung *33*, 119-123.

Borovjagin, A.V., Krendelchtchikov, A., Ramesh, N., Yu, D.C., Douglas, J.T., and Curiel, D.T. (2005). Complex mosaicism is a novel approach to infectivity enhancement of adenovirus type 5-based vectors. Cancer Gene Ther *12*, 475-486.

Brenner, S., and Horne, R.W. (1959). A negative staining method for high resolution electron microscopy of viruses. Biochim Biophys Acta *34*, 103-110.

Brouwer, E., Havenga, M.J., Ophorst, O., de Leeuw, B., Gijsbers, L., Gillissen, G., Hoeben, R.C., ter Horst, M., Nanda, D., Dirven, C.*, et al.* (2007). Human adenovirus type 35 vector for gene therapy of brain cancer: improved transduction and bypass of pre-existing anti-vector immunity in cancer patients. Cancer Gene Ther *14*, 211-219.

Brunger, A.T. (1992). Free R value: a novel statistical quantity for assessing the accuracy of crystal structures. Nature *355*, 472-475.

Brunger, A.T., Adams, P.D., Clore, G.M., DeLano, W.L., Gros, P., Grosse-Kunstleve, R.W., Jiang, J.-S., Kuszewski, J., Nilges, M., Pannu, N.S.*, et al.* (1998). Crystallography & NMR System: A New Software Suite for Macromolecular Structure Determination. Acta Crystallographica Section D *54*, 905-921.

Büchen-Osmond (2003). The Universal Virus Database, ICTVdB.

Burley, S.K., and Petsko, G.A. (1986). Amino-aromatic interactions in proteins. FEBS Lett *203*, 139-143.

Burmeister, W.P., Guilligay, D., Cusack, S., Wadell, G., and Arnberg, N. (2004). Crystal structure of species D adenovirus fiber knobs and their sialic acid binding sites. J Virol *78*, 7727-7736.

Burnett, R.M. (1985). The structure of the adenovirus capsid. II. The packing symmetry of hexon and its implications for viral architecture. J Mol Biol *185*, 125-143.

Burnett, R.M., Grutter, M.G., and White, J.L. (1985). The structure of the adenovirus capsid. I. An envelope model of hexon at 6 A resolution. J Mol Biol *185*, 105-123.

Buskens, C.J., Marsman, W.A., Wesseling, J.G., Offerhaus, G.J., Yamamoto, M., Curiel, D.T., Bosma, P.J., and van Lanschot, J.J. (2003). A genetically retargeted adenoviral vector enhances viral transduction in esophageal carcinoma cell lines and primary cultured esophageal resection specimens. Ann Surg *238*, 815-824; discussion 825-816.

Cardoso, A.I., Beauverger, P., Gerlier, D., Wild, T.F., and Rabourdin-Combe, C. (1995). Formaldehyde inactivation of measles virus abolishes CD46-dependent presentation of nucleoprotein to murine class I-restricted CTLs but not to class II-restricted helper T cells. Virology *212*, 255-258.

Carfi, A., Willis, S.H., Whitbeck, J.C., Krummenacher, C., Cohen, G.H., Eisenberg, R.J., and Wiley, D.C. (2001). Herpes simplex virus glycoprotein D bound to the human receptor HveA. Mol Cell *8*, 169-179.

Carson, M. (1997). Ribbons. Methods Enzymol *277*, 493-505.

Carson, S.D. (2001). Receptor for the group B coxsackieviruses and adenoviruses: CAR. Rev Med Virol *11*, 219-226.

Carter (1997). Methods in enzymology, Vol 276 (New York Academic Press).

Casasnovas, J.M., Larvie, M., and Stehle, T. (1999). Crystal structure of two CD46 domains reveals an extended measles virus-binding surface. EMBO J *18*, 2911-2922.

Cattaneo, R. (2004). Four viruses, two bacteria, and one receptor: membrane cofactor protein (CD46) as pathogens' magnet. J Virol *78*, 4385-4388.

CCP4 (1994). The CCP4 suite: programs for protein crystallography. Acta Crystallographica Section D *50*, 760-763.

CDC (2007). http://www.cdc.gov/.

Chappell, J.D., Prota, A.E., Dermody, T.S., and Stehle, T. (2002). Crystal structure of reovirus attachment protein sigma1 reveals evolutionary relationship to adenovirus fiber. EMBO J *21*, 1-11.

Cohen, C.J., Shieh, J.T., Pickles, R.J., Okegawa, T., Hsieh, J.T., and Bergelson, J.M. (2001). The coxsackievirus and adenovirus receptor is a transmembrane component of the tight junction. Proc Natl Acad Sci U S A *98*, 15191-15196.

Crawford-Miksza, L.K., and Schnurr, D.P. (1996). Adenovirus serotype evolution is driven by illegitimate recombination in the hypervariable regions of the hexon protein. Virology *224*, 357-367.

Cudney, R., Patel, S., Weisgraber, K., Newhouse, Y., and McPherson, A. (1994). Screening and optimization strategies for macromolecular crystal growth. Acta Crystallographica Section D *50*, 414-423.

Cusack, S. (2005). Adenovirus complex structures. Curr Opin Struct Biol *15*, 237-243.

Davison, A.J., Wright, K.M., and Harrach, B. (2000). DNA sequence of frog adenovirus. J Gen Virol *81*, 2431-2439.

Davison, E., Diaz, R.M., Hart, I.R., Santis, G., and Marshall, J.F. (1997). Integrin alpha5beta1-mediated adenovirus infection is enhanced by the integrin-activating antibody TS2/16. J Virol *71*, 6204-6207.

Defer, C., Belin, M.T., Caillet-Boudin, M.L., and Boulanger, P. (1990). Human adenovirus-host cell interactions: comparative study with members of subgroups B and C. J Virol *64*, 3661-3673.

DeLano, W.L. (2002). The PyMOL Molecular Graphics System (San Carlos).

Diederichs, K., and Karplus, P.A. (1997). Improved R-factors for diffraction data analysis in macromolecular crystallography. Nat Struct Biol *4*, 269-275.

Dimmock, E.a.L. (2007). Introduction to modern virology, Sixth Edition edn (Malden, Blackwell Publishing).

Dingle, J.H., and Langmuir, A.D. (1968). Epidemiology of acute, respiratory disease in military recruits. Am Rev Respir Dis *97*, Suppl:1-65.

Durmort, C., Stehlin, C., Schoehn, G., Mitraki, A., Drouet, E., Cusack, S., and Burmeister, W.P. (2001). Structure of the fiber head of Ad3, a non-CAR-binding serotype of adenovirus. Virology *285*, 302-312.

Edelstein, M.L., Abedi, M.R., and Wixon, J. (2007). Gene therapy clinical trials worldwide to 2007--an update. J Gene Med *9*, 833-842.

Einfeld, D.A., Brough, D.E., Roelvink, P.W., Kovesdi, I., and Wickham, T.J. (1999). Construction of a pseudoreceptor that mediates transduction by adenoviruses expressing a ligand in fiber or penton base. J Virol *73*, 9130-9136.

Elward, K., Griffiths, M., Mizuno, M., Harris, C.L., Neal, J.W., Morgan, B.P., and Gasque, P. (2005). CD46 plays a key role in tailoring innate immune recognition of apoptotic and necrotic cells. J Biol Chem *280*, 36342-36354.

Emsley et al. (2004). Coot: model-building tools for molecular graphics. Acta Crystallogr D Biol Crystallogr *60*, 2126-2132.

Fabry, C.M., Rosa-Calatrava, M., Conway, J.F., Zubieta, C., Cusack, S., Ruigrok, R.W., and Schoehn, G. (2005). A quasi-atomic model of human adenovirus type 5 capsid. EMBO J *24*, 1645-1654.

Farkas, S.L., Benko, M., Elo, P., Ursu, K., Dan, A., Ahne, W., and Harrach, B. (2002). Genomic and phylogenetic analyses of an adenovirus isolated from a corn snake (Elaphe guttata) imply a common origin with members of the proposed new genus Atadenovirus. J Gen Virol *83*, 2403-2410.

Fields, K., Howley (1996). Fields Virology, Vol 2 (Philadelphia, Lippincott-Raven).

Fleischli, C., Sirena, D., Lesage, G., Havenga, M.J., Cattaneo, R., Greber, U.F., and Hemmi, S. (2007). Species B adenovirus serotypes 3, 7, 11 and 35 share similar binding sites on the membrane cofactor protein CD46 receptor. J Gen Virol *88*, 2925-2934.

Fleischli, C., Verhaagh, S., Havenga, M., Sirena, D., Schaffner, W., Cattaneo, R., Greber, U.F., and Hemmi, S. (2005). The distal short consensus repeats 1 and 2 of the membrane cofactor protein CD46 and their distance from the cell membrane determine productive entry of species B adenovirus serotype 35. J Virol *79*, 10013-10022.

Flint, E., Racaniello, Skalka (2004). Principels of Virology, Second Edition edn (Washington, D.C., ASM Press).

Flocco, M.M., and Mowbray, S.L. (1994). Planar stacking interactions of arginine and aromatic side-chains in proteins. J Mol Biol *235*, 709-717.

French, S., and Wilson, K. (1978). On the treatment of negative intensity observations. Acta Crystallographica Section A *34*, 517-525.

Fujinaga, K., and Green, M. (1967). Mechanism of Viral Carcinogenesis by DNA Mammalian Viruses, Ii. Viral-Specific Rna in Tumor Cells Induced by "Weakly" Oncogenic Human Adenoviruses. Proc Natl Acad Sci U S A *57*, 806-812.

Gaggar, A., Shayakhmetov, D.M., and Lieber, A. (2003). CD46 is a cellular receptor for group B adenoviruses. Nat Med *9*, 1408-1412.

Gaggar, A., Shayakhmetov, D.M., Liszewski, M.K., Atkinson, J.P., and Lieber, A. (2005). Localization of regions in CD46 that interact with adenovirus. J Virol *79*, 7503-7513.

Gall, J.G., Crystal, R.G., and Falck-Pedersen, E. (1998). Construction and characterization of hexon-chimeric adenoviruses: specification of adenovirus serotype. J Virol *72*, 10260-10264.

Gallivan, J.P., and Dougherty, D.A. (1999). Cation-pi interactions in structural biology. Proc Natl Acad Sci U S A *96*, 9459-9464.

Gardlik, R., Palffy, R., Hodosy, J., Lukacs, J., Turna, J., and Celec, P. (2005). Vectors and delivery systems in gene therapy. Med Sci Monit *11*, RA110-121.

Garman, E.F., and Owen, R.L. (2006). Cryocooling and radiation damage in macromolecular crystallography. Acta Crystallogr D Biol Crystallogr *62*, 32-47.

GenBank (2008). http://www.ncbi.nlm.nih.gov/Genbank/.

Gerlier, D., Trescol-Biemont, M.C., Varior-Krishnan, G., Naniche, D., Fugier-Vivier, I., and Rabourdin-Combe, C. (1994). Efficient MHC class II-restricted presentation of measles virus to T cells relies on its targeting to its cellular receptor human CD46 and involves an endosomal pathway. Cell Biol Int *18*, 315-320.

Giannakis, E., Jokiranta, T.S., Ormsby, R.J., Duthy, T.G., Male, D.A., Christiansen, D., Fischetti, V.A., Bagley, C., Loveland, B.E., and Gordon, D.L. (2002). Identification of the streptococcal M protein binding site on membrane cofactor protein (CD46). J Immunol *168*, 4585-4592.

Gill, D.B., and Atkinson, J.P. (2004). CD46 in Neisseria pathogenesis. Trends Mol Med *10*, 459-465.

Greber, U.F. (2002). Signalling in viral entry. Cell Mol Life Sci *59*, 608-626.

Greber, U.F., Suomalainen, M., Stidwill, R.P., Boucke, K., Ebersold, M.W., and Helenius, A. (1997). The role of the nuclear pore complex in adenovirus DNA entry. EMBO J *16*, 5998-6007.

Green, N.M., Wrigley, N.G., Russell, W.C., Martin, S.R., and McLachlan, A.D. (1983). Evidence for a repeating cross-beta sheet structure in the adenovirus fibre. EMBO J *2*, 1357-1365.

Greenstone, H.L., Santoro, F., Lusso, P., and Berger, E.A. (2002). Human Herpesvirus 6 and Measles Virus Employ Distinct CD46 Domains for Receptor Function. J Biol Chem *277*, 39112-39118.

Gustafsson, D.J., Segerman, A., Lindman, K., Mei, Y.F., and Wadell, G. (2006). The Arg279Gln [corrected] substitution in the adenovirus type 11p (Ad11p) fiber knob abolishes EDTA-resistant binding to A549 and CHO-CD46 cells, converting the phenotype to that of Ad7p. J Virol *80*, 1897-1905.

Hakim, F.A., and Tleyjeh, I.M. (2008). Severe adenovirus pneumonia in immunocompetent adults: a case report and review of the literature. Eur J Clin Microbiol Infect Dis *27*, 153-158.

Harrach, B., Meehan, B.M., Benko, M., Adair, B.M., and Todd, D. (1997). Close phylogenetic relationship between egg drop syndrome virus, bovine adenovirus serotype 7, and ovine adenovirus strain 287. Virology *229*, 302-308.

Hoffman, J.A. (2006). Adenoviral disease in pediatric solid organ transplant recipients. Pediatr Transplant *10*, 17-25.

Holterman, L., Vogels, R., van der Vlugt, R., Sieuwerts, M., Grimbergen, J., Kaspers, J., Geelen, E., van der Helm, E., Lemckert, A., Gillissen, G*., et al.* (2004). Novel replication-incompetent vector derived from adenovirus type 11 (Ad11) for vaccination and gene therapy: low seroprevalence and non-cross-reactivity with Ad5. J Virol *78*, 13207-13215.

Hynes, R.O. (2002). Integrins: bidirectional, allosteric signaling machines. Cell *110*, 673-687.

Jancarik, J., and Kim, S.H. (1991). Sparse matrix sampling: a screening method for crystallization of proteins. Journal of Applied Crystallography *24*, 409-411.

Jason-Moller, L., Murphy, M., and Bruno, J. (2006). Overview of Biacore systems and their applications. Curr Protoc Protein Sci *Chapter 19*, Unit 19 13.

Johansson, S.M., Nilsson, E.C., Elofsson, M., Ahlskog, N., Kihlberg, J., and Arnberg, N. (2007). Multivalent sialic acid conjugates inhibit adenovirus type 37 from binding to and infecting human corneal epithelial cells. Antiviral Res *73*, 92-100.

Jones (1992). CCP4 Proceedings. 91-105.

Kabsch, W. (1993). Automatic processing of rotation diffraction data from crystals of initially unknown symmetry and cell constants. Journal of Applied Crystallography *26*, 795-800.

Kallstrom, H., Blackmer Gill, D., Albiger, B., Liszewski, M.K., Atkinson, J.P., and Jonsson, A.B. (2001). Attachment of Neisseria gonorrhoeae to the cellular pilus receptor CD46: identification of domains important for bacterial adherence. Cell Microbiol *3*, 133-143.

Kirby, I., Davison, E., Beavil, A.J., Soh, C.P., Wickham, T.J., Roelvink, P.W., Kovesdi, I., Sutton, B.J., and Santis, G. (1999). Mutations in the DG loop of adenovirus type 5 fiber knob protein abolish high-affinity binding to its cellular receptor CAR. J Virol *73*, 9508-9514.

Kirby, I., Davison, E., Beavil, A.J., Soh, C.P., Wickham, T.J., Roelvink, P.W., Kovesdi, I., Sutton, B.J., and Santis, G. (2000). Identification of contact residues and definition of the CAR-binding site of adenovirus type 5 fiber protein. J Virol *74*, 2804-2813.

Kirby, I., Lord, R., Davison, E., Wickham, T.J., Roelvink, P.W., Kovesdi, I., Sutton, B.J., and Santis, G. (2001). Adenovirus type 9 fiber knob binds to the coxsackie B virus-adenovirus receptor (CAR) with lower affinity than fiber knobs of other CAR-binding adenovirus serotypes. J Virol *75*, 7210-7214.

Kirchner, M., Heuer, D., and Meyer, T.F. (2005). CD46-independent binding of neisserial type IV pili and the major pilus adhesin, PilC, to human epithelial cells. Infect Immun *73*, 3072-3082.

Kleywegt, Z., Kjeldgaard, Jones (2001). International Tables for Crystallography, Vol F.

Kovacs, G.M., LaPatra, S.E., D'Halluin, J.C., and Benko, M. (2003). Phylogenetic analysis of the hexon and protease genes of a fish adenovirus isolated from white sturgeon (Acipenser transmontanus) supports the proposal for a new adenovirus genus. Virus Res *98*, 27-34.

Kwong, P.D., Wyatt, R., Robinson, J., Sweet, R.W., Sodroski, J., and Hendrickson, W.A. (1998). Structure of an HIV gp120 envelope glycoprotein in complex with the CD4 receptor and a neutralizing human antibody. Nature *393*, 648-659.

Larochelle, N., Deol, J.R., Srivastava, V., Allen, C., Mizuguchi, H., Karpati, G., Holland, P.C., and Nalbantoglu, J. (2008). Downregulation of CD46 during muscle differentiation: implications for gene transfer to human skeletal muscle using group B adenoviruses. Hum Gene Ther *19*, 133-142.

Larvie, M. (2001). X-ray Crystallography and Electron Microscopy of Cell Surface Receptors. In The Devision of Medical Sciences (Boston, Harvars University).

Leen, A.M., and Rooney, C.M. (2005). Adenovirus as an emerging pathogen in immunocompromised patients. Br J Haematol *128*, 135-144.

Lehmkuhl, H.D., and Cutlip, R.C. (1999). A new goat adenovirus isolate proposed as the prototype strain for goat adenovirus serotype 1. Arch Virol *144*, 1611-1618.

Levy, J., Wodell, R.A., August, C.S., and Bayever, E. (1990). Adenovirus-related hemophagocytic syndrome after bone marrow transplantation. Bone Marrow Transplant 6, 349-352.

Li, E., Brown, S.L., Stupack, D.G., Puente, X.S., Cheresh, D.A., and Nemerow, G.R. (2001). Integrin alpha(v)beta1 is an adenovirus coreceptor. J Virol *75*, 5405-5409.

Li, E., Stupack, D., Bokoch, G.M., and Nemerow, G.R. (1998a). Adenovirus endocytosis requires actin cytoskeleton reorganization mediated by Rho family GTPases. J Virol *72*, 8806-8812.

Li, E., Stupack, D., Klemke, R., Cheresh, D.A., and Nemerow, G.R. (1998b). Adenovirus endocytosis via alpha(v) integrins requires phosphoinositide-3-OH kinase. J Virol *72*, 2055-2061.

Liles, W.C., Cushing, H., Holt, S., Bryan, C., and Hackman, R.C. (1993). Severe adenoviral nephritis following bone marrow transplantation: successful treatment with intravenous ribavirin. Bone Marrow Transplant *12*, 409-412.

Liszewski, M.K., Farries, T.C., Lublin, D.M., Rooney, I.A., and Atkinson, J.P. (1996). Control of the complement system. Adv Immunol *61*, 201-283.

Liszewski, M.K., Kemper, C., Price, J.D., and Atkinson, J.P. (2005). Emerging roles and new functions of CD46. Springer Semin Immunopathol *27*, 345-358.

Liszewski, M.K., Post, T.W., and Atkinson, J.P. (1991). Membrane cofactor protein (MCP or CD46): newest member of the regulators of complement activation gene cluster. Annu Rev Immunol 9, 431-455.

Ludford-Menting, M.J., Thomas, S.J., Crimeen, B., Harris, L.J., Loveland, B.E., Bills, M., Ellis, S., and Russell, S.M. (2002). A functional interaction between CD46 and DLG4: a role for DLG4 in epithelial polarization. J Biol Chem *277*, 4477-4484.

Madisch, I., Hofmayer, S., Moritz, C., Grintzalis, A., Hainmueller, J., Pring-Akerblom, P., and Heim, A. (2007). Phylogenetic analysis and structural predictions of human adenovirus penton proteins as a basis for tissue-specific adenovirus vector design. J Virol *81*, 8270-8281.

Marsh, M., and Helenius, A. (2006). Virus entry: open sesame. Cell *124*, 729-740.

Marttila, M., Persson, D., Gustafsson, D., Liszewski, M.K., Atkinson, J.P., Wadell, G., and Arnberg, N. (2005). CD46 is a cellular receptor for all species B adenoviruses except types 3 and 7. J Virol *79*, 14429-14436.

Matthews, B.W. (1968). Solvent content of protein crystals. J Mol Biol *33*, 491-497.

McCoy (2005). http://www-structmed.cimr.cam.ac.uk/Course/Crystals/theory.html, University of Cambridge.

McCoy, A.J., Grosse-Kunstleve, R.W., Adams, P.D., Winn, M.D., Storoni, L.C., and Read, R.J. (2007). Phaser crystallographic software. Journal of Applied Crystallography *40*, 658-674.

McPherson, A. (1990). Current approaches to macromolecular crystallization. Eur J Biochem *189*, 1-23.

McPherson, A. (2003). Introduction to macromolecular crystallography (New Jersey, Wiley-Liss).

Medina-Kauwe, L.K. (2003). Endocytosis of adenovirus and adenovirus capsid proteins. Adv Drug Deliv Rev *55*, 1485-1496.

Mercier, G.T., Campbell, J.A., Chappell, J.D., Stehle, T., Dermody, T.S., and Barry, M.A. (2004). A chimeric adenovirus vector encoding reovirus attachment protein sigma1 targets cells expressing junctional adhesion molecule 1. Proc Natl Acad Sci U S A *101*, 6188-6193.

Messerschmidt (2007). X-ray Crystallography of Biomacromolecules, A Practical Guide, (Weinheim, Wiley-VCH).

Metzgar, D., Osuna, M., Kajon, A.E., Hawksworth, A.W., Irvine, M., and Russell, K.L. (2007). Abrupt emergence of diverse species B adenoviruses at US military recruit training centers. J Infect Dis *196*, 1465-1473.

Metzgar, D., Osuna, M., Yingst, S., Rakha, M., Earhart, K., Elyan, D., Esmat, H., Saad, M.D., Kajon, A., Wu, J., *et al.* (2005). PCR analysis of egyptian respiratory adenovirus isolates, including identification of species, serotypes, and coinfections. J Clin Microbiol *43*, 5743-5752.

Michael, S.I., Hong, J.S., Curiel, D.T., and Engler, J.A. (1995). Addition of a short peptide ligand to the adenovirus fiber protein. Gene Ther *2*, 660-668.

Miyazawa, N., Crystal, R.G., and Leopold, P.L. (2001). Adenovirus serotype 7 retention in a late endosomal compartment prior to cytosol escape is modulated by fiber protein. J Virol *75*, 1387-1400.

Mizuguchi, H., and Hayakawa, T. (2004). Targeted adenovirus vectors. Hum Gene Ther *15*, 1034-1044.

Mullen, M.M., Haan, K.M., Longnecker, R., and Jardetzky, T.S. (2002). Structure of the Epstein-Barr virus gp42 protein bound to the MHC class II receptor HLA-DR1. Mol Cell *9*, 375-385.

Mullis, K., Faloona, F., Scharf, S., Saiki, R., Horn, G., and Erlich, H. (1986). Specific enzymatic amplification of DNA in vitro: the polymerase chain reaction. Cold Spring Harb Symp Quant Biol *51 Pt 1*, 263-273.

Navaza, J. (1994). AMoRe: an automated package for molecular replacement. Acta Crystallographica Section A *50*, 157-163.

Nemerow, G.R., and Stewart, P.L. (1999). Role of alpha(v) integrins in adenovirus cell entry and gene delivery. Microbiol Mol Biol Rev *63*, 725-734.

Neu, U., Woellner, K., Gauglitz, G., and Stehle, T. (2008). Structural basis of GM1 ganglioside recognition by simian virus 40. Proc Natl Acad Sci U S A *105*, 5219-5224.

Nicholls, A., Sharp, K.A., and Honig, B. (1991). Protein folding and association: insights from the interfacial and thermodynamic properties of hydrocarbons. Proteins *11*, 281-296.

Notredame, C., Higgins, D.G., and Heringa, J. (2000). T-Coffee: A novel method for fast and accurate multiple sequence alignment. J Mol Biol *302*, 205-217.

O'Neill, P., Stevens, D.L., and Garman, E.F. (2002). Physical and chemical considerations of damage induced in protein crystals by synchrotron radiation: a radiation chemical perspective. J Synchrotron Radiat 9, 329-332.

Oliaro, J., Pasam, A., Waterhouse, N.J., Browne, K.A., Ludford-Menting, M.J., Trapani, J.A., and Russell, S.M. (2006). Ligation of the cell surface receptor, CD46, alters T cell polarity and response to antigen presentation. Proc Natl Acad Sci U S A *103*, 18685-18690.

Otwinowski, M. (1997). Processing of X-ray Diffraction Data Collected in Oscillation Mode, Methods in Enzymology, Macromolecular Crystallography, Part A, Vol 276 (New York, Academic Press).

Patterson, A.L. (1934). A Fourier Series Method for the Determination of the Components of Interatomic Distances in Crystals. Phys Rev 46, 372-376.

Persson, B.D., Reiter, D.M., Marttila, M., Mei, Y.F., Casasnovas, J.M., Arnberg, N., and Stehle, T. (2007). Adenovirus type 11 binding alters the conformation of its receptor CD46. Nat Struct Mol Biol *14*, 164-166.

Pierce, M.M., Raman, C.S., and Nall, B.T. (1999). Isothermal titration calorimetry of protein-protein interactions. Methods *19*, 213-221.

Pitcovski, J., Mualem, M., Rei-Koren, Z., Krispel, S., Shmueli, E., Peretz, Y., Gutter, B., Gallili, G.E., Michael, A., and Goldberg, D. (1998). The complete DNA sequence and genome organization of the avian adenovirus, hemorrhagic enteritis virus. Virology *249*, 307-315.

Post, T.W., Liszewski, M.K., Adams, E.M., Tedja, I., Miller, E.A., and Atkinson, J.P. (1991). Membrane cofactor protein of the complement system: alternative splicing of serine/threonine/proline-rich exons and cytoplasmic tails produces multiple isoforms that correlate with protein phenotype. J Exp Med *174*, 93-102.

Read, R. (2001). Pushing the boundaries of molecular replacement with maximum likelihood. Acta Crystallographica Section D *57*, 1373-1382.

Riley-Vargas, R.C., Gill, D.B., Kemper, C., Liszewski, M.K., and Atkinson, J.P. (2004). CD46: expanding beyond complement regulation. Trends Immunol *25*, 496-503.

Ritter, T., Lehmann, M., and Volk, H.D. (2002). Improvements in gene therapy: averting the immune response to adenoviral vectors. BioDrugs *16*, 3-10.

Roberts, M.M., White, J.L., Grutter, M.G., and Burnett, R.M. (1986). Three-dimensional structure of the adenovirus major coat protein hexon. Science *232*, 1148-1151.

Rowe, W.P., Huebner, R.J., Gilmore, L.K., Parrott, R.H., and Ward, T.G. (1953). Isolation of a cytopathogenic agent from human adenoids undergoing spontaneous degeneration in tissue culture. Proc Soc Exp Biol Med *84*, 570-573.

Ruoslahti, E. (1997). Integrins as signaling molecules and targets for tumor therapy. Kidney Int *51*, 1413-1417.

Russell, K.L., Hawksworth, A.W., Ryan, M.A., Strickler, J., Irvine, M., Hansen, C.J., Gray, G.C., and Gaydos, J.C. (2006). Vaccine-preventable adenoviral respiratory illness in US military recruits, 1999-2004. Vaccine *24*, 2835-2842.

Russell, S. (2004). CD46: a complement regulator and pathogen receptor that mediates links between innate and acquired immune function. Tissue Antigens *64*, 111-118.

Rux, J.J., and Burnett, R.M. (2000). Type-specific epitope locations revealed by X-ray crystallographic study of adenovirus type 5 hexon. Mol Ther *1*, 18-30.

Rux, J.J., Kuser, P.R., and Burnett, R.M. (2003). Structural and phylogenetic analysis of adenovirus hexons by use of high-resolution x-ray crystallographic, molecular modeling, and sequence-based methods. J Virol *77*, 9553-9566.

Salone, B., Martina, Y., Piersanti, S., Cundari, E., Cherubini, G., Franqueville, L., Failla, C.M., Boulanger, P., and Saggio, I. (2003). Integrin alpha3beta1 is an alternative cellular receptor for adenovirus serotype 5. J Virol *77*, 13448-13454.

San Martín, B. (2003). Structural Studies on Adenoviruses, Vol 272.

Santoro, F., Kennedy, P.E., Locatelli, G., Malnati, M.S., Berger, E.A., and Lusso, P. (1999). CD46 is a cellular receptor for human herpesvirus 6. Cell 99, 817-827.

Schleputz, C.M., Herger, R., Willmott, P.R., Patterson, B.D., Bunk, O., Bronnimann, C., Henrich, B., Hulsen, G., and Eikenberry, E.F. (2005). Improved data acquisition in grazing-incidence X-ray scattering experiments using a pixel detector. Acta Crystallographica Section A *61*, 418-425.

Schoehn, G., Fender, P., Chroboczek, J., and Hewat, E.A. (1996). Adenovirus 3 penton dodecahedron exhibits structural changes of the base on fibre binding. EMBO J *15*, 6841-6846.

Schrenzel, M., Oaks, J.L., Rotstein, D., Maalouf, G., Snook, E., Sandfort, C., and Rideout, B. (2005). Characterization of a new species of adenovirus in falcons. J Clin Microbiol *43*, 3402-3413.

Segerman, A., Arnberg, N., Erikson, A., Lindman, K., and Wadell, G. (2003a). There are two different species B adenovirus receptors: sBAR, common to species B1 and B2 adenoviruses, and sB2AR, exclusively used by species B2 adenoviruses. J Virol *77*, 1157-1162.

Segerman, A., Atkinson, J.P., Marttila, M., Dennerquist, V., Wadell, G., and Arnberg, N. (2003b). Adenovirus type 11 uses CD46 as a cellular receptor. J Virol *77*, 9183-9191.

Segerman, A., Lindman, K., Mei, Y.F., Allard, A., and Wadell, G. (2006). Adenovirus types 11p and 35 attach to and infect primary lymphocytes and monocytes, but hexon expression in T-cells requires prior activation. Virology *349*, 96-111.

Seiradake, E., and Cusack, S. (2005). Crystal structure of enteric adenovirus serotype 41 short fiber head. J Virol *79*, 14088-14094.

Seiradake, E., Lortat-Jacob, H., Billet, O., Kremer, E.J., and Cusack, S. (2006). Structural and mutational analysis of human Ad37 and canine adenovirus 2 fiber heads in complex with the D1 domain of coxsackie and adenovirus receptor. J Biol Chem *281*, 33704-33716.

Shayakhmetov, D.M., Li, Z.Y., Gaggar, A., Gharwan, H., Ternovoi, V., Sandig, V., and Lieber, A. (2004). Genome size and structure determine efficiency of postinternalization steps and gene transfer of capsid-modified adenovirus vectors in a cell-type-specific manner. J Virol *78*, 10009-10022.

Short, J.J., Pereboev, A.V., Kawakami, Y., Vasu, C., Holterman, M.J., and Curiel, D.T. (2004). Adenovirus serotype 3 utilizes CD80 (B7.1) and CD86 (B7.2) as cellular attachment receptors. Virology *322*, 349-359.

Short, J.J., Vasu, C., Holterman, M.J., Curiel, D.T., and Pereboev, A. (2006). Members of adenovirus species B utilize CD80 and CD86 as cellular attachment receptors. Virus Res *122*, 144-153.

Shortridge, K.F., and Biddle, F. (1970). The proteins of adenovirus type 5. Arch Gesamte Virusforsch *29*, 1-24.

Sirena, D., Lilienfeld, B., Eisenhut, M., Kalin, S., Boucke, K., Beerli, R.R., Vogt, L., Ruedl, C., Bachmann, M.F., Greber, U.F., *et al.* (2004). The human membrane cofactor CD46 is a receptor for species B adenovirus serotype 3. J Virol *78*, 4454-4462.

Sliz, P., Harrison, S.C., and Rosenbaum, G. (2003). How does radiation damage in protein crystals depend on X-ray dose? Structure *11*, 13-19.

Sousa, R. (1995). Use of glycerol, polyols and other protein structure stabilizing agents in protein crystallization. Acta Crystallographica Section D *51*, 271-277.

Stanley, P. (1989). Chinese hamster ovary cell mutants with multiple glycosylation defects for production of glycoproteins with minimal carbohydrate heterogeneity. Mol Cell Biol 9, 377-383.

Stanton, A. (1895). Wilhelm Conrad Röntgen On a New Kind of Rays: translation of a paper read before the Würzburg Physical and Medical Society. Nature *53*, 274-276.

Stewart, P.L., Burnett, R.M., Cyrklaff, M., and Fuller, S.D. (1991). Image reconstruction reveals the complex molecular organization of adenovirus. In Cell, pp. 145-154.

Stewart, P.L., Fuller, S.D., and Burnett, R.M. (1993). Difference imaging of adenovirus: bridging the resolution gap between X-ray crystallography and electron microscopy. In EMBO J, pp. 2589-2599.

Stone, D., Ni, S., Li, Z.Y., Gaggar, A., DiPaolo, N., Feng, Q., Sandig, V., and Lieber, A. (2005). Development and assessment of human adenovirus type 11 as a gene transfer vector. J Virol *79*, 5090-5104.

Thomson, D., Meers, J., and Harrach, B. (2002). Molecular confirmation of an adenovirus in brushtail possums (Trichosurus vulpecula). Virus Res *83*, 189-195.

Torreri, P., Ceccarini, M., Macioce, P., and Petrucci, T.C. (2005). Biomolecular interactions by Surface Plasmon Resonance technology. Ann Ist Super Sanita *41*, 437-441.

Tuve, S., Wang, H., Ware, C., Liu, Y., Gaggar, A., Bernt, K., Shayakhmetov, D., Li, Z., Strauss, R., Stone, D.*, et al.* (2006). A new group B adenovirus receptor is expressed at high levels on human stem and tumor cells. J Virol *80*, 12109-12120.

van Oostrum, J., and Burnett, R.M. (1985). Molecular composition of the adenovirus type 2 virion. J Virol *56*, 439-448.

van Raaij, M.J., Louis, N., Chroboczek, J., and Cusack, S. (1999a). Structure of the human adenovirus serotype 2 fiber head domain at 1.5 A resolution. Virology *262*, 333-343.

van Raaij, M.J., Mitraki, A., Lavigne, G., and Cusack, S. (1999b). A triple beta-spiral in the adenovirus fibre shaft reveals a new structural motif for a fibrous protein. Nature *401*, 935-938.

Varki, A. (2007). Glycan-based interactions involving vertebrate sialic-acid-recognizing proteins. Nature *446*, 1023-1029.

Vellinga, J., Van der Heijdt, S., and Hoeben, R.C. (2005). The adenovirus capsid: major progress in minor proteins. J Gen Virol *86*, 1581-1588.

Vigne, E., Mahfouz, I., Dedieu, J.F., Brie, A., Perricaudet, M., and Yeh, P. (1999). RGD inclusion in the hexon monomer provides adenovirus type 5-based vectors with a fiber knob-independent pathway for infection. J Virol *73*, 5156-5161.

Voet Donald, V.G.J. (2004). Biochemistry, Biomolecules, Mechanisms of Enzyme Action, and Metabolism, Vol 1, 3 edn (Hoboken, John Wiley & Sons).

Vogels, R., Zuijdgeest, D., van Rijnsoever, R., Hartkoorn, E., Damen, I., de Bethune, M.P., Kostense, S., Penders, G., Helmus, N., Koudstaal, W.*, et al.* (2003). Replication-deficient human adenovirus type 35 vectors for gene transfer and vaccination: efficient human cell infection and bypass of preexisting adenovirus immunity. J Virol *77*, 8263-8271.

Von Seggern, D.J., Chiu, C.Y., Fleck, S.K., Stewart, P.L., and Nemerow, G.R. (1999). A helper-independent adenovirus vector with E1, E3, and fiber deleted: structure and infectivity of fiberless particles. J Virol *73*, 1601-1608.

Wadell, G., and Norrby, E. (1969). Immunological and other biological characteristics of pentons of human adenoviruses. J Virol *4*, 671-680.

Wang, H., Liaw, Y.C., Stone, D., Kalyuzhniy, O., Amiraslanov, I., Tuve, S., Verlinde, C.L., Shayakhmetov, D., Stehle, T., Roffler, S.*, et al.* (2007). Identification of CD46 binding sites within the adenovirus serotype 35 fiber knob. J Virol *81*, 12785-12792.

Wickham, T.J. (2003). Ligand-directed targeting of genes to the site of disease. Nat Med *9*, 135-139.

Wickham, T.J., Granados, R.R., Wood, H.A., Hammer, D.A., and Shuler, M.L. (1990). General analysis of receptor-mediated viral attachment to cell surfaces. Biophys J *58*, 1501-1516.

Wickham, T.J., Mathias, P., Cheresh, D.A., and Nemerow, G.R. (1993). Integrins alpha v beta 3 and alpha v beta 5 promote adenovirus internalization but not virus attachment. Cell *73*, 309-319.

Wickham, T.J., Tzeng, E., Shears, L.L., 2nd, Roelvink, P.W., Li, Y., Lee, G.M., Brough, D.E., Lizonova, A., and Kovesdi, I. (1997). Increased in vitro and in vivo gene transfer by adenovirus vectors containing chimeric fiber proteins. J Virol *71*, 8221-8229.

Wilson, A. (1949). X-ray diffraction by random layers: ideal line profiles and determination of structure amplitudes from observed line profiles. Acta Crystallographica *2*, 245-251.

Wu, E., Pache, L., Von Seggern, D.J., Mullen, T.M., Mikyas, Y., Stewart, P.L., and Nemerow, G.R. (2003). Flexibility of the adenovirus fiber is required for efficient receptor interaction. J Virol *77*, 7225-7235.

Wu, E., Trauger, S.A., Pache, L., Mullen, T.M., von Seggern, D.J., Siuzdak, G., and Nemerow, G.R. (2004). Membrane cofactor protein is a receptor for adenoviruses associated with epidemic keratoconjunctivitis. J Virol *78*, 3897-3905.

Xia, D., Henry, L.J., Gerard, R.D., and Deisenhofer, J. (1994). Crystal structure of the receptor-binding domain of adenovirus type 5 fiber protein at 1.7 A resolution. Structure *2*, 1259-1270.

Xiong, J.P., Stehle, T., Diefenbach, B., Zhang, R., Dunker, R., Scott, D.L., Joachimiak, A., Goodman, S.L., and Arnaout, M.A. (2001). Crystal structure of the extracellular segment of integrin alpha Vbeta3. Science *294*, 339-345.

Xu, W., and Erdman, D.D. (2001). Type-specific identification of human adenovirus 3, 7, and 21 by a multiplex PCR assay. J Med Virol *64*, 537-542.

Youil, R., Toner, T.J., Su, Q., Chen, M., Tang, A., Bett, A.J., and Casimiro, D. (2002). Hexon gene switch strategy for the generation of chimeric recombinant adenovirus. Hum Gene Ther *13*, 311-320.

Zacharias, N., and Dougherty, D.A. (2002). Cation-pi interactions in ligand recognition and catalysis. Trends Pharmacol Sci *23*, 281-287.

Zubieta, C., Schoehn, G., Chroboczek, J., and Cusack, S. (2005). The structure of the human adenovirus 2 penton. Mol Cell *17*, 121-135.

10 Curriculum vitae

Personal details

Name:	Björn **David** Niklas Persson
Date of birth:	13/05/1979
Place of birth:	Linköping (Sweden)
Address:	Scheefstrasse 49
	D-72074 Tübingen
	Germany
Email:	David.Persson@uni-tuebingen.de
Nationality:	Swedish

Education

1986-1995	Elementary school Linköping, Sweden
1995-1998	High school Linköping, Sweden
1999-2004	Studies at the University of Umeå, Sweden
2003	Degree in Bachelors of Science with a major in Biochemistry, *Is the transcription factor E2F4 involved in the cell cycle regulated expression of the mouse ribonucleotide reductase R1 gene?*, Department of Medical Chemistry and Biophysics, University of Umeå, Sweden
2004	Degree in Masters of Science with a major in molecular biology, *CD46 is a cellular receptor for multiple species B adenoviruses*, Department of virology, University of Umeå, Sweden
July 2005- July 2008	PhD University of Tuebingen, "*Structural Basis of Adenovirus Attachment to its Receptor CD46*"